Research in Astronomy and Astrophysics

INVITED REVIEW

Type Ia Supernova Explosions in Binary Systems: A Review

To cite this article: Zheng-Wei Liu *et al* 2023 *Res. Astron. Astrophys.* **23** 082001

View the article online for updates and enhancements.

You may also like

- NEAR-ULTRAVIOLET PROPERTIES OF A LARGE SAMPLE OF TYPE Ia SUPERNOVAE AS OBSERVED WITH THE *Swift* UVOT
Peter A. Milne, Peter J. Brown, Peter W. A. Roming et al.
- DEFINING PHOTOMETRIC PECULIAR TYPE Ia SUPERNOVAE
S. González-Gaitán, E. Y. Hsiao, G. Pignata et al.
- High-velocity Feature as the Indicator of the Stellar Population of Type Ia Supernovae
Xiang-Cun Meng

This content was downloaded from IP address 149.156.70.22 on 03/01/2024 at 13:03

Research in Astronomy and Astrophysics, 23:082001 (43pp), 2023 August https://doi.org/10.1088/1674-4527/acd89e
© 2023. National Astronomical Observatories, CAS and IOP Publishing Ltd. Printed in China and the U.K.

Type Ia Supernova Explosions in Binary Systems: A Review

Zheng-Wei Liu[1,2,3,4], Friedrich K. Röpke[5,6], and Zhanwen Han[1,2,3,4]
[1] Yunnan Observatories, Chinese Academy of Sciences (CAS), Kunming 650216, China; zwliu@ynao.ac.cn
[2] Key Laboratory for the Structure and Evolution of Celestial Objects, CAS, Kunming 650216, China
[3] International Centre of Supernovae, Yunnan Key Laboratory, Kunming 650216, China
[4] University of Chinese Academy of Sciences, Beijing 100049, China
[5] Zentrum für Astronomie der Universität Heidelberg, Institut für Theoretische Astrophysik, Philosophenweg 12, D-69120 Heidelberg, Germany
[6] Heidelberger Institut für Theoretische Studien, Schloss-Wolfsbrunnenweg 35, D-69118 Heidelberg, Germany
Received 2023 March 9; revised 2023 April 28; accepted 2023 May 16; published 2023 July 26

Abstract

Type Ia supernovae (SNe Ia) play a key role in the fields of astrophysics and cosmology. It is widely accepted that SNe Ia arise from thermonuclear explosions of white dwarfs (WDs) in binary systems. However, there is no consensus on the fundamental aspects of the nature of SN Ia progenitors and their actual explosion mechanism. This fundamentally flaws our understanding of these important astrophysical objects. In this review, we outline the diversity of SNe Ia and the proposed progenitor models and explosion mechanisms. We discuss the recent theoretical and observational progress in addressing the SN Ia progenitor and explosion mechanism in terms of the observables at various stages of the explosion, including rates and delay times, pre-explosion companion stars, ejecta–companion interaction, early excess emission, early radio/X-ray emission from circumstellar material interaction, surviving companion stars, late-time spectra and photometry, polarization signals and supernova remnant properties. Despite the efforts from both the theoretical and observational sides, questions of how the WDs reach an explosive state and what progenitor systems are more likely to produce SNe Ia remain open. No single published model is able to consistently explain all observational features and the full diversity of SNe Ia. This may indicate that either a new progenitor paradigm or an improvement in current models is needed if all SNe Ia arise from the same origin. An alternative scenario is that different progenitor channels and explosion mechanisms contribute to SNe Ia. In the next decade, the ongoing campaigns with the James Webb Space Telescope, Gaia and the Zwicky Transient Facility, and upcoming extensive projects with the Vera C. Rubin Observatory's Legacy Survey of Space and Time and the Square Kilometre Array will allow us to conduct not only studies of individual SNe Ia in unprecedented detail but also systematic investigations for different subclasses of SNe Ia. This will advance theory and observations of SNe Ia sufficiently far to gain a deeper understanding of their origin and explosion mechanism.

Key words: (stars:) binaries (including multiple): close – methods: numerical – (stars:) supernovae: general

1. Introduction

Supernovae (SNe) are highly energetic explosions of some stars, which are so bright that they can outshine an entire galaxy. Their typical bolometric luminosities reach the order of 10^{43} erg s^{-1}, which is about ten billion times the solar luminosity. SNe play an important role in the fields of astrophysics and cosmology because they have been used as cosmic distance indicators, and they are heavy-element factories (especially for intermediate mass and iron-group elements), kinetic-energy sources, and cosmic-ray accelerators in galaxy evolution. SNe are also key players in the formation of new-generation stars by triggering the collapse of molecular clouds. SNe are generally classified into two main categories according to spectroscopic features: Type I and Type II SNe (Minkowski 1941; Filippenko 1997; Parrent et al. 2014). Type I SNe have no hydrogen (H) lines in their spectra, whereas Type II SNe contain obvious H lines. Type Ia SNe (SNe Ia) are a subclass of Type I, which exhibit strong singly ionized silicon (Si) absorption (Si II at 6150, 5800 and 4000 Å) features in their spectra.

SNe Ia are widely thought to be thermonuclear explosions of white dwarfs (WDs) in binary systems (Hoyle & Fowler 1960). They have been found to occur in all galaxy types. Their typical peak luminosity in the B-band is about $M_B = -19.5$ mag, and the typical kinetic energy is $\sim 10^{51}$ erg (Branch et al. 1993; Hillebrandt & Niemeyer 2000). The light curves of SNe Ia are powered by the Comptonization of γ-rays produced by the radioactive decay of ^{56}Ni $\rightarrow$ ^{56}Co $\rightarrow$ ^{56}Fe, with respective half-life times of 6.1 and 77 days (Truran et al. 1967; Colgate & McKee 1969; Arnett 1982; Hillebrandt et al. 2013). SNe Ia have been successfully used as cosmic distance indicators to constrain cosmological parameters, which has led to the discovery of the accelerating expansion of the Universe (Riess et al. 1998;

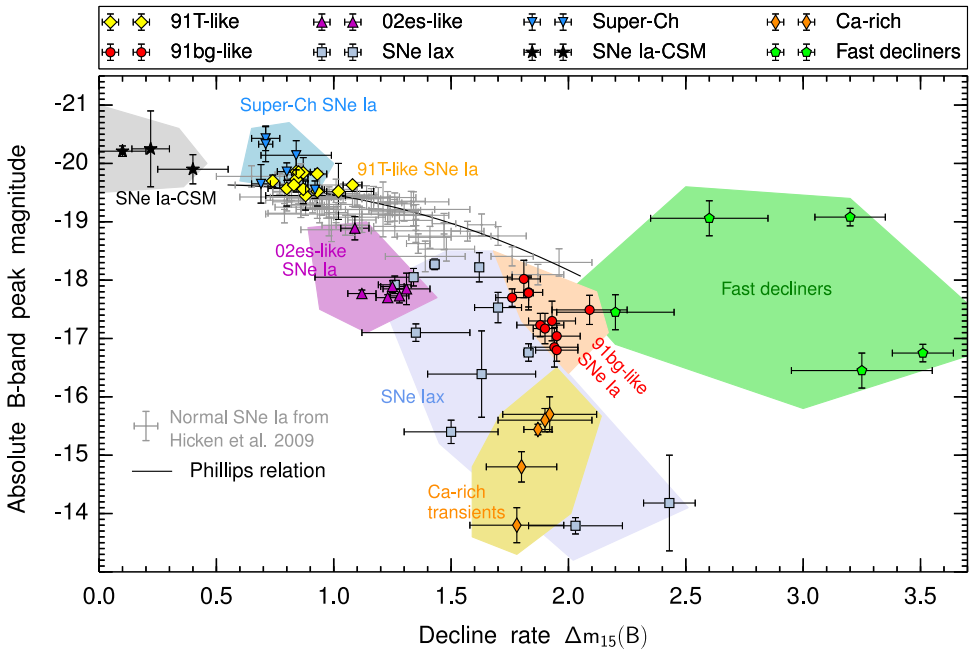


Figure 1. Distributions of normal SNe Ia and different subclasses in the peak luminosity vs. light curve width ($\Delta m_{15}(B)$; Phillips 1993) diagram. The figure is reproduced based on Figure 1 of Taubenberger (2017).

Schmidt et al. 1998; Perlmutter et al. 1999)—a breakthrough awarded with the 2011 Nobel Prize in Physics. Despite their importance and far-reaching implications, the specific progenitor systems as well as the explosion mechanism of SNe Ia remain enigmatic (e.g., Hillebrandt & Niemeyer 2000; Wang & Han 2012; Hillebrandt et al. 2013; Maoz et al. 2014; Ruiz-Lapuente 2014; Maeda & Terada 2016; Livio & Mazzali 2018; Röpke & Sim 2018; Soker 2019). This affects the reliability of necessary assumptions, such as those of universality of their calibration as distance indicators. Recently, it was found that the local measurements of the Hubble constant (H_0) based on SNe Ia are inconsistent with the value inferred from the cosmic microwave background radiation observed by the Planck satellite assuming a ΛCDM cosmological world model (Planck Collaboration et al. 2020). To determine whether this so-called H_0 tension hints at new physics, it is critical to improve our understanding of SNe Ia and, more specifically, their progenitors and explosion mechanisms.

2. Diversity of SNe Ia

A large fraction of observed SNe Ia (∼70%) are found to show remarkable homogeneity and quantifiable heterogeneity, and they exhibit a clear empirical relationship between light curve width and peak luminosity, i.e., the so-called "Phillips relation" (sometimes known as the width–luminosity relation [WLR]; Pskovskii 1977; Phillips 1993; Phillips et al. 1999). These SNe Ia are usually referred to as "normal SNe Ia," and they have long been used as standardizable candles for measuring cosmological distances (Leibundgut 2001, 2008; Goobar & Leibundgut 2011). However, an increasing number of SNe Ia have been observed that do not follow the Phillips relation (see Figure 1), and they are diverse in their observational characteristics, such as light curve shape, peak luminosity and spectral features (Benetti et al. 2005; Blondin et al. 2012; Jha 2017). For these reasons, SNe Ia have been classified into different subclasses diverging from normal events, which include 1991T-likes (Filippenko et al. 1992a; Phillips et al. 1992), 1991bg-likes (Filippenko et al. 1992b; Leibundgut et al. 1993), SNe Iax (i.e., SN 2002cx-likes; Li et al. 2003; Foley et al. 2013), 2002es-likes (Ganeshalingam et al. 2012), calcium (Ca)-rich objects (i.e., SN 2005E-like; Perets et al. 2010; Kasliwal et al. 2012), super-Chandrasekhar objects (i.e., SN 2003fg-likes; Howell et al. 2006; Hicken et al. 2007), SNe Ia-CSM (Hamuy et al. 2003) and fast decliners (Taubenberger 2017). The diversity of SNe Ia has recently been reviewed by Taubenberger (2017); we only skim the surface here (see also Jha et al. 2019; Ruiter 2020).

The 1991T-like objects form a luminous, slowly-declining subclass of SNe Ia, named after the well-observed SN 1991T (Filippenko et al. 1992a; Jeffery et al. 1992; Phillips et al. 1992). Their optical spectra at pre-maximum phases show extremely weak Ca II H and K and Si II λ6355 and strong Fe III absorption features. The 91T-like SNe are expected to be on average 0.2–0.5 mag more luminous than normal SNe Ia with similar decline rate (Blondin et al. 2012; Phillips et al. 2022). The 1991T-like SNe are found preferentially in late-type

galaxies, suggesting that they are likely associated with young stellar populations (Li et al. 2011c). It has been suggested that the 1991T-like SNe could contribute 2%–9% to all SNe Ia in the local Universe (Li et al. 2011c; Leaman et al. 2011; Blondin et al. 2012).

The 1991bg-like objects are a cool, subluminous and fast-declining subclass of SNe Ia with low ejecta velocity (Filippenko et al. 1992b; Ganeshalingam et al. 2012). Typically, they are fainter than normal SNe Ia in optical band up to 2.5 mag (Sullivan et al. 2011). Their spectra at maximum light show strong Ti II absorption, indicating a relatively cool photosphere. The 1991bg-like SNe are found preferentially in early-type (i.e., passive) galaxies (Howell 2001; Li et al. 2011c; Graur et al. 2017). Only few 1991bg-like SNe have been found in spiral galaxies. This suggests old stellar populations for the progenitors of the 1991bg-like SNe. There is no agreement about the rates of the 1991bg-like SNe in the literature; estimates range from 6% to 15% of all SNe Ia (Ganeshalingam et al. 2010; Li et al. 2011c; Silverman et al. 2012).

The SNe Iax are proposed as a hot, subluminous subclass of SNe Ia (e.g., Li et al. 2003; Foley et al. 2013). The SNe Iax are fainter than the normal SNe Ia and highly skewed to late-type galaxies (e.g., Foley et al. 2013). Their explosion ejecta are characterized by low expansion velocities and show strong mixing features. Their maximum-light spectra display similar features to those of the 1991T-like SNe, which are characterized by weak Si II λ6355 features and dominated by Fe III lines. In addition, strong He lines are identified in spectra of two events, i.e., SN 2004cs and SN 2007J. The late-time spectra of SNe Iax are dominated by narrow permitted Fe II (Jha et al. 2006; Jha 2017). It has been suggested that they contribute about $1/3$ of total SNe Ia (Li et al. 2001; Foley et al. 2013).

The 2002es-like objects are another cool, rapidly fading, subluminous subclass of SNe Ia, which have a peak luminosity and ejecta velocity ($\sim$6000 km s^{-1}) similar to SN 2002cx (Ganeshalingam et al. 2012; White et al. 2015). Their spectra at near-maximum light phases share some characteristics in common with the subluminous 1991bg-like SNe, which are clearly characterized by strong Ti II, Si II and O II absorption features (Taubenberger 2017). However, the 2002es-like SNe do not have fast-declining light curves characteristic of 1991bg-like events. White et al. (2015) suggested that 2002es-like events tend to explode preferentially (but not exclusively) in massive, early-type galaxies (Li et al. 2011c). Ganeshalingam et al. (2012) suggested that SN 2002es-like objects should account for $\sim$2.5% of all SNe Ia.

Ca-rich objects constitute a peculiar subclass of SNe Ia with SN 2005E as a prototype (Perets et al. 2010; Kasliwal et al. 2012; De et al. 2020). Ca-rich SNe are primarily characterized by peak magnitudes of -14 to -16.5 mag, rapid photometric evolution with typical rise times of 12–15 days and strong Ca features in nebular phase spectra (Kasliwal et al. 2012). They exhibit low ejecta and ^{56}Ni masses of $\lesssim 0.5\,M_{\odot}$ and $\lesssim 0.1\,M_{\odot}$, respectively (Lunnan et al. 2017). The majority of Ca-rich SNe have been observed in early-type galaxies (Kasliwal et al. 2012; Lyman et al. 2013), and the inferred rates of such SNe are likely in the range of 5%–20% of the normal SN Ia rates[7] (Perets et al. 2010; Kasliwal et al. 2012; De et al. 2020).

Super-Chandrasekhar objects are sometimes known as SN 2003fg-like SNe (Howell et al. 2006; Hicken et al. 2007; Scalzo et al. 2010; Silverman et al. 2011; Hsiao et al. 2020; Srivastav et al. 2023). They are referred to as "super-Chandrasekhar SNe" because a differentially rotating WD with a super-Chandrasekhar mass of $\sim 2.0\,M_{\odot}$ was used to interpret the observations of SN 2003fg (Howell et al. 2006). The main features of this subtype are summarized by Ashall et al. (2021). They are generally characterized by high luminosities (B-band peak absolute magnitudes of $-19 < M_B < -21$ mag), broad light curves ($\Delta m_{15}(B) < 1.3$ mag, defined as the decline in the B-band magnitude light curve from peak to 15 days later), and relatively low ejecta velocities. This is puzzling for a theoretical explanation; the first two properties point to a powerful explosion, which seems to be at odds with the low ejecta velocities. They have only one i-band maximum, which peaks after the epoch of the B-band maximum, but with weak (or without) i-band secondary maximum. Their maximum-light spectra do not show a Ti II feature; in addition, their nebular-phase spectra are characterized by a low ionization state. Super-Chandrasekhar SNe seem to be preferentially found in low-mass galaxies, indicating that they prefer a low-metallicity environment (Taubenberger et al. 2011). They seem to make up a small fraction of SNe Ia, but their exact rates are still unknown (Silverman et al. 2011; Taubenberger 2017; Ashall et al. 2021).

SNe Ia-CSM are a subclass named after the discovery of SN 2002ic (Hamuy et al. 2003; Deng et al. 2004), although there is still a debate on whether these objects are SNe Ia or in fact core-collapse SNe (Benetti et al. 2006; Silverman et al. 2013; Inserra et al. 2014). A list of several common features of SNe Ia-CSM has been compiled by Silverman et al. (2013). They have a range of R-band peak absolute magnitudes of $-19 < M_R < -21.3$ mag, and they exhibit narrow hydrogen emission features in their spectra (Dilday et al. 2012; Silverman et al. 2013). The presence of narrow H lines is thought to arise from circumstellar material (CSM), which is strongly indicative of mass loss (or outflows) of the progenitor system prior to the SN explosion. An initial systematic study of this subclass has been presented by Silverman et al. (2013), and it has been recently updated by Sharma et al. (2023). SNe Ia-CSM are preferentially found in late-type spirals and irregular galaxies, indicating the origin from a relatively young stellar population (Silverman et al. 2013). The rate of SNe Ia-CSM is estimated to be no more than a few percent of the SN Ia rates (Han &

[7] The fact that the rate estimates of the subclasses of SNe Ia do not add up to 100% indicates that there are large uncertainties on the estimated contributions of different subclasses.

Podsiadlowski 2006; Dilday et al. 2012; Silverman et al. 2013; Gal-Yam 2017; Meng & Podsiadlowski 2018; PhDubay et al. 2022; Sharma et al. 2023).

Fast decliners are rare and extremely rapidly declining SNe. So far, this class includes SN 1885A, SN 1939B, SN 2002bj, SN 2005ek and SN 2010X (Poznanski et al. 2010; Kasliwal et al. 2010; Perets et al. 2011; Drout et al. 2013; Taubenberger 2017). Whether these peculiar objects arise from thermonuclear explosions of WDs or core-collapse explosions of massive stars remains open (Bildsten et al. 2007; Shen et al. 2010; Kasliwal et al. 2010; Gal-Yam 2017). There is no conclusion on whether or not all of these objects actually belong to the same class of events (Taubenberger 2017; Jha et al. 2019).

3. Progenitors and explosion mechanisms

It is widely accepted that SNe Ia arise from thermonuclear explosions of WDs in binary systems (Hoyle & Fowler 1960). However, there is no consensus on the fundamental aspects of the nature of SN Ia progenitors and their explosion mechanism from both the theoretical and observational sides (see, e.g., Wang & Han 2012; Hillebrandt et al. 2013; Maoz et al. 2014; Maeda & Terada 2016; Livio & Mazzali 2018; Soker 2019, for reviews). In this section, potential progenitor models and explosion mechanisms of SNe Ia are briefly summarized.

3.1. Progenitor Scenarios

3.1.1. Single-degenerate Scenario

In the single-degenerate (SD) scenario, a WD accretes hydrogen-rich or helium-rich material from a non-degenerate companion star through Roche-lobe overflow (RLOF) or stellar wind until its mass approaches the Chandrasekhar mass ($\approx$1.4 $M_\odot$), at which point a thermonuclear explosion ensues (Whelan & Iben 1973; Nomoto 1982b, 1982a; Nomoto et al. 1984). The companion star could be either a main-sequence (MS) star, a subgiant (SG), a red giant (RG), an asymptotic giant branch (AGB) star, or a He star (Hachisu et al. 1999; Han & Podsiadlowski 2004; Ruiter et al. 2009; Meng et al. 2009; Wang et al. 2009). It has been suggested that a Chandrasekhar-mass WD can undergo a deflagration, a detonation (see, e.g., Röpke 2017, for an overview of thermonuclear combustion in WDs), or a delayed detonation to lead to an SN Ia explosion (e.g., Arnett 1969; Nomoto et al. 1984; Woosley et al. 1986; Khokhlov 1989; Hoeflich et al. 1995; Plewa et al. 2004; Röpke & Hillebrandt 2005; Röpke & Niemeyer 2007; Röpke et al. 2007b; Fink et al. 2014; Marquardt et al. 2015; Seitenzahl et al. 2016). In the SD scenario, SNe Ia are thought to arise from Chandrasekhar-mass WDs.[8] The homogeneity of the majority of SNe Ia therefore can be well explained by this scenario. A schematic illustration of main binary evolutionary paths for producing SNe Ia in the SD scenario is given in Figure 2.

One of the key questions in the SD scenario is how the WD retains the accreted companion material and grows in mass to approach the Chandrasekhar limit (i.e., the mass-retention efficiency onto the WD). The SD scenario requires that the WD accretes material at a relatively narrow range of accretion rates of a few $\times$ (10^{-8}–$10^{-7}\,M_\odot\,\mathrm{yr}^{-1}$) to allow steady burning of accreted material (Paczynski 1976; Fujimoto 1982a, 1982b; Livio et al. 1989; Nomoto et al. 2007; Shen & Bildsten 2007; Wolf et al. 2013; Piersanti et al. 2014; Wang 2018), which causes difficulties for explaining the observed nearby SN Ia rate (see Section 4). Moreover, some recent observations seem to pose a challenge to the SD scenario (see Section 5), such as the missing surviving companion stars in supernova remnants (SNRs) (Kerzendorf et al. 2012; Schaefer & Pagnotta 2012; Ruiz-Lapuente et al. 2018), the absence of swept-up H/He in their late spectra (Leonard 2007; Tucker et al. 2020) and low X-ray flux from nearby elliptical galaxies (Gilfanov & Bogdán 2010; Woods et al. 2017; Kuuttila et al. 2019). In addition, although the SD scenario makes the explosion rather homogeneous, it turns out to be difficult to cover the observed ranges in brightness and decline rates in this scenario. However, to conclude whether the SD scenario is promising for producing the majority of SNe Ia requires comparing a full range of predicted observational consequences from this scenario with the observations of SNe Ia (see discussions in Section 5).

A number of candidate progenitors have been suggested for the SD scenario, including cataclysmic variable stars, like classic novae, recurrent novae and dwarf novae (Webbink et al. 1987; Hachisu & Kato 2001; Warner 2003), supersoft X-ray sources (SSSs, van den Heuvel et al. 1992), symbiotic systems (Webbink et al. 1987; Yungelson & Livio 1998) and WD + hot subdwarf binaries (see Section 3.2.3; Iben & Tutukov 1994; Nelemans & Tauris 1998; Geier et al. 2013).

In the SD scenario, a WD accretes and retains companion matter that carries angular momentum. As a consequence, the WD spins with a short period, which leads to an increase in the critical explosion mass. If the critical mass is higher than the actual mass of the WD, the SN explosion could only occur after the WD increases the spin period with a specific spin-down timescale. This scenario is known as the "spin-up/spin-down model" (Di Stefano et al. 2011; Justham 2011; Hachisu et al. 2012b). In this model, if the spin-down timescale is longer than about 10^6 yrs, the CSM around the progenitor system could become diffuse and reach a density similar to that of the interstellar medium (ISM). This could explain the lack of radio and X-ray emission from SNe Ia in agreement with the current radio and X-ray observations (Margutti et al. 2012; Chomiuk et al. 2016; Lundqvist et al. 2020; see Section 5.4.1). Also, the H-rich or He-rich companion star (i.e., MS, SG, RG and He star) may shrink rapidly before the SN Ia explosion occurs by

[2] Double-detonation explosions of sub-Chandrasekhar-mass WDs could happen when accreting from a He star companion; see Section 3.2.3.

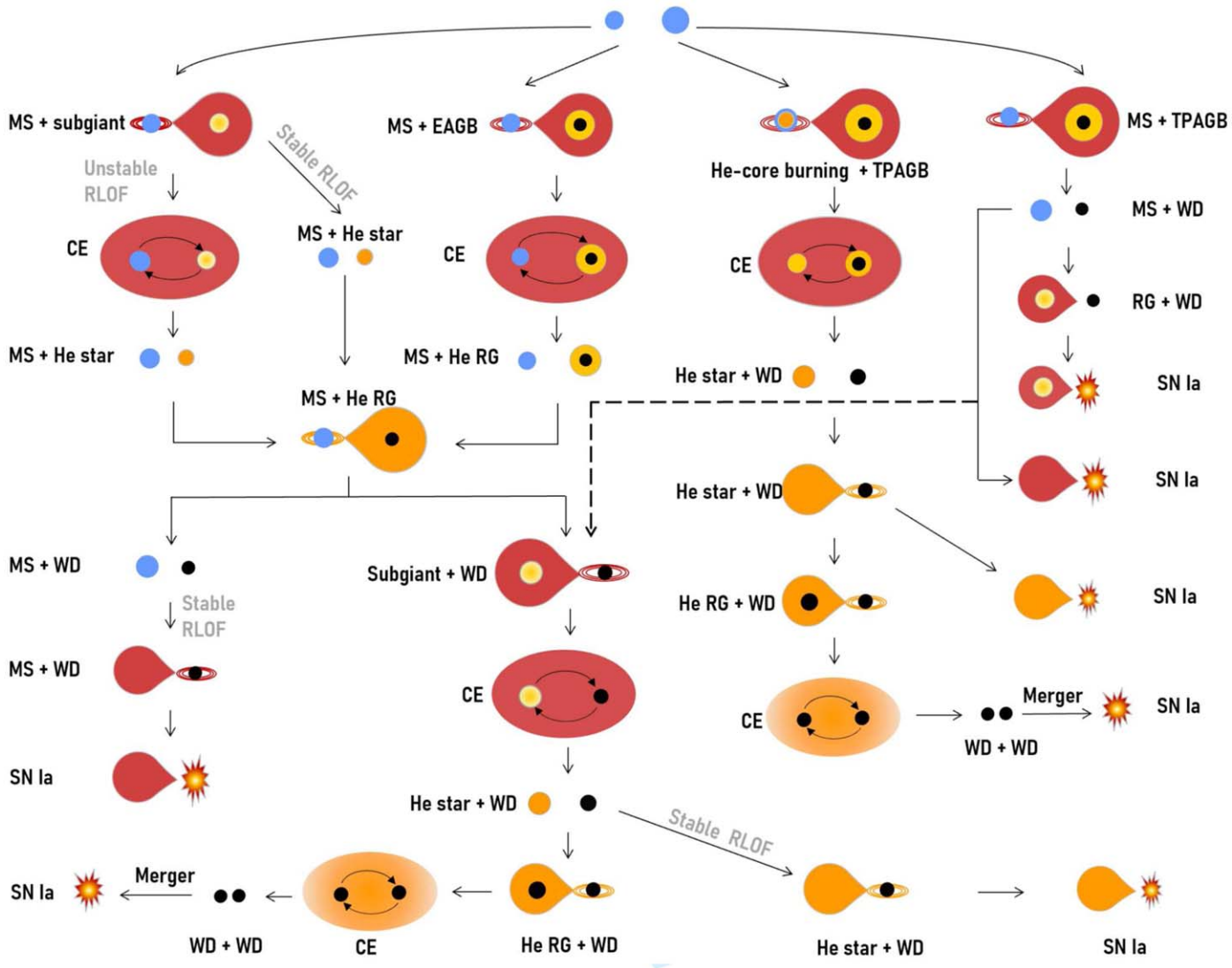


Figure 2. Schematic illustration of binary evolutionary paths for SNe Ia in the SD and DD scenarios (see also Wang 2018). Note that evolutionary channels here are not complete and that new channels may still be proposed in the future.

exhausting most of its H-rich or He-rich envelope during a long spin-down ($\gtrsim 10^8$ yrs) phase to become a WD or a hot subdwarf star (Hachisu et al. 2012a; Meng & Li 2019; Meng & Luo 2021). This would explain the non-detection of a pre-explosion companion star (Maoz & Mannucci 2008; Bloom et al. 2012; Kelly et al. 2014; see Section 5.1) in SNe Ia and the absence of swept-up H/He in their late spectra (Leonard 2007; Tucker et al. 2020; see Section 5.2.1). However, no (or weak) interaction signature of shocked gas is predicted in this scenario, which makes it difficult to explain the early excess luminosity (see Section 5.2.2) seen in some SNe Ia, such as iPTF14atg (Cao et al. 2015) and SN 2012cg (Marion et al. 2016). The exact spin-down timescale of the WD in this model is uncertain (Hachisu et al. 2012b; Meng & Podsiadlowski 2013; Maoz et al. 2014; Wang et al. 2014a) but a key to the success of the model.

3.1.2. Double-degenerate Scenario

In the original double-degenerate (DD) scenario, two carbon–oxygen (CO) WDs in a binary system are brought into contact by the emission of gravitational wave radiation and merge via tidal interaction into one single object, triggering an SN Ia explosion if the combined mass exceeds the Chandrasekhar-mass limit (Iben & Tutukov 1984; Webbink 1984). There are a number of evolutionary paths that can lead to SN Ia explosions in the DD scenario (Han 1998; Toonen et al. 2012; Yungelson & Kuranov 2017; Liu et al. 2018; see

Figure 2). The key question of the original DD scenario is whether the merger of two WDs could successfully lead to an SN Ia explosion. Different calculations have predicted that the merger of two WDs would likely cause the formation of neutron stars through accretion-induced collapse (AIC) rather than SN Ia explosions (Nomoto & Iben 1985; Kawai et al. 1987; Timmes et al. 1994; Saio & Nomoto 1998; Shen et al. 2012; Schwab et al. 2016; Schwab 2021). The accretion from the secondary WD onto the primary WD during the merger process may lead to burning in the outer layers of the WD rather than central burning, which would turn the original CO WD into an oxygen–neon–magnesium (ONeMg) WD. A Chandrasekhar-mass ONe WD is thought to be prone to collapse into a neutron star via AIC. However, there are possibilities to avoid AIC after the merger of two CO WDs. For instance, Yoon et al. (2007) concluded that the merger of two CO WDs could avoid off-center C-burning and explode as an SN Ia in the thermal-evolution phase if the rotation of the WDs is taken into account.

In the past decades, a number of numerical simulations have investigated the merger of two WDs (Benz et al. 1990; Rasio & Shapiro 1995; Segretain et al. 1997; Guerrero et al. 2004; Lorén-Aguilar et al. 2009; Fryer et al. 2010; Pakmor et al. 2010, 2012; Dan et al. 2011; Raskin et al. 2012, 2014; Moll et al. 2014; Sato et al. 2015). More importantly, some recent theoretical studies have shown that the merger of two WDs can eventually trigger an SN Ia explosion in ways that are different from the original DD scenario. For instance, a carbon detonation can be directly triggered by the interaction of the debris of the secondary WD with the primary WD during the violent merger phase of two CO WDs to eventually trigger an SN Ia explosion (i.e., the "violent merger model"; see Section 3.2.4; Pakmor et al. 2010, 2012; Sato et al. 2015). If the secondary WD in a DD binary system is a pure He WD, an initial He detonation could be triggered by accumulating a He shell on top of the primary CO WD through stable mass transfer, eventually triggering the C-core detonation near the center to successfully cause an SN Ia. This corresponds to the sub-Chandrasekhar-mass double-detonation scenario (see Section 3.2.3; Fink et al. 2007, 2010; Moll & Woosley 2013; Gronow et al. 2020, 2021a; Boos et al. 2021). In addition, unstable mass transfer could also lead to the presence of He in the surface layers of the primary CO WD if the secondary WD is either a He WD or a hybrid HeCO WD, which could successfully give rise to an SN Ia during the coalescence itself through the double-detonation mechanism (i.e., the He-ignited violent merger model described in Section 3.2.5; Guillochon et al. 2010; Dan et al. 2011; Pakmor et al. 2013, 2021, 2022; Roy et al. 2022).

There are some evidences in favor of the DD scenario (see Sections 4 and 5 for a detailed discussion). Binary population synthesis (BPS) calculations have shown that the predicted SN Ia rates and delay times from the DD scenario could well reproduce those inferred from the observations (Nelemans et al. 2001; Ruiter et al. 2009, 2013; Mennekens et al. 2010; Toonen et al. 2012; Yungelson & Kuranov 2017). In addition, the non-detection of pre-explosion companion stars in normal SNe Ia (Li et al. 2011b; Bloom et al. 2012; Kelly et al. 2014), the lack of radio and X-ray emission around peak brightness (Chomiuk et al. 2012b; Horesh et al. 2012; Margutti et al. 2014), the absence of a surviving companion star in SN Ia remnants (Kerzendorf et al. 2009; Schaefer & Pagnotta 2012; Ruiz-Lapuente et al. 2018), and the fact that no signatures of the swept-up H/He have been detected in the nebular spectra of SNe Ia (Leonard 2007; Lundqvist et al. 2013; Maguire et al. 2016) and the lack of X-ray flux (i.e., SSSs) expected for accreting WDs seem to favor the DD scenario. Also, it has been suggested that some superluminous SNe Ia that have ejecta masses of $\gtrsim 2.0\,M_{\odot}$ may arise from the merger of two WDs (Howell et al. 2006; Hicken et al. 2007; Silverman et al. 2011). However, the DD scenario predicts a relatively wide range of explosion masses, and thus makes it difficult to explain the observed homogeneity of the majority of SNe Ia.

Double WDs (DWDs) are the primary targets of some upcoming space gravitational-wave missions and observatories, such as the Laser Interferometer Space Antenna (Amaro-Seoane et al. 2017), TianQin (Luo et al. 2016; Huang et al. 2020) and Taiji (Ruan et al. 2018). Searches for DWDs have been carried out by different surveys, like the dedicated ESO Supernovae Type Ia Progenitor Survey (SPY; Napiwotzki et al. 2001), the Sloan Digital Sky Survey (York et al. 2000), the Sloan White dwArf Radial velocity data Mining Survey (SWARMS; Badenes et al. 2009), the Extremely Low Mass survey (Brown et al. 2010), the Kepler–K2 survey (Howell et al. 2014) and the large all-sky survey Gaia (Gaia Collaboration et al. 2016, 2018). However, to date, only about 150 DWD systems have been detected with detailed orbital parameters (Badenes et al. 2009; Hallakoun et al. 2016; Breedt et al. 2017; Brown et al. 2020; Burdge et al. 2020; Napiwotzki et al. 2020; Korol et al. 2022). A comprehensive list of close DWD systems (periods below 35 days) containing two low-mass WDs is given by Schreiber et al. (2022). Only a few DWDs have been reported to be possible SN Ia progenitors that would merge in a Hubble time, including two systems with sub-Chandrasekhar total masses obtained by SPY (WD2020-425 and HE2209-1444; Napiwotzki et al. 2020), two super-Chandrasekhar progenitor candidates composed of a WD and a hot subdwarf (KPD 1930+2752 and HD 265435; Maxted et al. 2000; Pelisoli et al. 2021), CD-30°11223 (Vennes et al. 2012; Geier et al. 2013), the Henize 2-428 system (Santander-García et al. 2015; but see also Reindl et al. 2020), 458 Vulpeculae (Rodríguez-Gil et al. 2010), SBS 1150+599A (Tovmassian et al. 2010) and GD 687 (Geier et al. 2010). Besides, Kawka et al. (2017) suggested that NLTT 12758 is a super-Chandrasekhar DWD system, but it would merge in a timescale longer than the Hubble time.

3.1.3. Other proposed progenitor scenarios

Some subtypes of the SD model and other possible progenitor scenarios have been proposed for SNe Ia, including (1) the common-envelope (CE) wind model, in which the SD models are assumed to drive CE winds rather than optically thick winds when the mass transfer rate exceeds the critical accretion rate (Meng & Podsiadlowski 2017); (2) the hybrid C–O–Ne WD model, in which a hybrid carbon–oxygen–neon (C–O–Ne) WD with a mass of $\gtrsim 1.3\,M_{\odot}$ accretes material from its companion star to approach the Chandrasekhar-mass limit and explodes as a faint SN Ia (García-Berro et al. 1997; Chen et al. 2014; Denissenkov et al. 2015; Wang et al. 2014b; Meng & Podsiadlowski 2014; Liu et al. 2015c; Kromer et al. 2015; Marquardt et al. 2015); (3) the M-dwarf donor model, in which the WD accretes material from an M-dwarf star so that it approaches the Chandrasekhar-mass limit and triggers an SN Ia explosion (Wheeler 2012); (4) the core-degenerate model, in which an SN Ia is produced from the merger of a CO WD with the core of an AGB companion star during a CE evolution (Livio & Riess 2003; Kashi & Soker 2011; Ilkov & Soker 2012; Soker et al. 2013, 2014; Soker 2018); (5) the triple channel, in which thermonuclear explosions in triple-star systems are triggered through both the SD and DD channels (Katz & Dong 2012; Hamers et al. 2013; Toonen et al. 2018; Swaruba Rajamuthukumar et al. 2023); and (6) the single-star model, in which AGB stars or He stars with a highly degenerate CO core near the Chandrasekhar mass ignite carbon at the center to subsequently cause an SN Ia explosion if they have lost their H-rich or He-rich envelopes (Iben & Renzini 1983; Tout 2005; Antoniadis et al. 2020). Note that this list may not be complete and that new channels may still be proposed. Ultimately, the question of SN Ia progenitor systems has to be settled by observations.

For a coarse and sketchy overview of the different progenitor scenarios of SNe Ia, we compile the different characteristics in Table 1. We would like to caution here that usually the arguments to be made in favor or against specific scenarios are more complex than what can be listed in a table. Therefore, we emphasize that they are only intended for a quick overview. The main benefit of our table is to highlight open research questions that are marked with "unclear."

3.2. Explosion Models

The explosion mechanism depends mainly on the question of whether the WD explodes near the Chandrasekhar mass (e.g., Nomoto et al. 1984; Livio & Riess 2003; Röpke & Niemeyer 2007; Röpke et al. 2007b; Mazzali et al. 2007; Kasen et al. 2009; Ilkov & Soker 2012; Rabinak et al. 2012; Jordan et al. 2012b; Seitenzahl et al. 2013b; Fink et al. 2014; Lach et al. 2022, 2022c) or at a mass below this limit (the "sub-Chandrasekhar-mass" explosion scenario, e.g., Woosley et al. 1986; Benz et al. 1989; Fink et al. 2007; Shen & Bildsten 2007; Rosswog et al. 2009a; Raskin et al. 2009; Sim et al. 2010; Pakmor et al. 2010; Kushnir et al. 2013; Townsley et al. 2019; Gronow et al. 2020, 2021a). To provide clues on the yet poorly understood origin and explosion mechanism of SNe Ia, one needs to compare the observational features predicted by different explosion mechanisms in the context of the progenitor models discussed in Section 3.1 with the observations.

A number of explosion models have been proposed to cover various progenitor scenarios of SNe Ia (Hillebrandt et al. 2013, for a recent review), including near-Chandrasekhar-mass deflagrations (Nomoto et al. 1984; Jordan et al. 2012a; Kromer et al. 2013a; Fink et al. 2014; Lach et al. 2022), near-Chandrasekhar-mass delayed detonations (Arnett 1969; Khokhlov 1991; Gamezo et al. 2005; Röpke & Niemeyer 2007; Rabinak et al. 2012; Seitenzahl et al. 2013b), gravitationally confined detonations (Jordan et al. 2008; Seitenzahl et al. 2016; Lach et al. 2022c), sub-Chandrasekhar-mass double detonations (Nomoto 1982b, 1982a; Woosley et al. 1986; Iben et al. 1987; Livne 1990; Woosley & Weaver 1994; Fink et al. 2007; Moll & Woosley 2013; Gronow et al. 2020, 2021a; Boos et al. 2021) and violent mergers (Pakmor et al. 2010, 2011). A schematic overview of various SN Ia explosion models proposed in the framework of either Chandrasekhar-mass or sub-Chandrasekhar-mass explosion is presented in Figure 3.

3.2.1. Chandrasekhar-mass pure Deflagrations

Near-Chandrasekhar-mass explosions in the SD scenario have long been proposed as a potential model for SNe Ia because they could reproduce some observational features, such as the light curves and spectra (e.g., Nomoto et al. 1984; Branch et al. 1985; Hoeflich et al. 1995, 1996; Mazzali et al. 2007; Kasen et al. 2009; Blondin et al. 2011; Sim et al. 2013). Moreover, Yamaguchi et al. (2015) suggested that the detection of strong K-shell emission from stable Fe-peak elements in SN Ia remnant 3C 397 requires electron captures at high density that can only be achieved by a near-Chandrasekhar-mass explosion. In such a configuration, a supersonic prompt detonation would turn essentially the entire star into iron-group elements, which is inconsistent with the observed features of SNe Ia; to produce the intermediate-mass elements (IMEs), such as Si and S, observed in their spectra, burning must start out as a subsonic deflagration. The WD then expands prior to being incinerated. Compared with a prompt detonation, this reduces the production of ^{56}Ni and can in principle increase the IME yields. The outward propagation of the subsonic deflagration flame leads to Rayleigh–Taylor instabilities that generate turbulence at the contact between hot ashes and cold fuel. This enlarges the surface area of the burning front and accelerates it.

One of the commonly used near Chandrasekhar-mass explosion models is the so-called "W7 model" of Nomoto

Table 1
Progenitor Scenarios of SNe Ia

Scenario	Bright pre-SN object expected?	H/He present in late-time spectra	CSM expected	Reproduction of SN Ia rate?	Reproduction of SN Ia DTDs	Reproduction of SN Ia brightness distribution	Associated thermonuclear explosion scenario	Surviving companion?
SD (SD general)	Yes	Yes	Yes	No	No	No	M_{Ch}	Yes
SD with MS donor	Yes	Yes	Yes	No	No	No	M_{Ch}	MS star
SD with giant donor	Yes	Yes	Yes	No	No	No	M_{Ch}	Compact stellar core
SD with He star donor	Yes	Yes	Yes	No	No	No	M_{Ch}	He star
SD with M-dwarf donor	No	Yes	Yes	No	No	No	M_{Ch}	M-dwarf star
SD spin-up/spin-down	Unclear	Unclear	Unclear	No	Unclear	Unclear	M_{Ch}; super-M_{Ch}	Compact object
SD with hybrid CONe WD	Yes	Unclear	Yes	No	No	No	M_{Ch}; sub-M_{Ch}	Unclear
DD (DD general)	No	No	Yes/no, depending on explosion mechanism	Yes	Yes	Yes	Sub-M_{Ch}; M_{Ch}; super-M_{Ch}	Yes/no, depending on explosion mechanism
Core degenerate	Yes	Yes	Unclear	Unclear	Unclear	Unclear	M_{Ch}	No
Triple system	Unclear	Unclear	Unclear	Unclear	Unclear	Unclear	Unclear	Unclear
Single star	Yes	Yes	No	Unclear	Unclear	Unclear	M_{Ch}; e-capture induced	No

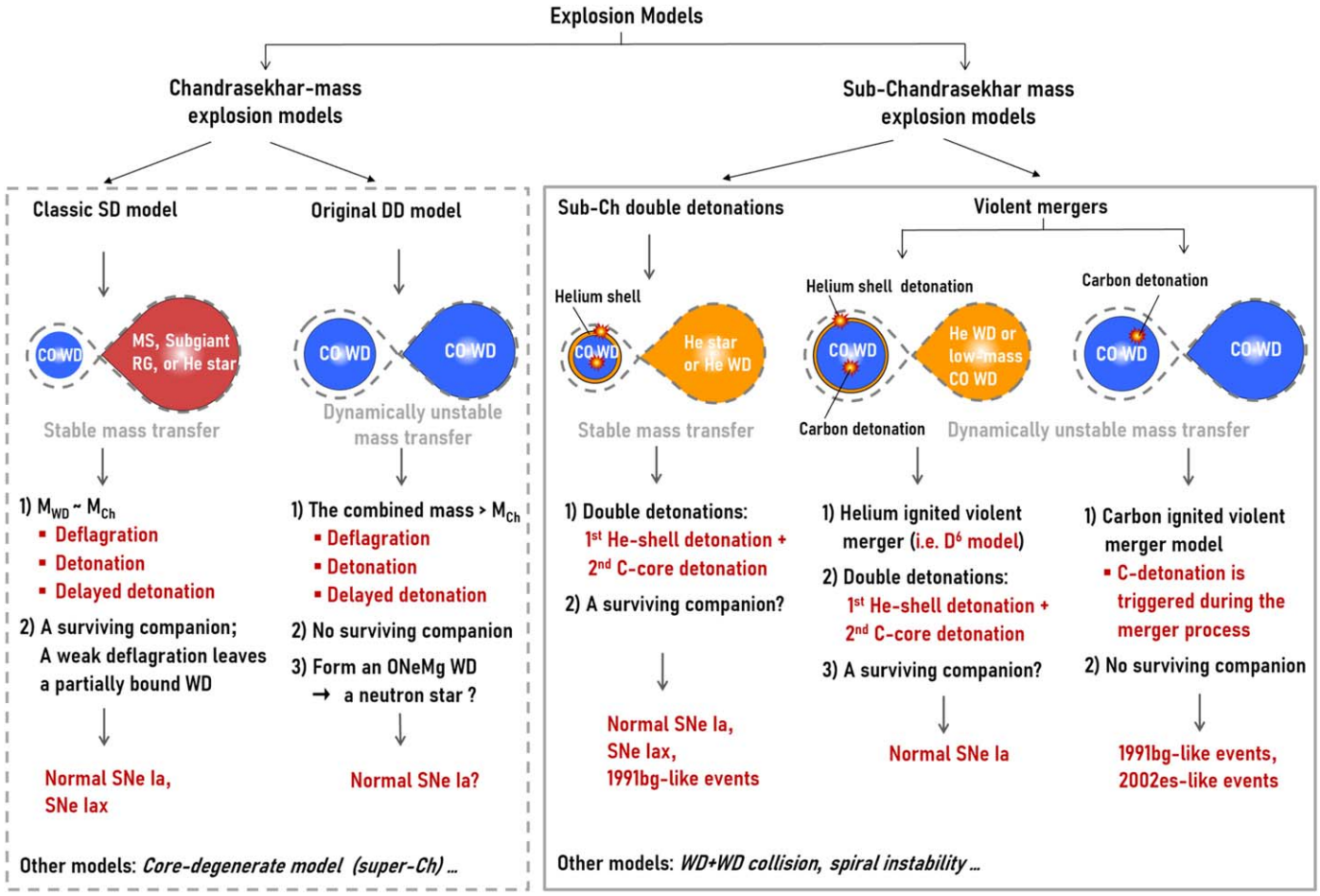


Figure 3. Different explosion models of SNe Ia in the context of either Chandrasekhar-mass or sub-Chandrasekhar-mass explosion (see also Hillebrandt et al. 2013, and references therein). Note that the models presented here are not complete.

et al. (1984). The W7 model is a one-dimensional (1D) pure deflagration explosion of a Chandrasekhar-mass WD, in which a parameterized description was used for the turbulent burning process. To avoid free parameters in the model, multi-dimensional simulations (for an example, see top panels of Figure 4) have been carried out (e.g., Reinecke et al. 2002; Gamezo et al. 2003; García-Senz & Bravo 2005; Röpke et al. 2006b, 2006a, 2007a; Jordan et al. 2012a; Ma et al. 2013; Long et al. 2014; Fink et al. 2014; Lach et al. 2022). The result of these simulations is that pure deflagrations are not able to reproduce the majority of normal SNe Ia (Sim et al. 2013; Kromer et al. 2013a). In the framework of the Chandrasekhar-mass deflagration model, it is difficult to produce the canonical 0.5 $M_\odot$ ^{56}Ni for normal SNe Ia because the flame ultimately cannot catch up with the expansion of the WD and much of its material remains unburned. Enhancing the burning efficiency with multi-spot ignitions had only limited success (Röpke et al. 2006b, 2006a; Long et al. 2014; Fink et al. 2014; Lach et al. 2022). Moreover, the ignition process itself is rather uncertain and multi-spot ignition does not seem very likely according to the simulations of Nonaka et al. (2012).

However, off-center ignited weak deflagration models have been suggested to explain the particular subclass of SNe Iax (Kromer et al. 2013a, 2015; Magee et al. 2016; Kawabata et al. 2021; McCully et al. 2022; Dutta et al. 2022). Figure 4 presents an example of a three-dimensional (3D) explosion simulation for a Chandrasekhar-mass pure deflagration model from Lach et al. (2022c). In the weak pure deflagration model of Chandrasekhar-mass WDs (sometimes known as "failed detonation model"), an off-center ignited pure deflagration of a Chandrasekhar-mass CO WD (or hybrid CONe WD) fails to completely unbind the entire WD, leaving behind a bound WD remnant (Jordan et al. 2012b; Kromer et al. 2013a; Ma et al. 2013; Long et al. 2014; Fink et al. 2014). It has been shown that pure deflagrations in near-Chandrasekhar-mass CO WDs and hybrid CONe WDs can respectively reproduce the observational light curves and spectra of brighter SNe Iax such as SN 2005hk (Kromer et al. 2013a) and, less confidently,

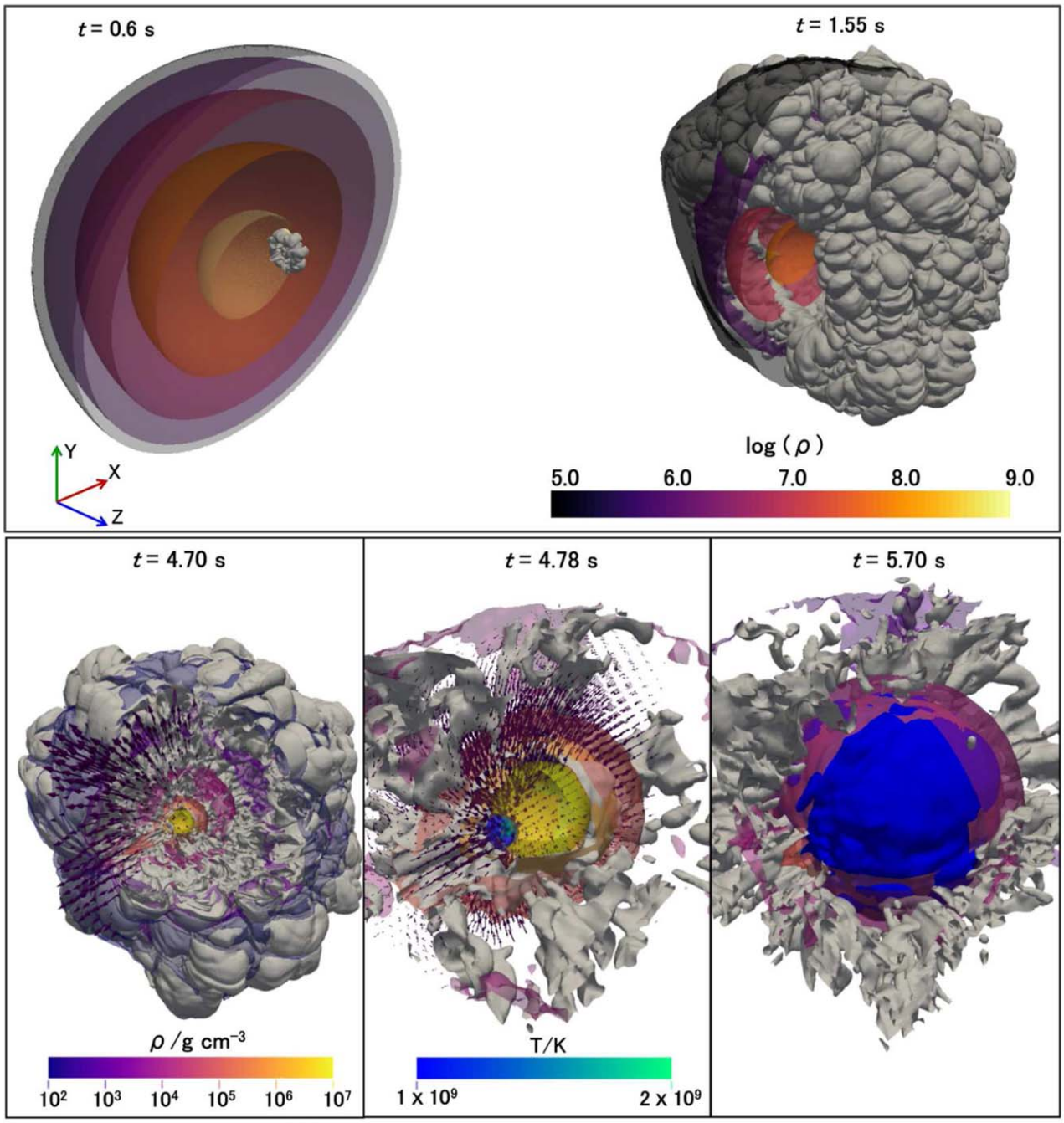


Figure 4. Examples of 3D explosion simulations for two different Chandrasekhar-mass models. *Top panels*: flame surface (*gray*) and density isosurfaces (*color coded*) from a 3D simulation for a Chandrasekhar-mass pure deflagration model at $t = 0.6$ s when flame is rising (*left*) and $t = 1.55$ s when flame front has almost wrapped around the WD. *Bottom panels*: similar to *top panels*, but for a delayed-detonation model (i.e., a GCD). Situations prior to detonation initiation, at the moment of detonation initiation, and at about 1 s after initiation are given from *left* to *right*. The hotspot with temperatures of 1×10^9 K is marked by the blue-green contour in *middle panel*. The blue surface in *right panel* corresponds to detonation front. Note that the illustration is not to scale. The figure is reprinted from Lach et al. (2022, see their Figure 3) and Lach et al. (2022c, see their Figure 1) with permission © ESO.

the faint Iax event SN 2008ha (Kromer et al. 2015; Lach et al. 2022). Bulla et al. (2020) have shown that the maximum-light polarization signal observed in SN 2005hk can be explained in the context of a weak deflagration explosion of a Chandrasekhar-mass WD if asymmetries caused by both the SN explosion itself and the ejecta–companion interaction are considered. Therefore, the weak deflagration explosion of a Chandrasekhar-mass WD seems to be a potential model for

SNe Iax (but see also Hoeflich et al. 1995; Stritzinger et al. 2015), at least for the brighter members of this subclass (Lach et al. 2022).

Interestingly, the weak pure deflagration model of Chandrasekhar-mass WDs predicts the existence of a surviving bound WD remnant which is significantly heated by the explosion and highly enriched by heavy elements from SN ejecta. Searches for such surviving WD remnants would be very helpful for assessing the validity of this explosion model (see Section 5.3.3; Jordan et al. 2012a; Kromer et al. 2013a; Fink et al. 2014; Shen et al. 2017; Zhang et al. 2019; Vennes et al. 2017; Lach et al. 2022).

3.2.2. Chandrasekhar-mass Delayed Detonations

Besides pure deflagration models, pure detonations of near-Chandrasekhar-mass WDs have also been proposed for SNe Ia. As already mentioned, the first numerically studied pure detonation model of a near-Chandrasekhar-mass WD in hydrostatic equilibrium (Arnett 1969) showed that this model produces too much ^{56}Ni and too little IMEs to explain the observations of normal SNe Ia. This conflict indicates that an expansion of the WD is needed prior to the detonation in order to reduce the production of ^{56}Ni and to increase that of IMEs. To achieve this, the *"delayed detonation model"* of a near Chandrasekhar-mass WD was proposed by Khokhlov (1989): The WD expands first due to an initial deflagration and causes the subsequent detonation to burn at relatively low fuel densities (Khokhlov 1991; Hoeflich et al. 1995; Gamezo et al. 2005; Bravo & García-Senz 2006; Röpke & Niemeyer 2007; Röpke et al. 2007b; Plewa 2007; Jordan et al. 2008; Seitenzahl et al. 2013b), reducing the production of ^{56}Ni and enhancing the yields of IMEs compared with the earlier pure detonation models. This therefore makes the delayed detonation model more favorable for explaining normal SNe Ia. Figure 4 shows an example of 3D explosion simulations for a Chandrasekhar-mass delayed detonation model (i.e., a GCD from Lach et al. 2022c).

The key features of Chandrasekhar-mass delayed-detonation models have been summarized by Seitenzahl et al. (2013b). Several scenarios for the transition from the initial deflagration to a subsequent detonation have been proposed for SNe Ia such as the deflagration to detonation transition model (DDT; Khokhlov 1991; Gamezo et al. 2005; Röpke & Niemeyer 2007; Bravo & García-Senz 2008; Kasen et al. 2009; Seitenzahl et al. 2013b; Willcox et al. 2016), the pulsating delayed detonation model (PDD; Ivanova et al. 1974; Hoeflich et al. 1995), gravitationally confined detonation model (GCD; Plewa et al. 2004; Jordan et al. 2008, 2012b; Townsley et al. 2007; Seitenzahl et al. 2016; Lach et al. 2022c) and the pulsational reverse detonation model (PRD; Bravo & García-Senz 2006, 2009; Bravo et al. 2009). Despite substantial effort, none of the simulations could demonstrate from first principles that the transition of the deflagration to a detonation really occurs (Röpke 2007; Pan et al. 2008; Woosley et al. 2009, 2011; Schmidt et al. 2010; Ciaraldi-Schoolmann et al. 2013; Poludnenko et al. 2019).

3.2.3. Sub-Chandrasekhar-mass Double-detonations

Sub-Chandrasekhar-mass WDs can be ignited through a *double-detonation mechanism* to give rise to thermonuclear explosions in the context of either the SD or DD progenitor scenario (see Section 3.1). The initial detonation in this model is triggered by accumulating a He shell on top of the primary WD through either stable mass transfer (i.e., the sub-Chandrasekhar-mass double-detonation model; Taam 1980; Nomoto 1982b, 1982a; Woosley et al. 1986; Tutukov & Yungelson 1996; Bildsten et al. 2007; Shen & Bildsten 2009; Fink et al. 2007, 2010; Moll & Woosley 2013; Neunteufel et al. 2016; Townsley et al. 2019; Gronow et al. 2020; Boos et al. 2021) or unstable mass-transfer (i.e., the so-called D^6 model; Guillochon et al. 2010; Dan et al. 2011; Pakmor et al. 2013; Boos et al. 2021; Shen et al. 2021b; Roy et al. 2022) from a secondary in a binary system.

In the sub-Chandrasekhar-mass double-detonation scenario (see Figure 3), the WD accretes material from a He-burning star or a He WD companion via stable mass-transfer to accumulate a He-layer on its surface. If the He shell reaches a critical mass of $\sim$0.02–0.2 $M_\odot$ (which is, however, quite uncertain; Woosley et al. 1986; Bildsten et al. 2007; Woosley et al. 2011; Neunteufel et al. 2016; Polin et al. 2019), an initial detonation of the He shell is triggered and eventually ignites a second detonation in the core. This leads to a thermonuclear explosion of the entire sub-Chandrasekhar-mass WD (e.g., Nomoto 1982b; Woosley et al. 1986; Iben et al. 1987; Livne & Glasner 1990; Woosley & Weaver 1994; Livne & Arnett 1995; Fink et al. 2007, 2010; Sim et al. 2010; Moll & Woosley 2013; Gronow et al. 2020, 2021a; Boos et al. 2021).

On the one hand, several binary systems composed of a WD and a He-rich companion star have been detected observationally (KPD 1930+2752, V445 Pup, HD 49798, CD-30°11223 and PTF1J2238+7430; Maxted et al. 2000; Geier et al. 2007; Kato & Hachisu 2003; Kudritzki & Simon 1978; Vennes et al. 2012; Geier et al. 2013; Kupfer et al. 2022), which seems to support this scenario. For example, CD-30°11223 is a binary system containing a WD and a subdwarf-B (sdB) star, in which the WD mass is $M_{\rm WD} = 0.76\,M_\odot$, the companion mass is $M_{\rm sdB} = 0.51\,M_\odot$ and the orbital period is only $P_{\rm orb} \simeq 1.2$ hours. Vennes et al. (2012) and Geier et al. (2013) suggested that CD-30°11223 will likely explode as an SN Ia via the sub-Chandrasekhar double-detonation mechanism during its future evolution. Very recently, Kupfer et al. (2022) predicted that PTF1J2238+7430 would lead to a thermonuclear explosion in the context of the sub-Chandrasekhar double-detonation scenario with a thick He shell of $\sim$0.17 $M_\odot$.

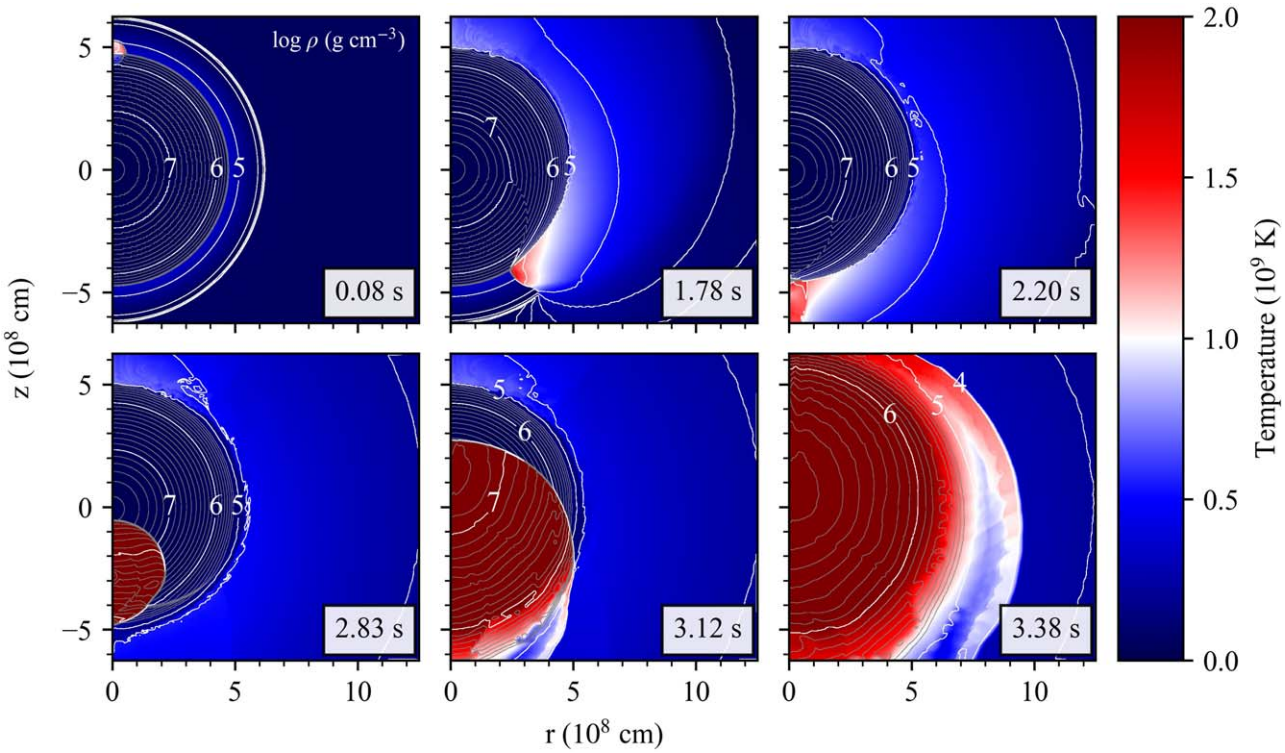


Figure 5. Time sequence of density (*white and gray lines*) and temperature (*color coded*) from a 2D simulation for a sub-Chandrasekhar double-detonation explosion of a 1.0 $M_\odot$ CO WD with a thin He shell of 0.016 $M_\odot$. At 0.08 s, an initial He-ignition is observed, and the He burning starts to grow. The inward-traveling shock then surrounds the whole core and converges at the south pole at 2.20 s. The shock wave propagates into the core to trigger the second detonation in the core at around 2.83 s, and the core detonation proceeds to give rise to a thermonuclear runaway. The figure is reprinted from Boos et al. (2021, see their Figure 2) with the permission of the AAS.

On the other hand, different studies in the literature have shown that the sub-Chandrasekhar-mass double-detonation models with a thick He shell (0.1–0.2 $M_\odot$) produce an outer layer of SN ejecta enriched with titanium (Ti), chromium (Cr) and nickel (Ni), leading to predicted spectra and light curves that are inconsistent with the observations of SNe Ia (Hoeflich & Khokhlov 1996; Kromer et al. 2010; Woosley et al. 2011; Sim et al. 2012). However, numerous complications remain to be solved in such a model, and both the production of IGEs in the outer layers and the predicted observables (such as spectra and color) are rather sensitive to the total mass, the thermal and the chemical conditions of the He shell (Bildsten et al. 2007; Fink et al. 2010; Waldman et al. 2011; Moore et al. 2013; Shen & Moore 2014; Piro 2015; Townsley et al. 2019; Gronow et al. 2020, 2021a, 2021b) and to details of the treatment of radiative transfer modeling (Collins et al. 2022). For instance, Kromer et al. (2010) showed that polluting the He shell with ^{12}C helps to bring the predicted observables into better agreement with observations of normal SNe Ia. More recently, some updated simulations have shown that double detonations of sub-Chandrasekhar-mass WDs with a thin and C-polluted He shell holds promise for explaining SNe Ia, including normal SNe Ia and peculiar objects (Pakmor et al. 2013; Townsley et al. 2019; Gronow et al. 2021a; Boos et al. 2021; Magee et al. 2021; Shen et al. 2021a, 2021b; Rivas et al. 2022; Collins et al. 2022). Figure 5 shows an example of the sub-Chandrasekhar-mass double-detonation simulation of a 1.0 $M_\odot$ CO WD with a thin He shell of 0.016 $M_\odot$ from Boos et al. (2021). Townsley et al. (2019) suggested that the sub-Chandrasekhar-mass double-detonation scenario might be viable for producing spectroscopically normal SNe Ia if the He layer is sufficiently thin ($\sim$0.01 $M_\odot$) and modestly enriched with core material. This indicates that double detonations of sub-Chandrasekhar-mass WDs may contribute the bulk of observed SNe Ia. However, the exact critical He shell mass required for successfully initiating double detonations of the entire sub-Chandrasekhar-mass WD remains uncertain. In addition, the exact He-retention efficiency of the accreting WD in the progenitor system is still poorly constrained (e.g., Ruiter et al. 2014; Toonen et al. 2014).

3.2.4. Carbon-ignited Violent Mergers

The "C-ignited violent merger model" (see Figure 3) is one of the modern versions of the DD scenario. In this model, unstable dynamical accretion of material from the secondary

(less massive) WD onto the primary WD causes compressional heating sufficient to directly trigger a detonation of a CO core in the primary WD, producing an SN Ia (Pakmor et al. 2010, 2011, 2012; Sato et al. 2015, 2016). While the *original* DD scenario assumes an explosion of a merged object exceeding the Chandrasekhar-mass limit, in the violent merger model the explosion is already triggered during the merger process before the two stars are completely disrupted (Guillochon et al. 2010; Pakmor et al. 2010, 2011, 2012; Kromer et al. 2013b; Sato et al. 2015, 2016). Therefore it proceeds in sub-Chandrasekhar-mass WDs. This scenario avoids the problem of a potential collapse to a neutron star in an AIC (Nomoto & Kondo 1991; Saio & Nomoto 1998; Timmes et al. 1994; Schwab et al. 2016).

It has been shown that the violent mergers of two CO WDs that involve a single carbon detonation in the primary star can generally explain the observational properties of subluminous SNe Ia such as 1991bg-like events (Pakmor et al. 2010, 2011), SN 2010lp (Kromer et al. 2013b) and SN 2002es-like event iPTF14atg (Kromer et al. 2016). However, the triggering of the detonation during the violent merger phase is still poorly constrained (Hillebrandt et al. 2013).

3.2.5. Helium-ignited Violent Mergers

The He-ignited violent merger model—or "*dynamically driven double-degenerate double-detonation*" (D^6) model—is another modern version of sub-Chandrasekhar explosions in the DD scenario, in which SNe Ia are produced through the double-detonation mechanism during the merger of two WDs (see Figure 3). In the D^6 model, an initial He detonation triggers on the surface of a heavier CO WD primary due to unstable dynamical He accretion from the less massive secondary which could be either another CO WD with thin surface He layers, a He WD, or a hybrid HeCO WD. Via a double-detonation mechanism, the initial He detonation initiates into a detonation of the CO core, producing an SN Ia (see Figure 6; e.g., Guillochon et al. 2010; Pakmor et al. 2013; Boos et al. 2021; Shen et al. 2021b; Roy et al. 2022). Because the He detonation in this model proceeds in a dynamic stage and not in a massive He layer at hydrostatic equilibrium conditions (see Section 3.2.3), the impact of the He detonation products on the observables is reduced compared to the classical sub-Chandrasekhar-mass double-detonation scenario. For instance, Pakmor et al. (2012) have shown that the double-detonation explosion in the violent merger of two CO WDs with masses of 0.9 $M_\odot$ and 1.1 $M_\odot$ can closely resemble normal SNe Ia, indicating that the D^6 model has the potential to explain the bulk of normal SNe Ia.

Interestingly, the secondary WD may survive from the explosion in the D^6 model and become a hypervelocity WD with a velocity of $\gtrsim$1000 km s^{-1} (see Section 5.3.3; Shen et al. 2018b; Igoshev et al. 2023). Shen et al. (2018b) suggested that three hypervelocity runaway stars with a velocity of $\gtrsim$1000 km s^{-1} detected in the Gaia survey (Gaia Collaboration et al. 2016, 2018) are likely to be WD companions that survived the D^6 SN Ia scenario (see also Bauer et al. 2021). However, the fate of the secondary WD in this model is rather unclear. Pakmor et al. (2022) recently investigated the fate of the secondary WD with self-consistent 3D hydrodynamical simulations, confirming that the primary WD can explode as an SN Ia, but they find that there is a large uncertainty on the question of whether the secondary WD detonates or not (Pakmor et al. 2022). In contrast, Roy et al. (2022) claim that an initial He detonation does not ignite a carbon detonation in the underlying WD.

3.2.6. Other proposed Explosion Models

In the framework of either a Chandrasekhar-mass or sub-Chandrasekhar-mass explosion, some other possible explosion models have been proposed for SNe Ia, including: (1) The core-degenerate model, in which the WD merges with the core of an AGB star during the CE phase, triggering a thermonuclear explosion inside the envelope (Livio & Riess 2003; Kashi & Soker 2011; Ilkov & Soker 2012; Soker et al. 2013, 2014); (2) Tidal disruptions, in which the tidal interaction of a WD with a black hole triggers a thermonuclear explosion (Rosswog et al. 2009b); (3) Head-on collisions of two WDs, in which two WDs collide in a binary or triple-star system, leading to a thermonuclear explosion due to the resultant shock compression (Benz et al. 1989; Rosswog et al. 2009a; Raskin et al. 2009, 2010; Katz & Dong 2012; Kushnir et al. 2013; Papish & Perets 2016); (4) The spiral instability model, in which a spiral mode instability in the accretion disk forms during the merger of two WDs and leads to a detonation on a dynamical timescale resulting in an SN Ia (Kashyap et al. 2015).

In Table 2, we present an overview of the main characteristics of different explosion mechanisms of SNe Ia. Again, the same cautionary remark as for Table 1 applies.

4. Rates and Delay Times

The observationally-inferred SN Ia rate in our Galaxy is about $2.84 \pm 0.60 \times 10^{-3}\,\mathrm{yr}^{-1}$ (e.g., van den Bergh & Tammann 1991; Cappellaro et al. 1997; Li et al. 2011c, 2011a; Brown et al. 2019; Wiseman et al. 2021). The observed delay-time distribution of SNe Ia (DTD, i.e., the distribution of durations between star formation and SN Ia explosion) covers a wide range from $\sim$10 Myr to about 10 Gyr (e.g., Maoz et al. 2010, 2011, 2012; Maoz & Graur 2017; Graur & Maoz 2013).

By comparing the expected rates and DTDs of SNe Ia from BPS calculations for different proposed progenitor models with those inferred from observations, several studies attempted to place constraints on the nature of SN Ia progenitor systems (see Figure 7; e.g., (Yungelson & Livio 1998; Yungelson 2010; Hachisu et al. 1999; Nelemans et al. 2001; Han & Podsiadlowski 2004; Botticella et al. 2008; Mannucci et al.

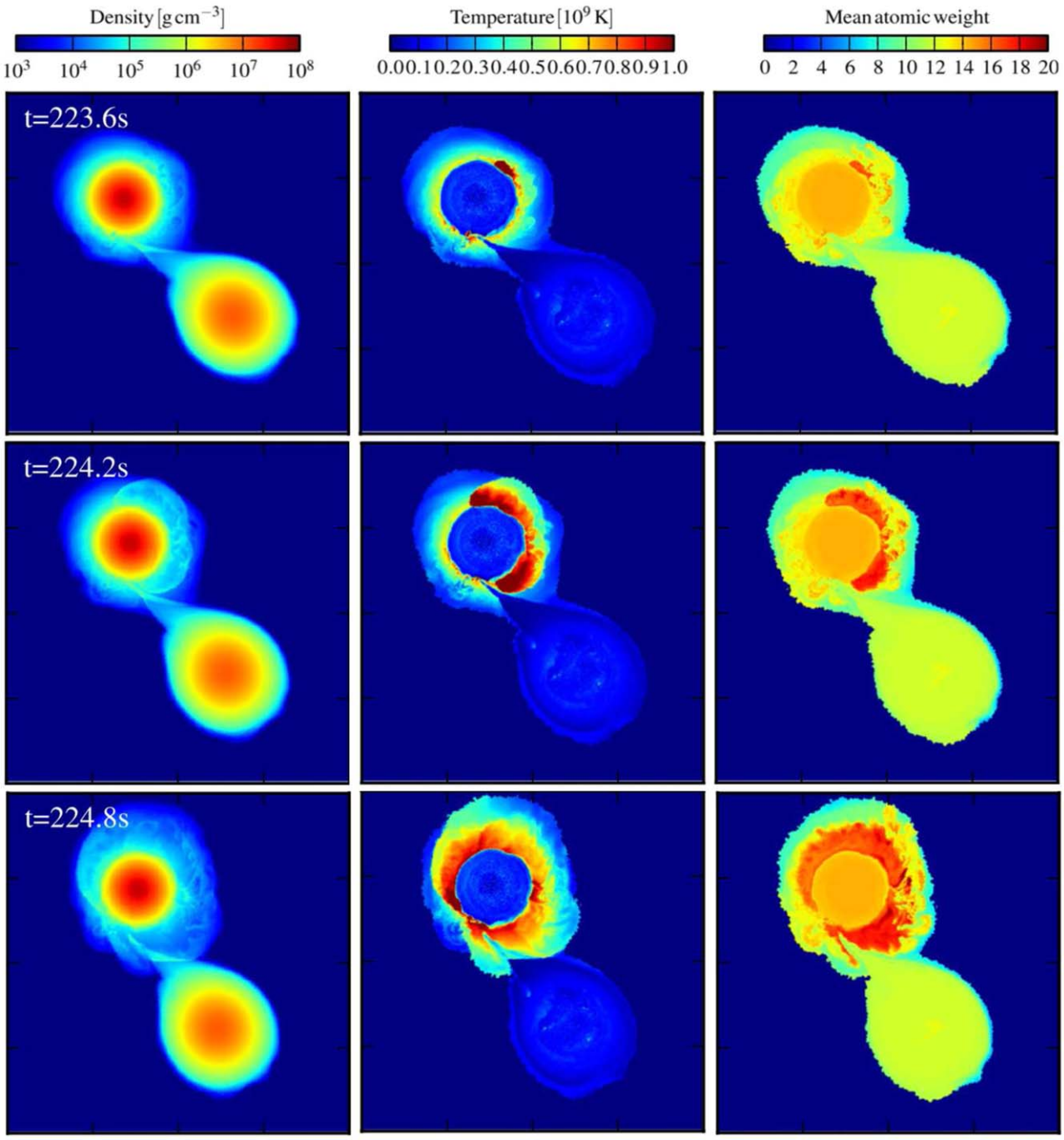


Figure 6. An example of explosion modeling for helium-ignited violent mergers of two WDs. The panels show slices of density, temperature and mean atomic weight in the orbital plane (*columns from left to right*) as a function of time when the He detonation forms on the surface of the primary WD in a simulation of the merger of a 1.1 $M_\odot$ primary CO WD and a 0.9 $M_\odot$ secondary CO WD. Note that all panels have the same length scale of 4×10^9 cm. The figure is reprinted from Pakmor et al. (2013, see their Figure 2) with the permission of the AAS.

2008; Ruiter et al. 2009, 2011, 2014; Maoz et al. 2010; Meng et al. 2009; Meng & Yang 2010; Wang et al. 2009, 2010; Mennekens et al. 2010; Toonen et al. 2012; Bours et al. 2013; Claeys et al. 2014; Graur et al. 2014b; Liu et al. 2015b; Liu & Stancliffe 2018; Liu et al. 2016, 2018; Ablimit et al. 2014, 2016; Shen et al. 2017). In summary, no single proposed progenitor model is able to consistently reproduce both the observed SN Ia rates and the DTDs (see Figure 7). The DD progenitor model generally predicts a broad range of delay times that follow a t^{-1} power-law, which is similar to the

Table 2
Explosion Mechanisms of SNe Ia

Scenario	Explosion triggering	Combustion mode	Imprint on nucleosynthesis	Associated SN Ia subclass	Reproduction of SN Ia brightness range	Reproduction of WLR
M_{Ch} deflagrations	spontaneous in C/O material	turbulent deflagration in C/O material	solar Mn/Fe ratio, potential overproduction of n-rich IGE	perhaps SNe Iax	no	no
M_{Ch} delayed detonations	spontaneous in C/O material	turbulent deflagration transitioning to detonation in C/O material	solar Mn/Fe ratio	normal SNe Ia? 91T-like objects?	yes, depending on deflagration ignition	no
sub-M_{Ch} double detonations	in He shell compressional heating → leads to core detonation	detonation in He shell, detonation in C/O core	solar Mn/Fe ratio due to He-shell detonation, low production of n-rich IGE (Z-dependent)	normal SNe Ia	yes, depending on mass of exploding WD	yes
He-ignited violent mergers ("D^6")	in He shell due to dynamical instabilities → leads to core detonation	detonation in low-mass He shell, detonation in C/O core	possibly low Mn/Fe ratio, low production of n-rich IGE (Z-dependent)	normal SNe Ia	yes, depending on mass of exploding WD	yes
C-ignited violent mergers	at edge of C-core due to accretion	detonation in C/O material	low Mn/Fe ratio, low production of n-rich IGE (Z-dependent)	normal SNe Ia? 91bg-like objects? 2010lp, 2002ex-like objects	yes, depending on mass of exploding WD	yes

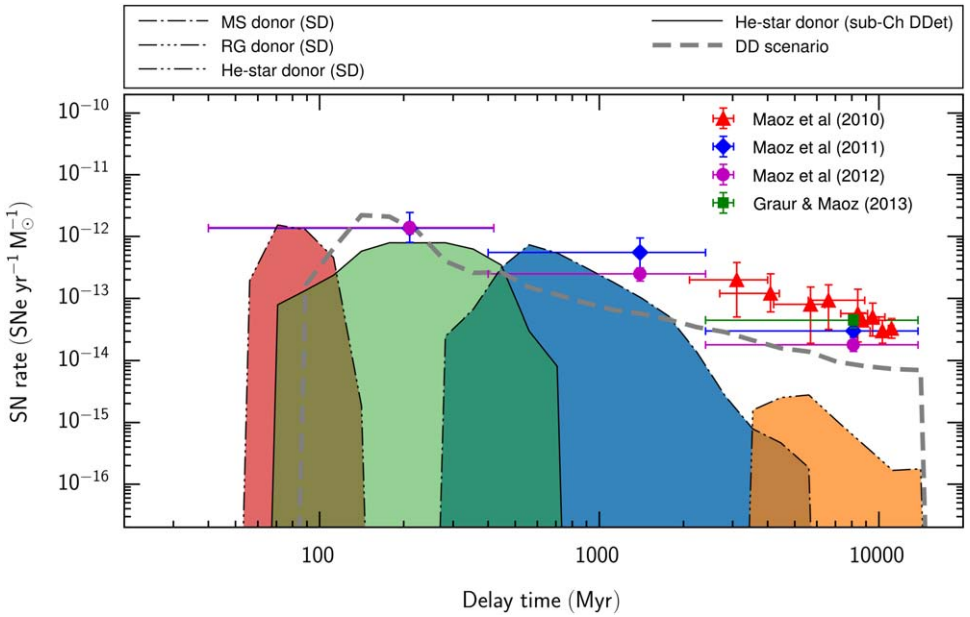


Figure 7. Distributions of delay times for different SN Ia progenitor channels predicted from BPS calculations. The observationally derived delay-time distributions are represented by points with error bars (Maoz et al. 2010, 2011, 2012; Graur & Maoz 2013). The figure is reproduced based on Figure 1 of Liu et al. (2015b). The results of the original DD scenario (gray dashed line) are taken from Wang et al. (2010, see also Han 1998). In the Sub-Chandrasekhar-mass double-detonation (i.e., Sub-Ch DDet) model, only the results for helium-star donors are included (see also Wang et al. 2013). Note that there is a large variation in the results among various BPS studies (Maoz et al. 2014, see their Figure 8).

overall behavior of the observed DTD, but a sharp decrease in SN Ia rates for delay times shorter than 200 Myr is seen in the DD model. This is inconsistent with a significant detection of prompt SNe Ia with delay times of $35 < t < 200$ Myr (Maoz et al. 2010). BPS calculations have predicted that SD models with an MS or an RG donor mainly contribute to intermediate delay times of $\sim$100 Myr to 1 Gyr and long delay times of $\gtrsim$3 Gyr, respectively (e.g., Han & Podsiadlowski 2004; Ruiter et al. 2009; Meng et al. 2009; Wang et al. 2010; Claeys et al. 2014; Liu et al. 2015b). SD models with a He star donor are expected to contribute to delay times shorter than 100 Myr (e.g., Wang et al. 2009; Claeys et al. 2014). The SD scenario generally tends to predict much lower SN Ia rates than those of the DD scenario (gray dashed line of Figure 7). However, a large variation of the results among different BPS studies is seen (Maoz et al. 2014, see their Figure 8). For recent reviews on the details of the topic, see Maoz & Mannucci (2012) and Maoz et al. (2014).

One should always keep in mind that there are significant uncertainties in the theoretical predictions of SN Ia rates and delay times from BPS calculations. On the one hand, constraints on the mass-retention efficiencies in the SD scenario are still rather weak (Shen & Bildsten 2007; Wolf et al. 2013; Piersanti et al. 2014; Wang 2018) yet studies show that there is a significant impact of the mass-retention efficiencies on BPS results such as rates and DTDs (Bours et al. 2013; Toonen et al. 2014; Ruiter et al. 2014; Piersanti et al. 2014). On the other hand, the predictions of BPS calculations sensitively rely on the assumed parameters in specific BPS codes such as the CE evolution, star formation rate and initial mass function. However, to date, strong constraints on these parameters (e.g., the CE efficiency, see Zorotovic et al. 2010; De Marco et al. 2011; Ivanova et al. 2013; Röpke & De Marco 2023) are still lacking. This limits the predictive power of the BPS results (Toonen et al. 2014; Claeys et al. 2014). For a recent review of BPS calculations, see Han et al. (2020).

5. Observables of Thermonuclear Supernovae

The approach to compare the observational features predicted by different progenitor models with observations has long been used to provide important clues to the yet poorly understood origin and explosion mechanism of SNe Ia. Over the past decades, substantial effort in modeling SNe Ia aimed at the prediction of optical observables (light curves and spectra; e.g., Kasen et al. 2006; Sim et al. 2010; Maeda et al. 2010; Kromer et al. 2010; Pakmor et al. 2010; Polin et al. 2019; Shen et al. 2021b). The main goal was to distinguish between explosions of Chandrasekhar-mass and sub-Chandrasekhar-mass WD explosions as well as different mechanisms of thermonuclear combustion in these events. Despite all efforts,

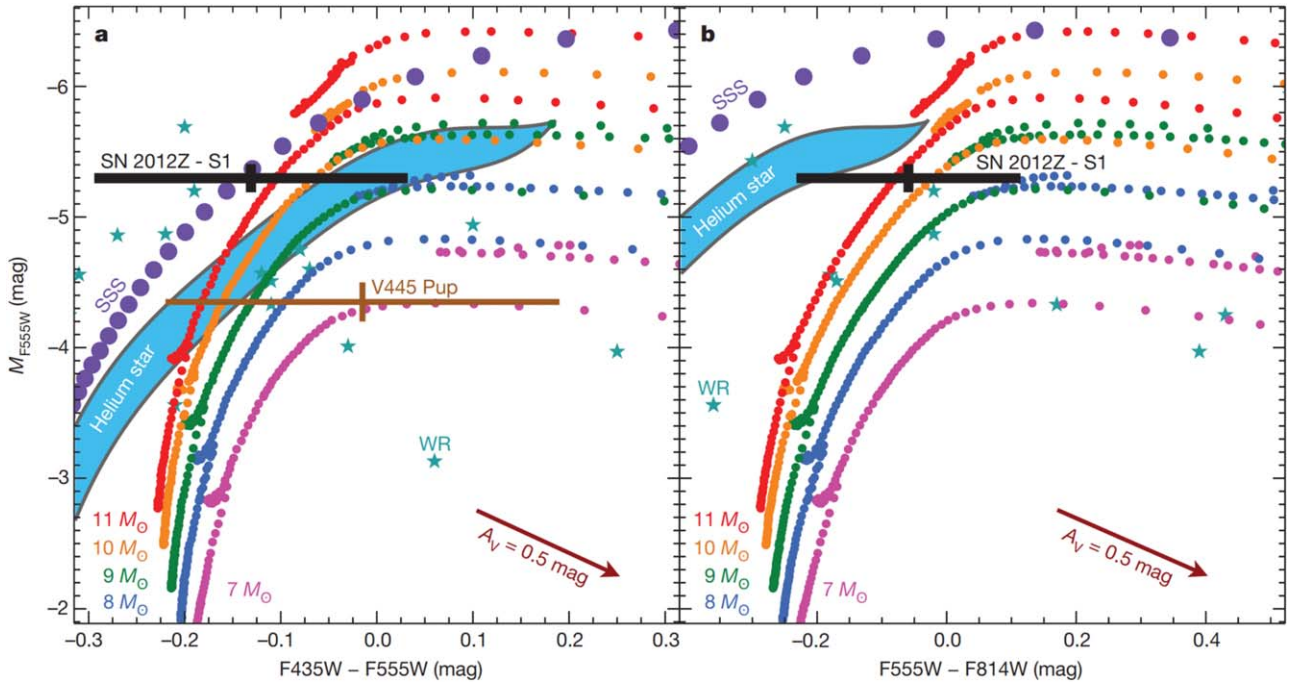


Figure 8. An example of constraints on the progenitor models of SNe Ia by searching for their pre-explosion companion stars. Here, the color-magnitude diagrams present a comparison between detected pre-explosion luminous source of SN 2012Z (i.e., SN 2012Z-S1; *black crosses*) and different theoretical models, including single stars with masses in a range of 7–11 $M_\odot$ (*colored dotted curves*), He-star donor model to a CO WD with an initial mass of 1.3 $M_\odot$ (*shaped blue regions*), candidates of Wolf-Rayet stars (*star symbols*) and thermal models for Eddington-luminosity SSSs (*purple dots*). The observations of a nova V445 Pup (*brown cross*) is also shown for comparison. The interstellar extinction of $A_V = 0.05$ (*magenta arrow*) is adopted. The figure is reprinted from McCully et al. (2014, see their Figure 2).

degeneracies make it difficult to draw firm conclusions (Röpke et al. 2012).

Besides optical light curves and spectra predicted by radiative transfer calculations in the context of different explosion mechanisms, certain other observational signatures are also expected to be indicative for different progenitor scenarios, including the detection of pre-explosion companions, H/He lines in SN Ia late-time spectra caused by material stripped from the companion during its interaction with the SN ejecta, early excess emission due to the ejecta–companion interaction, narrow absorption signatures of CSM, and radio and X-ray emission from CSM interactions, surviving companion stars (and WD remnants), polarization signals, SNR morphology, etc. In this section, we will give a detailed overview of the observables predicted for different phases (from the pre-explosion phase to the SNR phase) of SNe Ia from currently proposed progenitor scenarios and their comparisons with the observations. In particular, we focus on the question of how a binary companion star in the SD scenario shapes the observables of SNe Ia.

5.1. Pre-explosion Companion Stars

The companion stars in potential progenitor models of SNe Ia fall into two categories (see Section 3.1): (i) non-degenerate companion stars (MS, SG, RG, AGB or He-burning stars) in the SD scenario; (ii) WD companions in the DD scenario. Because non-degenerate companion stars are much brighter than WDs, luminous sources are expected to be detected in pre-explosion images at positions of SNe Iaif they are generated from the SD progenitor scenario. Therefore, analyzing pre-explosion images from the SN position provides a direct way to test the SD progenitor scenario (Foley et al. 2010; McCully et al. 2014).

On the theoretical side, Han (2008) comprehensively addressed the pre-explosion observable properties (luminosities, effective temperatures, masses, surface gravity, and orbital and spin velocities) of MS companion stars at the moment of an SN Ia explosion by performing BPS calculations for the WD + MS progenitor model. Following this work, Liu et al. (2015c) extended the calculations to present pre-explosion properties of different non-degenerate companion stars, including MS, SG and RG companions in the SD scenario, and the He-burning companion stars from both the SD and sub-Chandrasekhar-mass double-detonation scenarios. Wong et al. (2021) also made predictions for the properties of the He-star donors at the time of explosion for a set of progenitor systems involving a CO WD and a He star.

On the observational side, different studies have attempted to search for the expected non-degenerate companion stars by

analyzing pre-explosion images at the SN position, e.g., those taken by the Hubble Space Telescope (HST). To date, however, no progenitor companion star has been firmly detected in the analysis of pre-explosion images of normal SNe Ia (e.g., Maoz & Mannucci 2008; Li et al. 2011b; Bloom et al. 2012; Kelly et al. 2014), but there are some possible pre-explosion detections recently reported in several SNe Iax. For instance, McCully et al. (2014) detected a blue luminous source in the pre-explosion image of an SN Iax event, SN 2012Z. As shown in Figure 8, the properties of this pre-explosion luminous source (i.e., SN 2012Z-S1) have been found to be consistent with those of a He-star companion to the exploding WD (McCully et al. 2014; Liu et al. 2015c). Interestingly, late-time observations taken about 1400 days after the explosion by the HST have shown that SN 2012Z was brighter than the normal SN 2011fe by a factor of two at this epoch (McCully et al. 2022). Comparing with theoretical models, McCully et al. (2022) suggested this excess flux to be a composite of several sources: the shock-heated companion, a bound WD remnant that could drive a wind, and light from the SN ejecta due to radioactive decay. Foley et al. (2015) analyzed pre-explosion HST images of another SN Iax (SN 2014dt), but no source could be detected in this case.

5.2. Ejecta–Companion Interaction

After the explosion in the SD scenario, the ejecta expand freely for a few minutes to hours before hitting the non-degenerate companion star, engaging in ejecta–companion interaction (see Figure 9). The effect of an SN explosion on a nearby companion star has been studied since the 1970s (e.g., Colgate 1970; Wheeler et al. 1975; Fryxell & Arnett 1981; Marietta et al. 2000; Pakmor et al. 2008; Liu et al. 2012; Pan et al. 2012b; Boehner et al. 2017; McCutcheon et al. 2022). There are several ways in which the SN blast wave can modify the properties of companion stars during the ejecta–companion interaction, giving rise to observables that can be used to constrain SN Ia progenitors.

First, the SN ejecta significantly interact with the companion star after the explosion, stripping some H-rich and He-rich material from its surface. This effect is caused either by the direct transfer of momentum or by the conversion of the blast kinetic energy into internal heat, i.e., by evaporation/ablation. As a consequence, some H/He lines caused by the stripped material may be present in late-time spectra of SNe Ia (Wheeler et al. 1975; Mattila et al. 2005; Botyánszki et al. 2018; Dessart et al. 2020).

Second, the shock heating injects thermal energy into the companion star during the interaction, leading to a dramatic expansion of the surviving companion star so that it displays signatures that are different from a star that does not experience the ejecta–companion interaction. For example, it could become more luminous and have a lower surface gravity (Podsiadlowski 2003; Liu et al. 2023).

Third, radiative diffusion from shock-heated ejecta during the interaction is expected to produce an early excess in optical/ultraviolet (UV) or X-ray emission (Kasen 2010).

Fourth, the surface of a companion star may be enriched with heavy elements (e.g., Ni, Fe or Ca) deposited by the SN Ia ejecta (Pan et al. 2012b; Liu et al. 2013b), which might be detectable in the spectra of a surviving companion star.

Finally, the companion star survives the explosion and retains its pre-explosion orbital velocity after the SN explosion, which leads to a high peculiar velocity compared with other stars in the vicinity (Ruiz-Lapuente et al. 2004; Schaefer & Pagnotta 2012). The typical pre-explosion orbital velocities of the H-rich and He-rich companions in the SD Chandrasekhar-mass scenario are $\sim$80–280 km s^{-1} (Han 2008) and $\sim$250–500 km s^{-1} (Wang et al. 2009), respectively. The He-star companions in the sub-Chandrasekhar-mass double-detonation scenario and the He WD (or the CO WD which transfers its outer He layers) companions in the D^6 model are respectively expected to have pre-explosion orbital velocities of $\sim$400–1000 km s^{-1} (Neunteufel 2020) and $>$1000 km s^{-1} (Shen et al. 2018b; Igoshev et al. 2023).

5.2.1. Searches for Stripped Hydrogen and Helium

The earliest study of the effect of an SN explosion on a companion star was done by Colgate (1970). He suggested that the companion star receives a kick that is mainly caused by the evaporation from the stellar surface (i.e., the ablation), although there is also a small kick from the direct collision with the SN ejecta. Cheng (1974) further investigated the impact of an SN shell onto a 2.82 $M_\odot$ and a 20.0 $M_\odot$ MS companion star for various binary separations, SN shell masses and velocities. He concluded that the MS companion star could survive from the interaction with the SN shell. Upon these two works, several analytical models were developed to estimate the amount of stripped H mass and the kick velocity received by the companion star during the ejecta–companion interaction for MS companion stars with an $n = 3$ (Wheeler et al. 1975) and an $n = 2/3$ polytrope (which is appropriate for a low-mass MS; Applegate & Terman 1989), and for RG companion stars (Wheeler et al. 1975; Chugai 1986).

To test the analytic prescription of Wheeler et al. (1975), several numerical simulations were performed for low-mass MS companions (Fryxell & Arnett 1981; Taam & Fryxell 1984) and RG stars (Livne et al. 1992). In particular, Livne et al. (1992) suggested that almost the entire envelope of an RG star could be stripped off by the SN blast, imparting a velocity to the stripped material ($\lesssim 10^3$ km s^{-1}) much smaller than that of SN ejecta ($\sim 10^4$ km s^{-1}). Following the work of Wheeler et al. (1975); Meng et al. (2007) semi-analytically estimated the amount of stripped H mass due to SN Ia explosions by

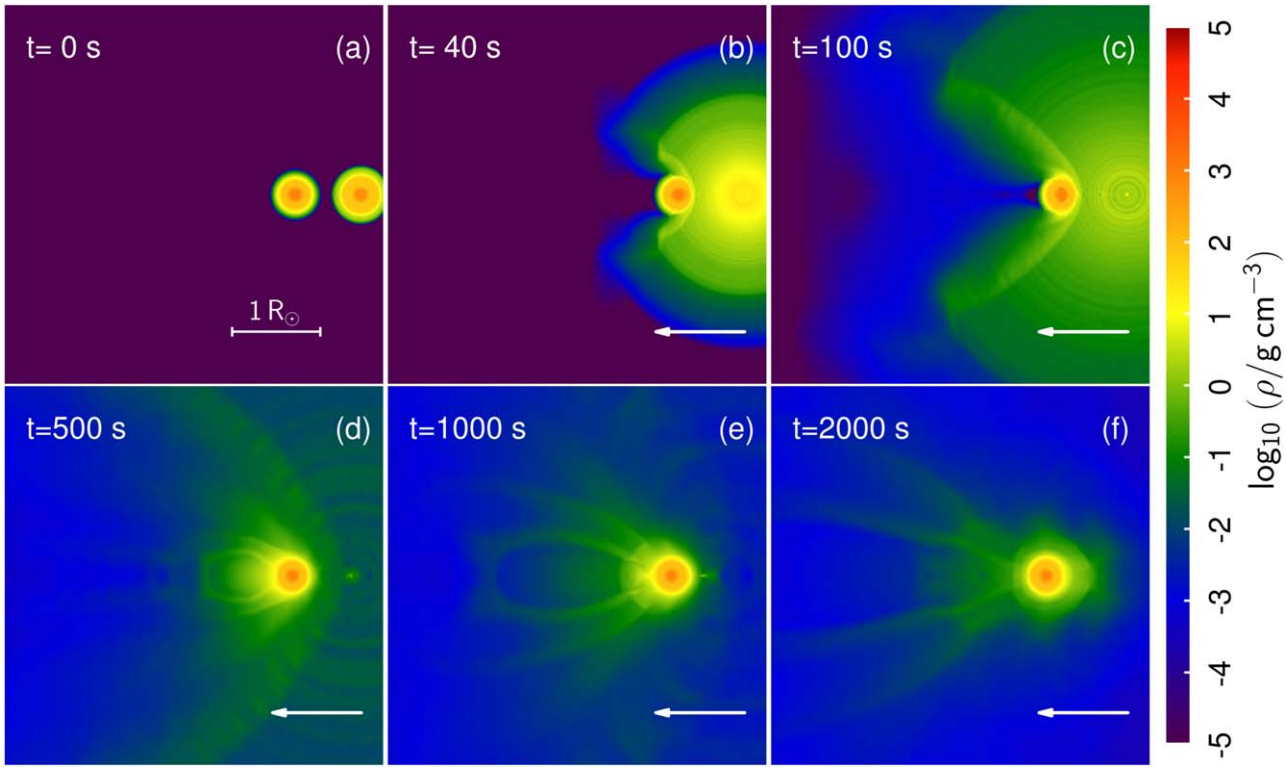


Figure 9. An example of the interaction between SN Ia ejecta and an MS companion star in 3D hydrodynamical simulations (Liu et al. 2012). The panels show slices in the orbital plane for three different times after the SN explosion as indicated. The direction of motion of the incoming SN Ia ejecta is from right to left (*arrow symbols*). Colors indicate density.

adopting the binary and companion properties constructed with detailed binary evolution calculations. However, they underestimated the total stripped companion masses because of neglecting the effect of the ablation on the companion surface.

More recently, updated two-dimensional (2D) and 3D simulations with grid-based or smoothed particle hydrodynamics (SPH) methods have been presented that investigate the details of the interaction between SN Ia ejecta and the companion star (Marietta et al. 2000; Pakmor et al. 2008; Pan et al. 2010, 2012b; Liu et al. 2012, 2013b, 2013c, 2013a; Boehner et al. 2017; Bauer et al. 2019; Zeng et al. 2020; McCutcheon et al. 2022). For instance, Marietta et al. (2000) performed high-resolution 2D simulations to comprehensively study the interaction of SN Ia ejecta in a variety of plausible progenitor systems with MS, SG and RG companions. However, they assumed the structure of single MS/SG/RG stars for the companion in their simulations. The study of Marietta et al. (2000) for MS companion stars was updated to 3D simulations with the SPH method by Pakmor et al. (2008), in which they considered the effect of pre-explosion mass transfer on the structures of a companion star at the moment of SN explosion. However, they computed their companion star models by constantly removing mass while evolving a single MS star to mimic the detailed mass-transfer processes in a binary system. This makes their MS star model much more compact than one constructed from a full binary evolution calculation. Therefore, they predicted a small amount of stripped H mass of 0.01–0.06 $M_{\odot}$ for the MS donor model. Liu et al. (2012, 2013b) further developed the work of Pakmor et al. (2008) by adopting more realistic companion star models constructed from detailed, state-of-the-art binary evolution calculations. They also extended simulations to cover different companion stars (MS, SG and He-star) and a range of binary separations and explosion energies (see also Liu et al. 2013c, 2013a). Pan et al. (2012b) employed adaptive mesh refinement (AMR) simulations to study the ejecta–companion interaction for MS, RG and He-star companions with different binary separations and explosion energies (see also Pan et al. 2010). In their simulations, however, they did not follow the full binary evolution but used initial conditions with a constant mass-loss rate when constructing their companion stars.

The main results of ejecta–companion interaction of SNe Ia in the literature can be summarized as follows.

1. 2D or 3D hydrodynamical simulations have predicted that about 5 per cent to 30 per cent of the companion

mass (i.e., $\gtrsim 0.1\,M_{\odot}$) can be stripped off from the outer layers of an MS or SG companion star (see top panel of Figure 10). For RG companions, almost the entire envelope is removed by the SN Ia blast wave. In the case of a He companion star, about one few per cent of the mass ($\sim$0.002–0.03 $M_{\odot}$) is lost in the interaction (see bottom panel of Figure 10).

2. The SN impact affects not only the companion star, but also the SN ejecta themselves. The presence of a companion star strongly breaks the symmetry of the SN Ia ejecta after the interaction (see panel c of Figure 9). The stripped companion material is largely confined to the downstream region behind the companion star, creating a hole in the SN debris with an opening angle of about 30°–115°.
3. Depending on the different stellar types, the companion stars receive kick velocities of a few ten kilometers per second to $\sim$100 km s^{-1}, which are lower than their pre-explosion orbital velocities. This indicates that the surviving companion star should move with a velocity which is largely determined by its pre-explosion orbital velocity.
4. The characteristic velocities of stripped companion material for the MS, SG, RG and He-star companions are $\sim$500–800 km s^{-1}, $\lesssim$900 km s^{-1}, $\sim$400–700 km s^{-1} and $\sim$800–1000 km s^{-1}, respectively, which are slower than the maximum velocity of SN Ia ejecta ($\sim 10^{4}$ km s^{-1}) by about one order of magnitude. This implies that H/He lines caused by stripped companion material become visible only at late-times when the photosphere recedes and moves to low velocity regions, revealing the inner SN Ia ejecta.
5. For a given companion model, the amount of stripped companion mass and kick velocity received by the companion star during the interaction decrease as the binary separation increases, which can be fitted by power-law relations.
6. The dependence of the amount of stripped mass and kick velocity on the explosion energy is in agreement with linear relations. Both quantities increase as the explosion energy increases.
7. The companion star is generally expected to survive the explosion and becomes a runaway or hypervelocity star. However, whether a He WD companion in the double-detonation model would survive the explosion is still unclear (Pakmor et al. 2022).
8. The companion surface could be enriched with heavy elements (contamination) from the low-expansion-velocity tail of SN Ia ejecta, which provides a way to observationally identify the surviving companion stars in SNRs. However, the exact level of contamination is still rather uncertain in current models because of uncertainties in mixing of the contaminants in the envelope.

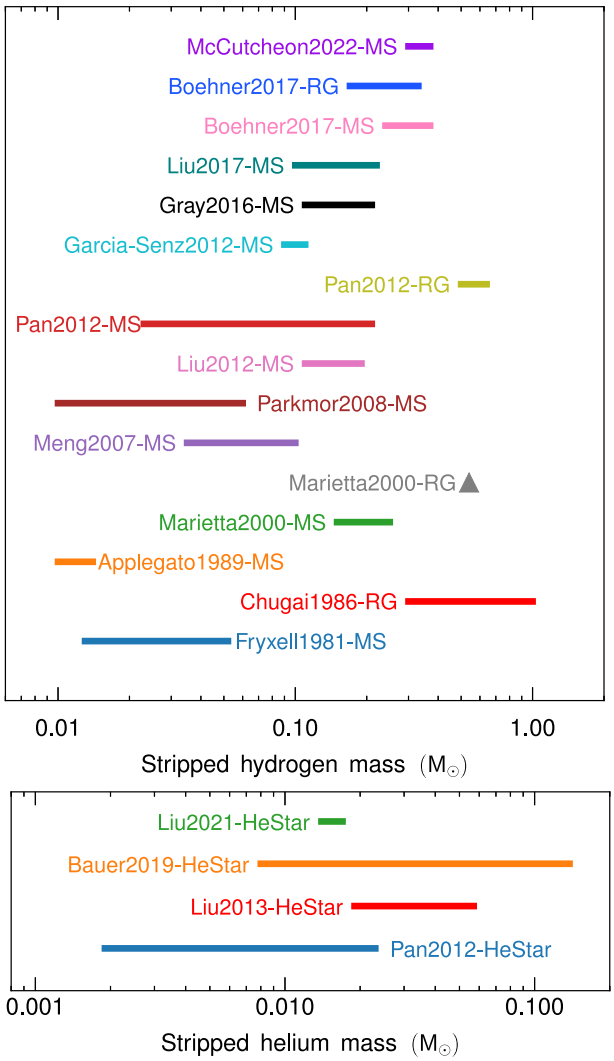


Figure 10. Theoretical predictions for the amount of companion mass swept up by the SN Ia explosion during the ejecta–companion interaction. *Top panel*: the swept-up H masses predicted either from analytical studies (Chugai 1986; Applegate & Terman 1989; Meng et al. 2007) or from 2D/3D hydrodynamical simulations (Fryxell & Arnett 1981; Marietta et al. 2000; Pakmor et al. 2008; Liu et al. 2012; Liu & Stancliffe 2017; Pan et al. 2012b; García-Senz et al. 2012; Gray et al. 2016; Boehner et al. 2017; McCutcheon et al. 2022). Suffixes "MS" and "RG" indicate that the companion star was an MS or RG star, respectively. *Bottom panel*: the swept-up He masses predicted by numerical simulations (Pan et al. 2012b; Liu et al. 2013b; Bauer et al. 2019; Liu et al. 2021).

One of the key questions of the SD scenario is whether the signatures of swept-up H or He due to the interaction can be detected in late-time spectra of SNe Ia. On the theoretical side, by performing the 1D parameterized spherically symmetric radiative transfer calculations, Mattila et al. (2005) concluded that Balmer lines should be detectable in SN Ia nebular spectra if the stripped H masses are $\gtrsim 0.03\,M_{\odot}$ (see also Lundqvist

et al. 2013, 2015). In their models, they artificially added some uniform-density solar-abundance material with a low expansion velocity of 1000 km s^{-1} at the center of SN Ia ejecta of the W7 model from Nomoto et al. (1984). Recently, Botyánszki et al. (2018) performed, for the first time, 3D Monte Carlo simulations with a non-local thermodynamic equilibrium (NLTE) radiative transport code to determine the signatures of stripped companion material in nebular spectra of SNe Ia as a function of viewing angle. In this study, more realistic distributions of stripped companion material and post-explosion SN Ia ejecta structures were adopted based on 2D hydrodynamical simulations of the ejecta–companion interaction by Boehner et al. (2017). However, the Sobolev approximation as well as the simplified treatment on line overlap and multiple scattering in Botyánszki et al. (2018) causes some uncertainties in their results. Dessart et al. (2020) further extended previous calculations with a set of 1D NLTE steady-state radiative transfer simulations by covering a broader parameter space (a large range of masses for the ejecta, ^{56}Ni and stripped material) and computing line overlap and line blanketing explicitly. These models adopted a 1D parameterized spherically symmetric SN ejecta structure as in Mattila et al. (2005).

In summary, all radiative transfer calculations in the literature for SNe Ia with stripped companion material have concluded that the ejecta–companion interaction in the SD scenario produces significant and detectable signatures of stripped H/He in late-time spectra. They further provided the dependence of line luminosities from stripped H/He-rich material on the amount of stripped H/He mass. This indicates that searching for H/He emission due to stripped companion material in late-time spectra of SNe Ia is promising for identifying the SD or DD nature of the progenitor system.

On the observational side, a series of observations have attempted to search for narrow, low-velocity H/He emission lines expected to be caused by swept-up H/He in late-time spectra of SNe Ia. But to date, no strong evidence for such H/He emission has been found in late-time spectra of most SNe Ia (even for the nearby SNe Ia with very high quality observations, i.e., SN 2011fe and SN 2014J; (Leonard 2007; Lundqvist et al. 2013, 2015; Shappee et al. 2013b, 2018; Maguire et al. 2016; Graham et al. 2015, 2017; Sand et al. 2018, 2019; Dimitriadis et al. 2017; Jacobson-Galán et al. 2019; Holmbo et al. 2019; Tucker et al. 2019, 2020, 2022a; Siebert et al. 2020; Elias-Rosa et al. 2021; Hosseinzadeh et al. 2017, 2022). A detection was reported only for two fast-declining, subluminous events (SN 2018cqj and ASASSN-18tb; Dimitriadis et al. 2019; Vallely et al. 2019; Prieto et al. 2020). However, the Hα emission lines detected in SN 2018cqj and ASASSN-18tb have been suggested to be caused by either CSM interaction or by H material stripped from a companion star.

Furthermore, by analyzing late-time spectra of SNe Ia, one can convert the line luminosity limits to limits on the mass of H/He in SN Ia progenitors based on the current radiative transfer calculations for stripped companion material (Mattila et al. 2005; Botyánszki et al. 2018; Dessart et al. 2020). Statistical limits on stripped H/He mass by analyzing a number of SN Ia late-time spectra have been given by Tucker et al. (2020), and they are summarized in Figure 11. Comparing these statistical limits from the observation with the stripped H/He masses derived from numerical simulations, we can examine the validity of the SD scenario for SNe Ia. As affirmed in Figure 11, the observational constraints on the swept-up H/He masses are generally much lower than those from theoretical predictions (Figure 10), which poses a serious challenge for the SD scenario.

Current radiative transfer simulations for SNe Ia with stripped material are still afflicted with uncertainties, because they either simply assume parameterized spherically-symmetric SN ejecta (Mattila et al. 2005; Dessart et al. 2020), or they treat line overlap and multiple scattering in an approximative way (Botyánszki et al. 2018). For stricter predictions of the strength of H and He lines in late-epoch spectra, multi-dimensional NLTE radiative transfer calculations are needed that use the output ejecta model from 3D impact simulations and treat line overlap and multiple scatterings in detail. Moreover, there are some other possibilities that may explain the lack of H/He emission in late-time spectra. For instance, the "spin-up/spin-down" model may lead to a compact companion star whose H/He-rich envelope has been stripped before the explosion, causing the absence of stripped H/He material during the interaction (see Section 3.1.1).

5.2.2. *Early Excess Emission*

Different progenitor models and explosion mechanisms for SNe Ia may produce distinct early light curves (Kasen 2010; Rabinak et al. 2012; Piro & Morozova 2016; Noebauer et al. 2017; Magee & Maguire 2020). Therefore, early light curves of SNe Ia have been thought to play an important role in constraining their progenitor systems and explosion mechanism. For example, Nugent et al. (2011) used the early light curves of the nearby SN 2011fe to constrain the radius of its exploding star, confirming that it must have been a WD (see also Bloom et al. 2012). In the literature, different mechanisms have been proposed to cause an excess emission (i.e., a "bump") in early light curves of SNe Ia within the days following explosion, which will be described in detail below (Figure 12; see also Maeda et al. 2018; Jiang et al. 2021; Magee et al. 2022).

Companion interaction: Kasen (2010) predicted that the shock caused by the ejecta–companion interaction significantly heats SN Ia ejecta to high temperatures, which causes a strong excess emission during the first few days after the explosion

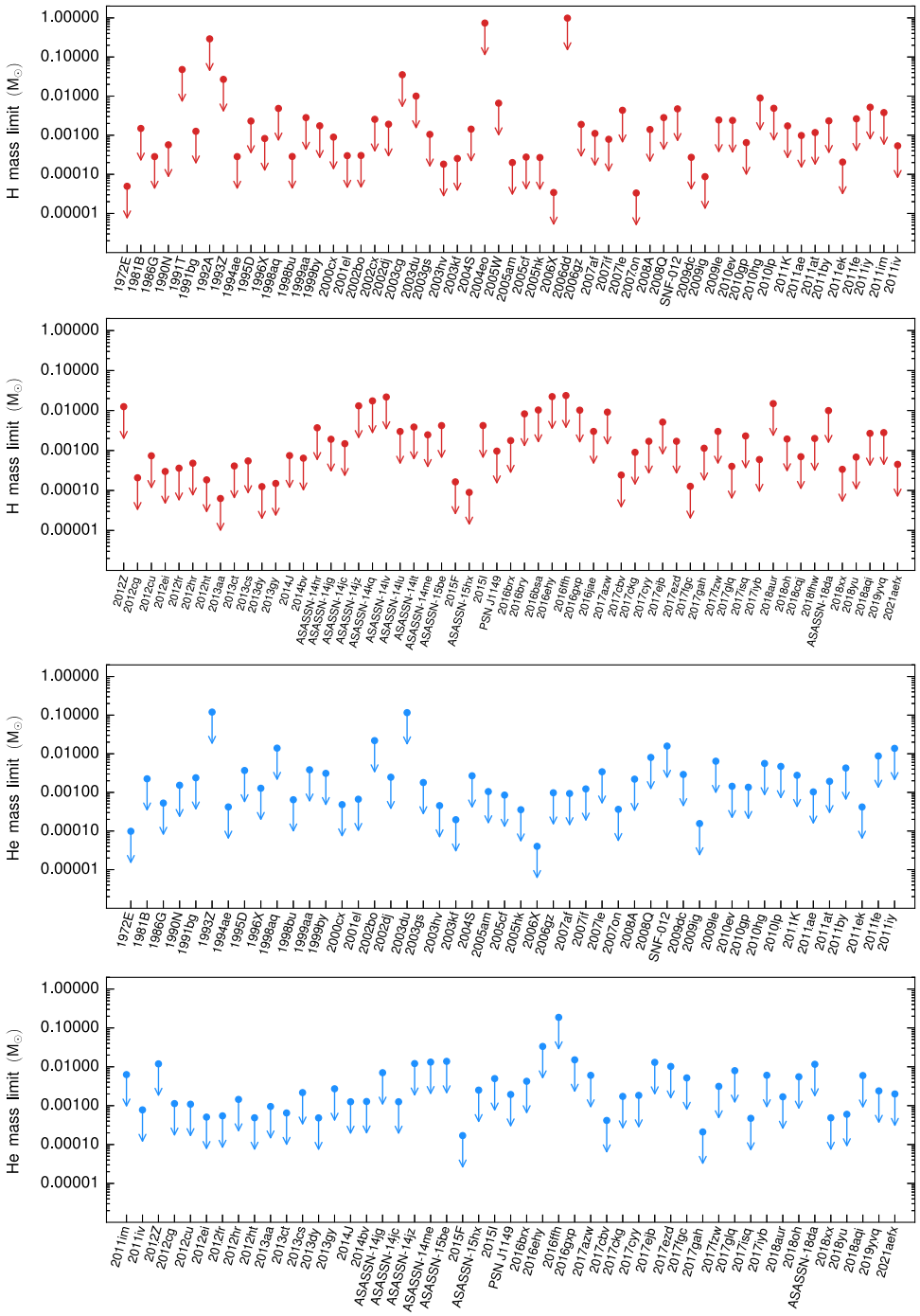


Figure 11. Distributions of observational mass limits on stripped H/He material by the explosion for a sample of SNe Ia (Tucker et al. 2020, and references therein). Data points are taken from Tucker et al. (2020).

that is observable in the light curves within certain viewing angles in the SD scenario (see also Maeda et al. 2014; Kutsuna & Shigeyama 2015; Magee et al. 2022). This early-time excess emission is expected to be brightest in the UV wavelengths and becomes subordinate at longer optical wavelengths. However, it can still cause a blue color evolution in the optical light curve. By applying BPS results to the analytical model of Kasen (2010); Liu et al. (2015a) presented the distributions of expected early UV emission for different SD progenitor systems. Because the DD scenario does not predict such early

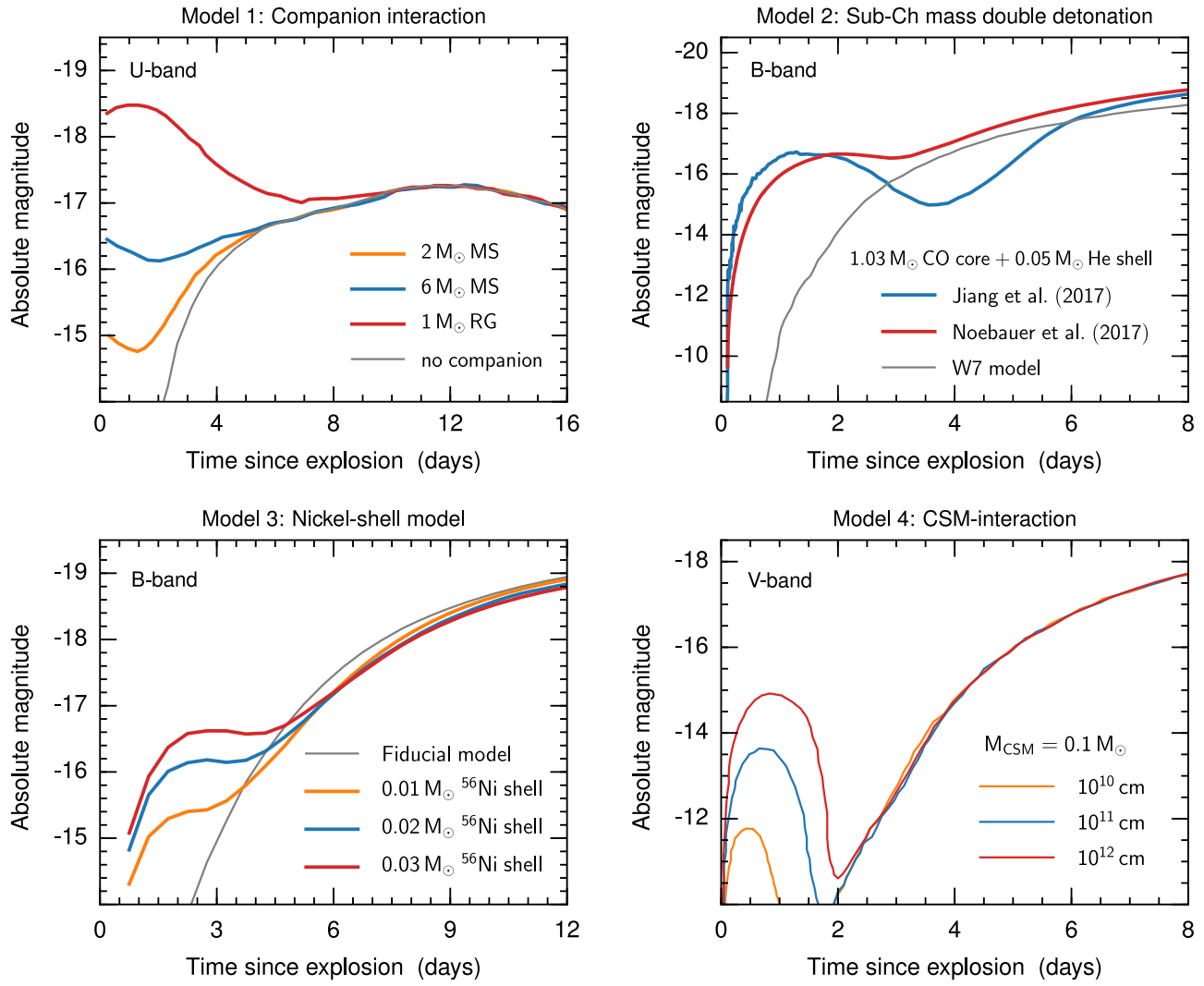


Figure 12. Examples of early excess emissions predicted from different scenarios. *Upper-left panel*: *U*-band early light curves given by the interaction of SN Ia ejecta with a 1 $M_\odot$ RG (*red line*), 2 $M_\odot$ MS (*yellow line*) and 6 $M_\odot$ MS (*blue line*) companion star, respectively. The figure is reproduced from Kasen (2010, see their Figure 3) with the permission of the AAS. *Lower-left panel*: *B*-band light curves predicted by the nickel-shell models with ^{56} Ni shells of 0.01 $M_\odot$-0.03 $M_\odot$ and a given shell width of 0.06 $M_\odot$. The fiducial model for SN 2018oh is shown as a *gray line*. The figure is created by taking the data points provided by Magee & Maguire (2020, see their Figure 3). *Upper-right panel*: *B*-band light curves of two sub-Chandrasekhar-mass double-detonation models presented by Noebauer et al. (2017, *red line*; see their Figure 3) and Jiang et al. (2017, *blue line*; see their Figure 3). The result of the W7 model (Nomoto et al. 1984) is also given as a *gray line* for comparison. *Lower-right panel*: *V*-band early light curves of the CSM-interaction model for a low ^{56} Ni mixing level with a boxcar width of 0.05 $M_\odot$ given by Piro & Morozova (2016), in which the mass and outer radius of CSM are set to be $M_{\rm CSM} = 0.1\ M_\odot$ and $R_{\rm CSM} = 10^{10}$–10^{12} cm, respectively. The figure is reproduced from Piro & Morozova (2016, see their Figure 10) with the permission of the AAS.

UV emission, detecting early strong UV emission within the days following explosion has long been considered a smoking gun for the SD scenario of SNe Ia (Kasen 2010; Hayden et al. 2010; Olling et al. 2015; Liu et al. 2015a; Magee et al. 2022). For a given explosion model, early UV emission caused by the ejecta–companion interaction is strongly dependent on the ratio of binary separation to companion radius (assuming RLOF) at the moment of SN explosion. Therefore, the properties of this early UV emission are expected to provide a clue to the types of non-degenerate companions (Cao et al. 2015; Marion et al. 2016).

Sub-Chandrasekhar-mass double-detonations: The burning of the initial He shell in sub-Chandrasekhar-mass double-detonation explosions can leave heavy, radioactive material in the outermost ejecta. A more massive He shell is expected to produce more radioactive material. The decay of this heavy, radioactive material could create an excess luminosity in the early light curves of SNe Ia (Sim et al. 2012; Noebauer et al.

2017; Jiang et al. 2017; Maeda et al. 2018; Polin et al. 2019; Magee et al. 2021). This may produce the early gamma emissions detected in SN 2014J (Diehl et al. 2014, 2015; Isern et al. 2016).

Nickel-shell models: Piro & Nakar (2013) suggested that the location of ^{56}Ni in SN Ia ejecta could have a noticeable impact on early-time light curves of SNe Ia. Piro & Morozova (2016) further investigated how the distribution of ^{56}Ni in the outer layers of the ejecta shapes early light curves of SNe Ia. More recently, Magee & Maguire (2020) comprehensively predicted early-time curves of SNe Ia from a series of models containing ^{56}Ni shells with different masses and widths in outer layers of SN Ia ejecta. They have shown that a ^{56}Ni shell in outer SN Ia ejecta will lead to an early excess luminosity a few days after the explosion (Piro & Nakar 2013; Piro & Morozova 2016; Noebauer et al. 2017; Magee et al. 2018; Magee & Maguire 2020; Magee et al. 2020).

CSM interaction: The presence of CSM is expected in different progenitor scenarios (see Section 5.4), which can also significantly affect early light curves of SNe Ia. Piro & Morozova (2016) have shown that the presence of CSM can lead to a significant shock cooling emission during the first few days after the explosion, which can affect the early-time rise of the light curves of SNe Ia (see also Maeda et al. 2018; Moriya et al. 2023). Depending on the degree of mixing of ^{56}Ni in the exploding WD and the detailed configurations of the CSM, this shock cooling emission can lead to early-time signatures (such as the early color evolution) similar to those caused by the ejecta interaction with a companion star (Piro & Morozova 2016). Figure 12 depicts early light curves of SNe Ia predicted from different proposed models described above.

Early light curves of SNe Ia have been studied since the 2010s to search for evidence of such early excess emission (Hayden et al. 2010; Brown et al. 2012b, 2012a; Olling et al. 2015; Burke et al. 2022a). To date, nearby SNe Ia with early excess emission have been reported and interpreted with the theoretical models discussed above: SN 2012cg (Marion et al. 2016; Shappee et al. 2018), SN 2012fr (Contreras et al. 2018), LSQ12gpw (Firth et al. 2015), SN 2013dy (Zheng et al. 2013) SN 2014J (Goobar et al. 2015), SN 2015ak (Jiang et al. 2018), SN 2015F (Im et al. 2015; Cartier et al. 2017), SN 2015bq (Li et al. 2022), iPTF14atg (Cao et al. 2015), SN 2016jhr (Jiang et al. 2017), iPTF16abc (Miller et al. 2018), SN 2017cbv (Hosseinzadeh et al. 2017), SN 2017erp (Jiang et al. 2018; Brown et al. 2019; Burke et al. 2022b), SN 2018yu (Burke et al. 2022b), SN 2018oh (Li et al. 2019c; Dimitriadis et al. 2019; Shappee et al. 2019), SN 2018aoz (Ni et al. 2022, 2023), SN 2019yvq (Miller et al. 2020; Siebert et al. 2020), SN 2019np (Sai et al. 2022), SN 2020hvf (Jiang et al. 2021), SN 2021aefx (Ashall et al. 2022; Hosseinzadeh et al. 2022), SN 2021zny (Dimitriadis et al. 2023), SN 2022ilv (Srivastav et al. 2023) and SN 2023bee (Hosseinzadeh et al. 2023; Wang et al. 2023).

Cao et al. (2015) suggested that an early UV excess emission seen in iPTF14atg is strong evidence of the ejecta–companion interaction in the SD scenario. Similarly, Marion et al. (2016) and Hosseinzadeh et al. (2017) respectively argued that the ejecta–companion interaction is likely to be the origin of early-excess signatures detected in SN 2012cg and SN 2017cbv. However, whether the early excess emission of these SNe Ia can be exclusively attributed to ejecta–companion interaction is still under debate (Kromer et al. 2013a; Liu & Stancliffe 2016; Shappee et al. 2018). Recently, Jiang et al. (2017) suggested that a He-detonation model provides a good explanation for early light curves of SN 2016jhr. In addition, it has been proposed that the CSM interaction and ^{56}Ni-mixing in the outer layers of SN Ia ejecta are likely to be the origin of early excess emissions of SN 2020hvf (Jiang et al. 2021) and SN iPTF16abc (Miller et al. 2018), respectively. Very recently, Dimitriadis et al. (2023) suggested that the interaction of SN ejecta with $0.04\,M_{\odot}$ H/He-poor CSM at a distance of about 10^{12} cm in the context of the merger of two CO WDs can provide an explanation for the early flux excess of SN 2021zny. In contrast to these studies, Hosseinzadeh et al. (2022) found that no available models can convincingly reproduce the early light curves of SN 2021aefx.

In summary, it is still hard to draw a strong conclusion on the exact origin of early excess emission detected in nearby SNe Ia. Current results seem to indicate that there may be various mechanisms at play that cause early excess emission in different SNe Ia.

5.3. Surviving Companion Stars

In the SD scenario, non-degenerate companion stars are expected to survive SN Ia explosions (see Section 5.2; Wheeler et al. 1975; Marietta et al. 2000; Pakmor et al. 2008; Liu et al. 2012, 2013a, 2013b, 2013c, 2021; Pan et al. 2012b; Maeda et al. 2014; Boehner et al. 2017; Bauer et al. 2019; Zeng et al. 2020). Searching for the surviving companion star in nearby SNRs has been commonly considered to be a promising way to test the SD progenitor scenario (e.g., Kerzendorf et al. 2009; Ruiz-Lapuente 2019). The surviving companion stars are expected to display distinct observational signatures due to the mass-stripping, shock heating and enrichment with heavy elements from SN ejecta during the ejecta–companion interaction. In addition, as the disruption of a binary progenitor system after the explosion, surviving companion stars will be runaway stars with a high peculiar space velocity compared to other stars in the vicinity (see Section 5.2).

5.3.1. Theoretical Predictions

Using 1D stellar evolution codes, early studies investigated the post-impact properties of surviving companions of SNe Ia by using simplified initial companion models instead of results from detailed modeling of the ejecta–companion interaction.

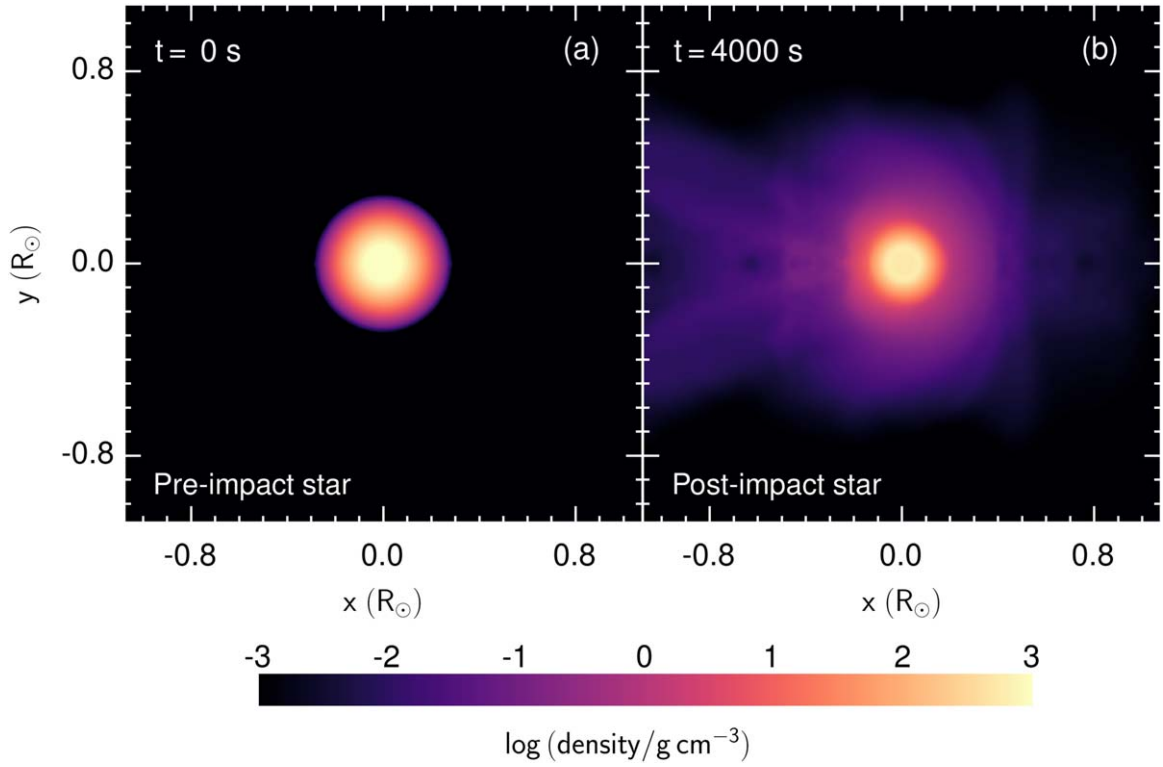


Figure 13. A He-star companion at pre-impact phase (*left panel*) and post-impact phase (*right panel*) from a 3D hydrodynamical simulation of the ejecta–companion interaction (Liu et al. 2013b, 2023).

For instance, Podsiadlowski (2003) and Shappee et al. (2013a) studied the post-impact evolution of a 1.0 $M_\odot$ SG star and a 1.0 $M_\odot$ MS companion star, respectively. Podsiadlowski (2003) found that the surviving SG star can become significantly overluminous by up to two orders of magnitude compared with its pre-SN luminosity for 10^3–10^4 yr after the explosion. Similar results and conclusion were derived by Shappee et al. (2013a) for their 1.0 $M_\odot$ MS companion star model. Both works claimed that the surviving companions become overluminous and detectable during the thermal re-equilibration phase after the impact. However, these two works did not perform detailed hydrodynamical impact simulations, and they mimicked the ejecta–companion interaction by adopting a rapid mass loss and extra heating during a single star evolution.

By mapping the results from 3D hydrodynamical simulations of the ejecta–companion interaction (see the right-hand panel of Figure 13) into 1D stellar evolution codes, the post-impact evolution of surviving MS star (Pan et al. 2012a; Rau & Pan 2022) and He-star (Pan et al. 2013; Liu et al. 2023) companions of normal SNe Ia have been followed over a long timescale of 10^4–10^7 yr after the explosion until the stars reestablish their thermal equilibrium. The same method was applied for the investigations of observational signatures of surviving companion stars from Chandrasekhar-mass pure deflagration explosions for SNe Iax (Liu & Zeng 2021; Zeng et al. 2022a, 2022b) and from the sub-Chandrasekhar-mass double-detonation explosions (Liu et al. 2021). The expected observational signatures of surviving companions from current studies in the literature are summarized as follows (Figures 13 and 14).

1. It is found that the ejecta–companion interaction causes an energy deposition in the companion star due to shock heating while removing some material from the companions' surface. Because the companion stars are strongly heated and inflated during the interaction (Figure 13), they continue to expand and become overluminous over a Kelvin–Helmholtz timescale after the impact. As the companion stars reestablish the thermal equilibrium, they continue to evolve on a track fairly close to that of an unperturbed star with the same mass.
2. Depending on different companion models and initial binary separations, the surviving MS and He-star companions of normal SNe Ia expand for a timescale of 10–10^4 yr and tens of years to reach a peak luminosity on the order of 10–1000 $L_\odot$ and $\sim 10^4$ $L_\odot$, respectively. The stars start to contract when they have radiated away the deposited energy.

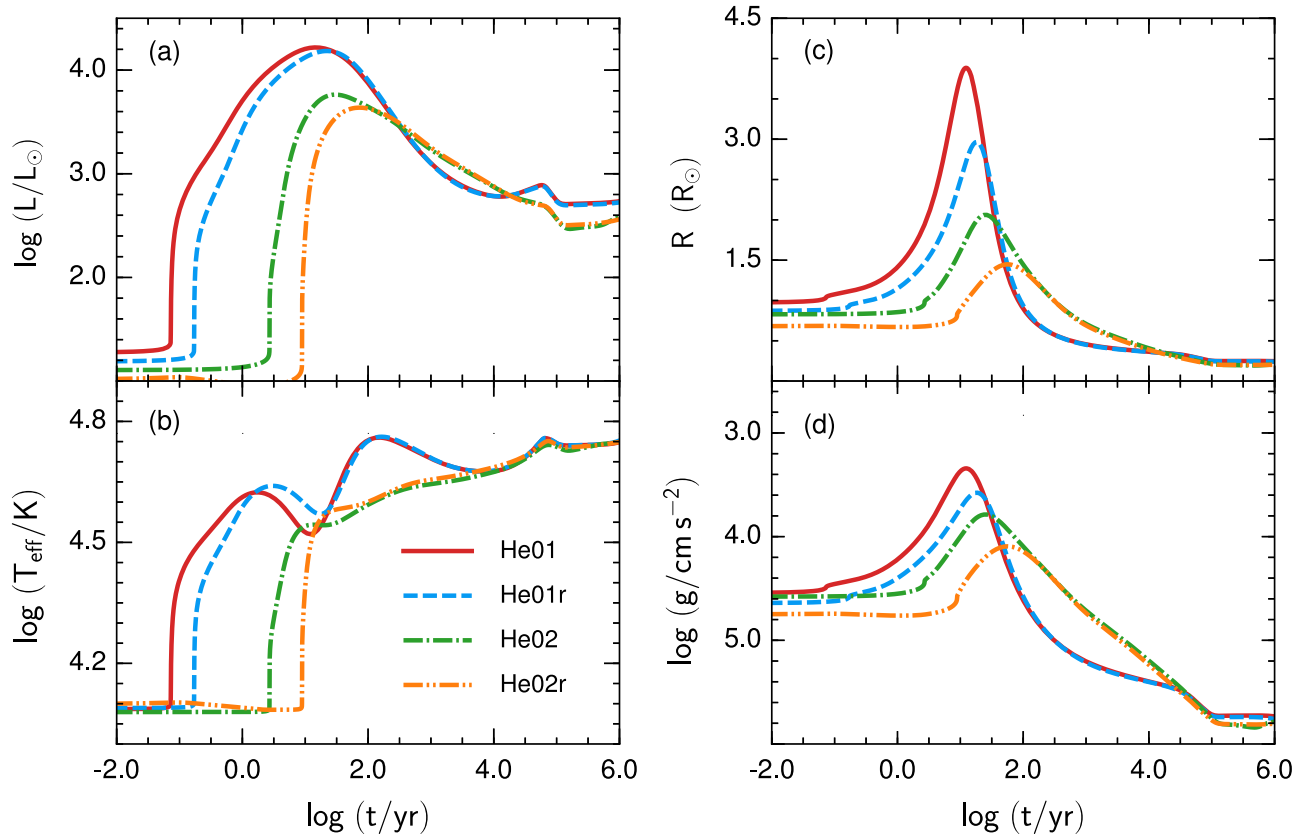


Figure 14. An example of post-evolution of the photosphere luminosity L, effective temperature $T_{\rm eff}$, radius R and surface gravity g of surviving He star companions as functions of time (Liu et al. 2023).

3. After the explosion, the surviving He-star companions of sub-Chandrasekhar-mass double-detonation SNe Ia inflate for about 100–1000 yr and reach peak luminosities of 10^2–10^3 $L_\odot$, exceeding their pre-explosion luminosities by 2–3 orders of magnitude.
4. The surface rotational speeds of companion stars could significantly decrease after the interaction due to the angular momentum loss and their dramatic expansion. As the deposited energy is radiated away, the stars shrink and their surface rotational speeds increase, becoming a fast-rotating object again after thermal equilibrium is reestablished. This suggests that the surviving companion stars could rotate slowly although they are fast-rotating stars originally (assuming that the star co-rotates with its orbit due to the strong tidal interaction during the pre-SN mass-transfer phase). The expected state of rotation of surviving companions thus depends on the age of the SNR.
5. The post-impact evolution of the surviving companion star is determined strongly by the competition between the amount and depth of energy deposition into the star during the interaction.
6. The inclusion of the orbital motion and the spin of the companion star in impact simulations does not affect the the post-impact properties of companion stars significantly.
7. When artificially adjusting the kinetic energy of the SN ejecta by scaling the velocities based on an original explosion model (e.g., the W7 model), it is found that a higher kinetic energy leads to a higher total amount of energy deposition and a greater depth of energy deposition for a given companion star model.

5.3.2. Searches for Surviving Companion Stars

In the past few decades, many studies have focused on searching for surviving companion stars as predicted for the SD scenario in the Galactic SNRs, such as Tycho (e.g., Ruiz-Lapuente et al. 2004; Ruiz-Lapuente 2019; Fuhrmann 2005; Ihara et al. 2007; González Hernández et al. 2009; Kerzendorf et al. 2009, 2013, 2018a; Bedin et al. 2014), Kepler (e.g., Kerzendorf et al. 2014; Ruiz-Lapuente et al. 2018) and SN 1006 (e.g., González Hernández et al. 2012; Kerzendorf et al. 2012, 2018b). Additionally, some SNRs in the Large

Magellanic Cloud (LMC): SNR 050967.5 (e.g., Schaefer & Pagnotta 2012; Pagnotta et al. 2014; Litke et al. 2017), SNR 051969.0 (e.g., Edwards et al. 2012; Li et al. 2019a), SNR 050567.9 (DEML71, Pagnotta & Schaefer 2015), SNR 050968.7 (N103B, e.g., (Pagnotta & Schaefer 2015; Li et al. 2017) and SNR 054870.4 (e.g., Li et al. 2019a) were searched. To date, no surviving companion could be firmly identified in these SNRs. Nevertheless, there are a few candidates showing special features in line with the expectations and have therefore been proposed as surviving companions in SN Ia events (e.g., Ruiz-Lapuente et al. 2004, 2023; Geier et al. 2015; Shen et al. 2018b).

Tycho G: Ruiz-Lapuente et al. (2004) suggested that Tycho G is a possible surviving companion because of its peculiar radial velocity and proper motion, and a lower surface gravity than an MS star (Bedin et al. 2014). Moreover, González Hernández et al. (2009) suggested that Tycho G has an overabundance of Ni relative to normal metal-rich stars, which seems to be consistent with the deposition of heavy elements from an SN Ia explosion (but see also Ihara et al. 2007). However, some other studies cast doubts on this identification (Fuhrmann 2005). For instance, Howell (2011) concluded that Tycho G is apparently not out of thermal equilibrium. Kerzendorf et al. (2013) showed that the measured [Ni/Fe] ratio of Tycho G seems to be not so unusual with respect to field stars with the same metallicity. In addition, Kerzendorf et al. (2009, 2012) suggested that Tycho G is unlikely to be the surviving companion star of SN 1572 because its measured rotational velocity of $\sim 6 \pm 1.5\,\mathrm{km\,s^{-1}}$ is much lower than rotational velocities of pre-explosion MS companion stars of 40–180 $\mathrm{km\,s^{-1}}$ (Han 2008). However, the ejecta–companion interaction can significantly reduce the rotational velocity of a companion star (Pan et al. 2012a; Liu et al. 2013b, 2023; Zeng et al. 2022b).

US 708: In the sub-Chandrasekhar double-detonation scenario, the companion stars are expected to have high orbital velocities of up to $\simeq$ 900–1000 $\mathrm{km\,s^{-1}}$ at the moment of explosion (Neunteufel 2020; Neunteufel et al. 2022). The surviving companion stars from this scenario are therefore good candidates of hypervelocity stars (e.g., Geier et al. 2013, 2015; Shen et al. 2018b; Neunteufel et al. 2019, 2022; Igoshev et al. 2023). The hypervelocity star US 708 has been classified as an sdO/B star. Based on a spectroscopic and kinematic analysis, Geier et al. (2015) reported that US 708 travels with a velocity of about 200 $\mathrm{km\,s^{-1}}$, suggesting that it is one of the fastest unbound stars in our Galaxy that was ejected from the Galactic disk 14.0 ± 3.1 Myr ago. Considering the possibilities of different acceleration mechanisms of hypervelocity stars, Geier et al. (2015) concluded that US 708 is very unlikely to originate from the Galactic center, but it is rather the ejected donor remnant of a sub-Chandrasekhar-mass double-detonation SN Ia. Very recently, comparing the long-term evolution and properties of surviving companion stars of sub-Chandrasekhar-mass double-detonation SNe Ia with the observations of US 708, Liu et al. (2021) suggested that US 708 would require the entire pre-SN progenitor binary to travel at a velocity of about 400 $\mathrm{km\,s^{-1}}$ if it is indeed the surviving He-star donor of a sub-Chandrasekhar-mass double-detonation SN Ia. It could have been ejected from a globular cluster in the direction of the current motion of the surviving companion star (see also Bauer et al. 2019).

MV-G272: Ruiz-Lapuente et al. (2023) explored the Galactic Type Ia remnant SNR G272.2-3.2 (about 7,500 yr old) with the Gaia EDR3, finding a kinematically peculiar star (M1-M2 type dwarf) Gaia EDR3 5323900215411075328, i.e., MV-G272. The past trajectory of MV G272 shows that it was ejected from the center of SNR G272.2-3.2 about 6,000–8,000 yr ago. The mass, radius, effective temperature, surface gravity and metallicity are measured to be $M = 0.44$–$0.50\,M_{\odot}$, $R = 0.446$–$0.501\,R_{\odot}$, $T_{\rm eff} = 3,\ 800$ K, $\log g = 4.46$ and $[\mathrm{Fe/H}] = -0.34$, respectively. Based on kinematical characteristics of MV-G272 and its trajectory, Ruiz-Lapuente et al. (2023) proposed that MV-G272 is the surviving companion candidate of the SN Ia that formed SNR G272.2-3.2. They also suggested that the discovery of MV-G272 hints at the possibility of an SD SN Ia progenitor system with an M-type dwarf companion (Wheeler 2012).

5.3.3. Searches for Surviving WD Remnants

In the D^6 model, the WD companion may survive the explosion (see Section 3.2.5; Pakmor et al. 2013; Shen et al. 2018b; Tanikawa et al. 2019; Boos et al. 2021). Such surviving WDs are expected to fly away with a velocity of $\gtrsim$1000 $\mathrm{km\,s^{-1}}$. Interestingly, Shen et al. (2018b) discovered three hypervelocity WDs with a velocity of 1000–1300 $\mathrm{km\,s^{-1}}$ in Gaia's second data release (Gaia Collaboration et al. 2016, 2018). Because these three hypervelocity runaway WDs have inflated radii that do not fit into any classical spectroscopic WD subtype, and show a much lower surface gravity and peculiar composition, Shen et al. (2018b) suggested that they are likely to be the WD companions ejected from SNe Ia explosions via the D^6 mechanism (see also Chandra et al. 2022). Shields et al. (2022) also attempted to search for fast-moving WDs predicted by the D^6 explosion in nearby SN Ia remnant SN 1006, but no such candidates were detected. However, the exact fate of the secondary WD in the D^6 model remains uncertain because it remains unclear whether it is detonated in the SN event (Pakmor et al. 2022). By artificially igniting a carbon detonation of the secondary WD in a D^6 model, Pakmor et al. (2022) found that the explosion of a secondary WD does not produce distinguishable observables (light curves and spectra) until $\sim$40 d after the explosion compared to a simulation without an explosion of the secondary WD. Furthermore, there is still no consensus on whether the first He detonation can eventually trigger a carbon detonation of the primary WD to cause an SN Ia (Roy et al. 2022).

It has been suggested that SNe Iax could arise from weak deflagration explosions of Chandrasekhar-mass WDs in which the stars are not fully disrupted. Such events would leave behind a bound WD remnant that has been shock heated significantly (Jordan et al. 2012a; Foley et al. 2013; Kromer et al. 2013a; Fink et al. 2014; Jha 2017). If binary systems are destroyed by the SN explosion in this model, such partly burnt WD remnants would be ejected with a high velocity and a peculiar atmosphere due to enrichment with heavy elements from the SN explosion, causing some unusual observational features (Shen et al. 2017; Zhang et al. 2019). To date, only a few candidates for such partly burnt WD remnants have been reported. Vennes et al. (2017) interpreted LP 40-365 as a partly burnt WD remnant due to its high proper motion and peculiar atmosphere that is dominated by IMEs (see also Raddi et al. 2018, 2019; Hermes et al. 2021). Ruffini & Casey (2019) suggested that a hyper-runaway WD in Gaia DR2, LP 93-21, could be another candidate for such events. Foley et al. (2014) reported a post-explosion detection of a thermally pulsing AGB-like source at the position of SN 2008ha by using HST images obtained 4.1 yr after the explosion. They suggested that this source might be a candidate of either the bound remnant of the WD or its companion star if this source is indeed related to SN 2008ha.

Pakmor et al. (2021) recently investigated the fate of a DD system containing a $0.80\,M_{\odot}$ primary CO WD and a secondary hybrid HeCO WD with a mass of $0.69\,M_{\odot}$. They found that the accretion from the secondary hybrid WD onto the more massive primary CO WD gives rise to a He-detonation when the accumulated He-shell reaches a critical mass limit. This He-detonation burns through the accretion stream to also incinerate the He-shell of the secondary HeCO WD, compressing the CO core of the HeCO WD to subsequently trigger a detonation. As a consequence, the HeCO WD explodes as a faint transient, and the primary CO WD survives from the explosion. This is different from the D^6 model, in which the surviving star is the secondary WD (Shen et al. 2018b; Kawabata et al. 2021) rather than the primary CO WD (Pakmor et al. 2022). Searches for such surviving primary WDs in future observations will help to confirm or rule out such an explosion mechanism.

5.3.4. Single (extremely) Low-mass WDs

In the SD scenario, depending on the actual mass of the companion star at the moment of SN Ia explosion and the total amount of mass lost from companion surface by the mass-stripping during the interaction (see Section 5.2), the surviving companion stars can become single low-mass WDs ($<0.5\,M_{\odot}$; Justham et al. 2009; Wang et al. 2010; Liu & Stancliffe 2018). In particular, hydrodynamical impact simulations for RG companion stars have shown that almost the whole envelope of the RG companion is stripped off by the explosion, leaving a low-mass He-core remnant (Marietta et al. 2000). This suggests that the surviving companion stars could have masses less than $\sim 0.3\,M_{\odot}$ (Brown et al. 2010), becoming single extremely low-mass WDs (ELWDs) if the companion stars had been RG stars (Liu et al. in prep). However, Brown et al. (2016) have shown that all of the ELWDs ($\lesssim 0.3\,M_{\odot}$) are found in binary systems rather than in isolation. If some SNe Ia were indeed produced from the RG donor scenario (despite the low SN Ia rates predicted by BPS calculations for this channel as shown in Figure 7; see also Maoz & Mannucci 2012; Liu et al. 2019; Liu & Stancliffe 2020; Ablimit et al. 2022), some single ELWDs are expected to exist. Future observations might be able to test the RG donor channel for SNe Ia by searching for such single ELWDs.

5.4. Ejecta–CSM Interaction

In the SD scenario, a significant amount of CSM is generally expected to exist around the progenitor due to pre-explosion outflows (Hachisu et al. 1999; Han & Podsiadlowski 2006; Patat et al. 2007; Sternberg et al. 2011; Dilday et al. 2012; Margutti et al. 2014):

(a) *Stellar winds*. The companion star in the SD scenario could be an RG star or an AGB star. In this case, the companion star loses mass in slow stellar winds at a rate of $5\times10^{-9}\,M_{\odot}\,\mathrm{yr}^{-1}$ to $5\times10^{-6}\,M_{\odot}\,\mathrm{yr}^{-1}$ with a typical velocity of 5–30 $\mathrm{km\,s}^{-1}$ (Seaquist & Taylor 1990; Vassiliadis & Wood 1993; Chen et al. 2011). Depending on models used for the description of wind accretion (e.g., Bondi-Hoyle-Lyttleton model, Bondi & Hoyle 1944; slow wind accretion, Liu & Stancliffe 2017; wind RLOF, Mohamed & Podsiadlowski 2007), mass loss rates from the binary system are expected to be $\gtrsim 10^{-8}\,M_{\odot}\,\mathrm{yr}^{-1}$.

(b) *Optically thick winds*. At high mass-transfer rates in the SD scenario, a so-called "optically thick wind (OTW)" has been proposed to be driven from the WD surface if the mass transfer rate is higher than the critical accretion rate for stable H/He burning (about $6\times10^{-6}\,M_{\odot}\,\mathrm{yr}^{-1}$, Hachisu et al. 1999). The WD accumulates companion material at a rate of the critical accretion rate, and the unprocessed material is lost by the OTW at a rate of $\gtrsim 10^{-8}\,M_{\odot}\,\mathrm{yr}^{-1}$ with a velocity of a few 1000 $\mathrm{km\,s}^{-1}$ (Hachisu et al. 1999; Han & Podsiadlowski 2006).

(c) *Non-conservative mass transfer*. At intermediate mass transfer rates, the steady mass-transfer happens through RLOF, and a small fraction of the transferred mass ($\lesssim 1\%$) may be lost over the outer Lagrangian points of the binary system with a velocity of several 100 $\mathrm{km\,s}^{-1}$ (up to $\sim$600 $\mathrm{km\,s}^{-1}$, see Deufel et al. 1999) when the WD undergoes steady nuclear burning (see also Chomiuk et al. 2012b; Margutti et al. 2014).

(d) *Nova explosions*. At low mass transfer rates, the accreting WD is expected to experience repeated nova outbursts

due to unsteady H/He burning on its surface (e.g., Starrfield et al. 1972; Nomoto 1982b; Yaron et al. 2005; Moore & Bildsten 2012; Wolf et al. 2013). In these, nova shells are ejected with a typical velocity of 1000–5000 $\mathrm{km\,s^{-1}}$ and a typical mass of 10^{-7}–$10^{-5}\,M_{\odot}$. Depending on the recurrence timescale and shell dynamics (Hachisu et al. 2000; Moore et al. 2013), the mass loss due to nova explosions is expected to be $\lesssim 10^{-6}\,M_{\odot}\,\mathrm{yr^{-1}}$ (Yaron et al. 2005).

While CSM interaction imprints on the observables were originally proposed as evidence for an SD progenitor evolution, it is now thought that also the DD scenario may produce significant amounts of CSM:

(a) *Tidal tail ejection*. Raskin & Kasen (2013) found that during the merger of two WDs (but prior to their final coalescence) $\approx 10^{-4} - 10^{-2}\,M_{\odot}$ of material can be tidally ejected (which is referred to as "tidal tail" mass loss) with a typical velocity of about 2000 $\mathrm{km\,s^{-1}}$ to form a CSM around the system. Therefore, a detectable shock emission in radio, optical/UV and X-ray wavelengths is expected to be caused by the interaction of the SN ejecta with this CSM (Raskin & Kasen 2013). Also, these "tidal tail" ejections are expected to produce relatively broad Na I D absorption features at late times.

(b) *The double-detonation scenario.* Shen et al. (2013) suggested that multiple mass ejection episodes could happen over hundreds to thousands of years prior to the merger of a CO WD + He WD binary system in the context of sub-Chandrasekhar-mass double-detonation explosion scenario (Pakmor et al. 2013). As a result, about $(3-\!-6) \times 10^{-5}\,M_{\odot}$ of material can be ejected from the binary system to the surrounding environment with a velocity of $\sim$1500 $\mathrm{km\,s^{-1}}$.

(c) *The core-degenerate scenario.* Soker et al. (2013) suggested that the violent merger of a CO WD with the core of an AGB star during the CE phase might eject some material (about $0.1 - 0.5\,M_{\odot}$) and show some signs of CSM if the SN Ia explodes soon after the mass ejections (Soker et al. 2013; Ruiter et al. 2013).

(d) *Mass outflows during rapid accretion*. By simulating the merger of two WDs, Dan et al. (2011) suggested that about 10^{-2} to $10^{-3}\,M_{\odot}$ material can be lost through the Lagrangian point with a possible velocity of about 1000 $\mathrm{km\,s^{-1}}$ during the rapid accretion phase of two WDs (see also Guillochon et al. 2010).

(e) *Disk winds*. Ji et al. (2013) simulated the merger of two WDs taking the effect of magnetic fields into account. They suggest that a rapidly rotating magnetized WD could be formed with a surrounding hot accretion disk if the WD-WD system fails to promptly detonate. They further suggested that a fraction of the disk ($\sim 10^{-3}\,M_{\odot}$) could be lost with a velocity of about 2600 $\mathrm{km\,s^{-1}}$ due to a magnetically driven wind.

5.4.1. Radio and X-ray Emission From CSM Interactions

After the SN explosion, the interaction of the SN Ia ejecta with the surrounding CSM or ISM produces a shock wave, accelerating particles and amplifying the magnetic field. This leads to the emission of synchrotron radiation in radio wavelengths (Chevalier 1977, 1982, 1998). Additionally, the SN shock heats the CSM or ISM to high enough temperatures (10^6–10^9 K) to produce X-ray emission by inverse Compton scattering (Chevalier & Fransson 2006; Fransson et al. 1996). Therefore, the detection of radio or X-ray from the CSM-interaction has long been suggested to provide a way to constrain the properties of the surrounding CSM, which can provide clues on the mass-loss history of the progenitor system prior to the SN explosion and thus place constraints on the nature of progenitor systems. However, no such radio or X-ray emission has been detected for most SNe Ia (e.g., Immler et al. 2006; Panagia et al. 2006; Russell & Immler 2012; Chomiuk et al. 2012b, 2016; Horesh et al. 2012; Margutti et al. 2012, 2014; Pérez-Torres et al. 2014; Kilpatrick et al. 2018; Sarbadhicary et al. 2019; Cendes et al. 2020; Lundqvist et al. 2020; Harris et al. 2021; Sand et al. 2021; Stauffer et al. 2021; Hosseinzadeh et al. 2022), even for the nearby, well-observed events SN 2011fe (Horesh et al. 2012; Margutti et al. 2012; Chomiuk et al. 2012b) and SN 2014J (Margutti et al. 2014; Chomiuk et al. 2016; Kundu et al. 2017).

Figure 15 displays an example of probing the CSM properties of the progenitor of SN 2011fe with its radio observations (Chomiuk et al. 2012a). The lack of early-time radio detection from SN 2011fe constrains the mass-loss rate of its progenitor system to $\dot{M} = 6 \times 10^{-10}\,M_{\odot}\,\mathrm{yr^{-1}}$ for a wind velocity of $v_{\rm w} = 100\,\mathrm{km\,s^{-1}}$ (see Figure 15; see also Chomiuk et al. 2012b). Moreover, an X-ray source in SN 2011fe was neither detected by the Swift X-Ray Telescope nor by Chandra, which constrains the progenitor system mass-loss rate $\dot{M} < 2 \times 10^{-9}\,M_{\odot}\,\mathrm{yr^{-1}}$ for a wind velocity of $v_{\rm w} = 100\,\mathrm{km\,s^{-1}}$ (Margutti et al. 2012). From the non-detection of early X-ray emission from SN 2014J, Margutti et al. (2014) derived an upper limit for the pre-explosion mass-loss rate of $\dot{M} < 10^{-9}\,M_{\odot}\,\mathrm{yr^{-1}}$ (for wind velocity of $v_{\rm w} = 100\,\mathrm{km\,s^{-1}}$) in the context of inverse Compton emission from upscattered optical photons by the SN shock (see also Kundu et al. 2017). Based on a sample of 53 SNe Ia observed with the Swift X-Ray Telescope, Russell & Immler (2012) calculated a 3σ upper limit for the X-ray luminosity of $1.7 \times 10^{38}\,\mathrm{erg\,s^{-1}}$ (Russell & Immler 2012), which corresponds to an upper limit on the mass-loss rate of $1.1 \times 10^{-6}\,M_{\odot}\,\mathrm{yr^{-1}} \times (v_{\rm wind})/(10\,\mathrm{km\,s^{-1}})$. More recently, Lundqvist et al. (2020) reported no radio detections for a sample of 21 nearby SNe Ia with deep radio observations, which constrains their pre-explosion mass-loss rates to

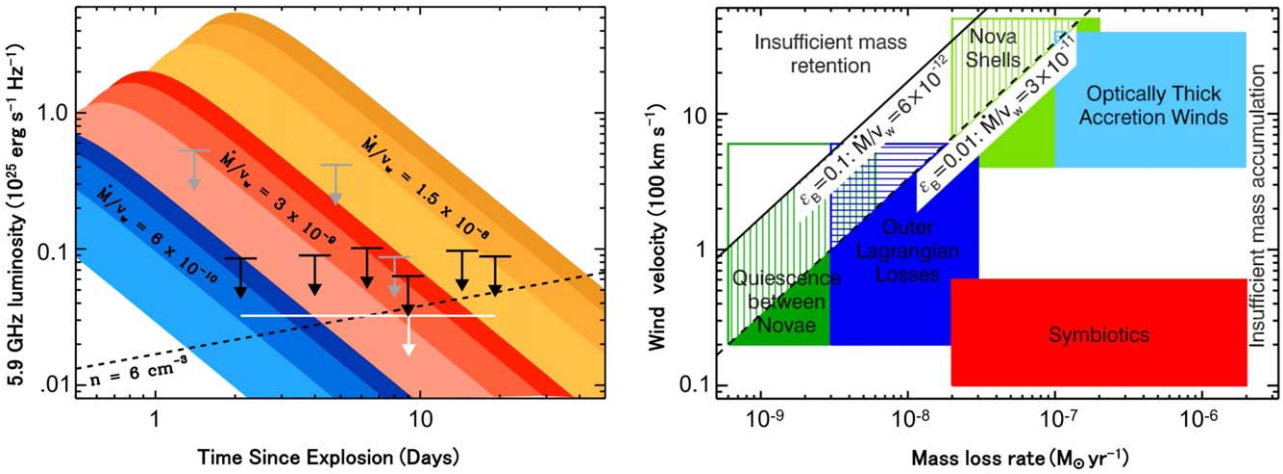


Figure 15. An example of using radio observations of SNe Ia to probe CSM properties of their progenitors (Chomiuk et al. 2012b). *Left panel*: A comparison between theoretical radio light curves (*colored swaths*) from synchrotron emissions due to the ejecta-CSM interaction and deep 3σ limits on the 5.9 GHz radio luminosity of SN 2011fe from Expanded Very Large Array (EVLA; *black arrows*). Additional data (*gray arrows*) from Horesh et al. (2012, scaled to 5.9 GHz) and a stacked limit (*white arrow*) are also shown. Different colored swaths give the theoretical expectations for three progenitor wind mass-loss rates highlighted in the figure in units of $M_\odot$ yr^{-1}/100 km s^{-1} by assuming $\epsilon_e = 0.1$. The value of ϵ_B ranges from 0.01 to 0.1 in each colored swath. The expected light curve from a model with uniform-density CSM of $n = 6$ cm^{-3} is presented in a *dashed black line*. *Right panel*: Constraints on the parameter space (mass-loss rate vs. wind speed) for different SD progenitor models discussed above (Section 5.4) for radio observations of SN 2011fe. Deep 3σ limits on progenitor wind mass-loss rates for the cases of $\epsilon_B = 0.1$ and $\epsilon_B = 0.01$ from *left panel* are marked by solid and dashed lines, respectively. The progenitor models located at the lower right regions of these two lines are expected to detect radio emissions by EVLA. Therefore, these progenitor models are likely to be ruled out for SN 2011fe. The figures are reprinted from Chomiuk et al. (2012b, see their Figure 2 and 3) with the permission of the AAS.

$\dot{M} \lesssim 4 \times 10^{-8}\, M_\odot$ yr^{-1} for a wind velocity of $v_w = 100$ km s^{-1}. All these results seem to disfavor the SD scenario because it usually predicts a significant amount of surrounding CSM.

In contrast, Kool et al. (2023) conducted radio searches with the electronic Multi-Element Radio Linked Interferometer Network (e-MERLIN) with a phase-referencing mode at the *C*-band (5.1 GHz) for SN 2020eyj, concluding that SN 2020eyj has shown significant signatures of CSM in its spectra (narrow He emission lines). Interestingly, Kool et al. (2023) also report that radio signals were observed for SN 2020eyj in two epochs. They argue that SN 2020eyj originated from a binary progenitor consisting of a WD and a He-star donor (i.e., WD + He-star model) because its spectra show features of interaction with He-rich CSM (narrow He emission lines) and their radio detection seems to be consistent with the prediction of the WD + He-star model (Moriya et al. 2019). This would therefore be the first detection of radio emission from an SNe Ia. However, whether the detected radio signals were indeed produced by SN 2020ejy still needs to be confirmed by higher-resolution radio observations.

5.4.2. Narrow Spectral Lines Caused By CSM Interaction

The CSM around SN Ia progenitor systems is expected be ionized by the UV radiation to produce time-varying absorption features in the SN spectra, which are expected to be detected by multi-epoch high spectral resolution observations (Patat et al. 2007; Sternberg et al. 2011). The detection of such absorption features may help to place constraints on the nature of SN Ia progenitor systems. Patat et al. (2007) reported the first detection of variable blueshifted neutral sodium (Na I; $\lambda\lambda$ 5890, 5896) absorption lines in SN 2006X. They interpreted this finding as strong evidence for an SD origin of SN 2006X. Following Patat et al. (2007), similar time-variable absorption features associated with CSM were reported in some other SNe Ia either from high spectral resolution observations (SN 2007le, Simon et al. 2009; PTF 11kx, Dilday et al. 2012) or from low spectral resolution observation (SN 1999cl, Blondin et al. 2009). Sternberg et al. (2011) studied variable Na I absorption features in a sample of 35 nearby SNe Ia with single-epoch high-resolution spectra. They found that 12 SNe Ia ($\sim$34%) displayed blueshifted absorption, but 13 SNe Ia did not show Na I absorption (these objects were preferentially located in early-type galaxies). They thus concluded that more than 20% of SNe Ia may result from the SD scenario. These results were confirmed by Maguire et al. (2013) who combined a new sample of 17 low-redshift SNe Ia observed with the XShooter intermediate-resolution spectrograph on the European Southern Observatory (ESO) Very Large Telescope with the sample given by Sternberg et al. (2011). Foley et al. (2012) suggested that SNe Ia with blueshifted absorptions generally have higher ejecta velocities and redder colors around maximum light compared with the other SN Ia population (see also Hachinger

et al. 2017). More recently, Graham et al. (2019) suggested that SN 2015cp was likely to have CSM properties similar to those of the well-studied event PTF 11kx.

5.4.3. Other Imprints Of CSM

The accreting WDs in the SD scenario are a powerful source to photoionize He II in the surrounding gas, producing emission in the He II recombination line at $\lambda 4686\,\mathring{A}$. These He II recombination lines can be used as a test of the nature of SN Ia progenitors (Rappaport et al. 1994; Woods & Gilfanov 2013; Johansson et al. 2014; Graur et al. 2014a; Chen et al. 2015).

If the OTW model is adopted in the SD scenario (Hachisu et al. 1996, 1999), a significant pre-explosion mass loss (or outflow) with high velocity of a few 1000 km s^{-1} is expected to modify the structure of the CSM at the time of the SN explosion. This evacuates a detectable low-density cavity around the WD (Badenes et al. 2007). However, neither a cavity around the WD nor He II recombination lines have been firmly detected in SNe Ia to date (Badenes et al. 2007; Johansson et al. 2014; Graur et al. 2014a).

5.4.4. Properties of SNRs

As the SN Ia ejecta interact with their surrounding CSM or ISM on timescales of hundreds or thousands of years, a shock wave is generated and propagates outward into the surroundings, and the SNR phase begins. The region enclosed by this shock wave, which contains both the SN ejecta and the swept-up material, is known as an SNR (Woltjer 1972). In general, Type Ia SNRs appear to be more spherical than those of core-collapse SNe, but some of them do show asymmetries either in their morphologies or in their emission patterns. Examples for asymmetric SNRs are Tycho (SN 1574; Warren et al. 2005; Vigh et al. 2011), SN 1006 (Winkler et al. 2014), Kepler (SN 1604; Kasuga et al. 2018) and the youngest known Galactic SNR G1.9 + 0.3 (Borkowski et al. 2013, 2017). In particular, the observations of SNR G1.9+ 0.3 demonstrated that the spatial distributions of both IMEs and Fe are significantly asymmetric (Borkowski et al. 2013, 2017; Griffeth Stone et al. 2021).

The interaction of the SN blast wave with the CSM has been modeled in numerical simulations to make predictions on the properties of the resulting SNRs. Again, the goal is to to constrain progenitor models and explosion mechanisms (Chevalier et al. 1992; Blondin & Ellison 2001; Badenes et al. 2007; Vigh et al. 2011; Chiotellis et al. 2012; Warren et al. 2005; Orlando et al. 2012; Borkowski et al. 2013; Burkey et al. 2013; Williams et al. 2013, 2017; Ferrand et al. 2019, 2022; Kasuga et al. 2021). For instance, Badenes et al. (2007) presented 1D hydrodynamic simulations of the ejecta–CSM interaction by assuming a pre-SN time-dependent wind. They found that the OTW from the WD surface excavates large low-density cavities around the progenitors, which is incompatible with currently observed features of known SNRs such as the Kepler and Tycho cases and SN 1006. Chiotellis et al. (2012) performed a 2D simulation with a spherically symmetric density profile of the SN ejecta and a wind-bubble CSM model, finding that the observed characteristics of the Kepler remnant are in good agreement with predictions from an explosion in a dense, bow-shaped bubble formed by the wind of the AGB donor star.

Some asymmetries in SN Ia ejecta are expected to be caused by the SN explosion itself and by the presence of a companion star in the SD scenario (see Section 5.2). These asymmetries in SN Ia ejecta might affect the subsequent ejecta-CSM interaction and therefore have an imprint on the observable properties of Type Ia SNRs such as their morphologies (Ferrand et al. 2019) and the spatial distributions of different chemical elements. A long-standing question is whether asymmetries in SN Ia ejecta caused by the explosion process contribute noticeably to the shaping of SNRs or whether the remnant properties are entirely determined by the interaction of the SN ejecta with the CSM. To test this, Ferrand et al. (2019) compared the SNR evolution in 3D simulations initialized with a spherically symmetric SN Ia ejecta model to that of an asymmetric ejecta model derived from a 3D explosion model (the N100 model of Seitenzahl et al. 2013b). Figure 16 shows the time evolution of the density of all material (i.e., both SN Ia ejecta and CSM) in the 3D SNR simulations of Ferrand et al. (2019). They concluded that the impact of explosion asymmetries on the SNR morphology is still visible after hundreds of years (Figure 16). However, they neglected the effect of the ejecta–companion interaction in their SNR modeling. Vigh et al. (2011) presented 2D and 3D numerical simulations of young SNRs with an asymmetric ejecta model, in which the ejecta structure is artificially modified by considering the effect of the companion star. They concluded that the asymmetries of the SN ejecta due to the presence of a companion star can have a strong effect on the subsequent evolution of the SNR. Gray et al. (2016) found that a hole in the SN Ia ejecta caused by the presence of a nearby companion remains visible for many centuries after the interaction between the ejecta and the ISM (see also García-Senz et al. 2012). Ferrand et al. (2022) performed 3D SNR simulations in the context of the D^6 model by considering the effect of the presence of a WD companion, suggesting that the WD companion produces a large conical shadow in the ejecta, visible in projection as a dark patch surrounded by a bright ring.

For firm conclusions, further SNR modeling is required to comprehensively take into account the asymmetries in the ejecta caused by the ejecta–companion interaction in the context of different SD progenitor systems (e.g., the MS, SG, or He-star donor model) and to cover different explosion models. This may provide a new way to distinguish the SD and DD scenarios of SNe Ia through SNR observations.

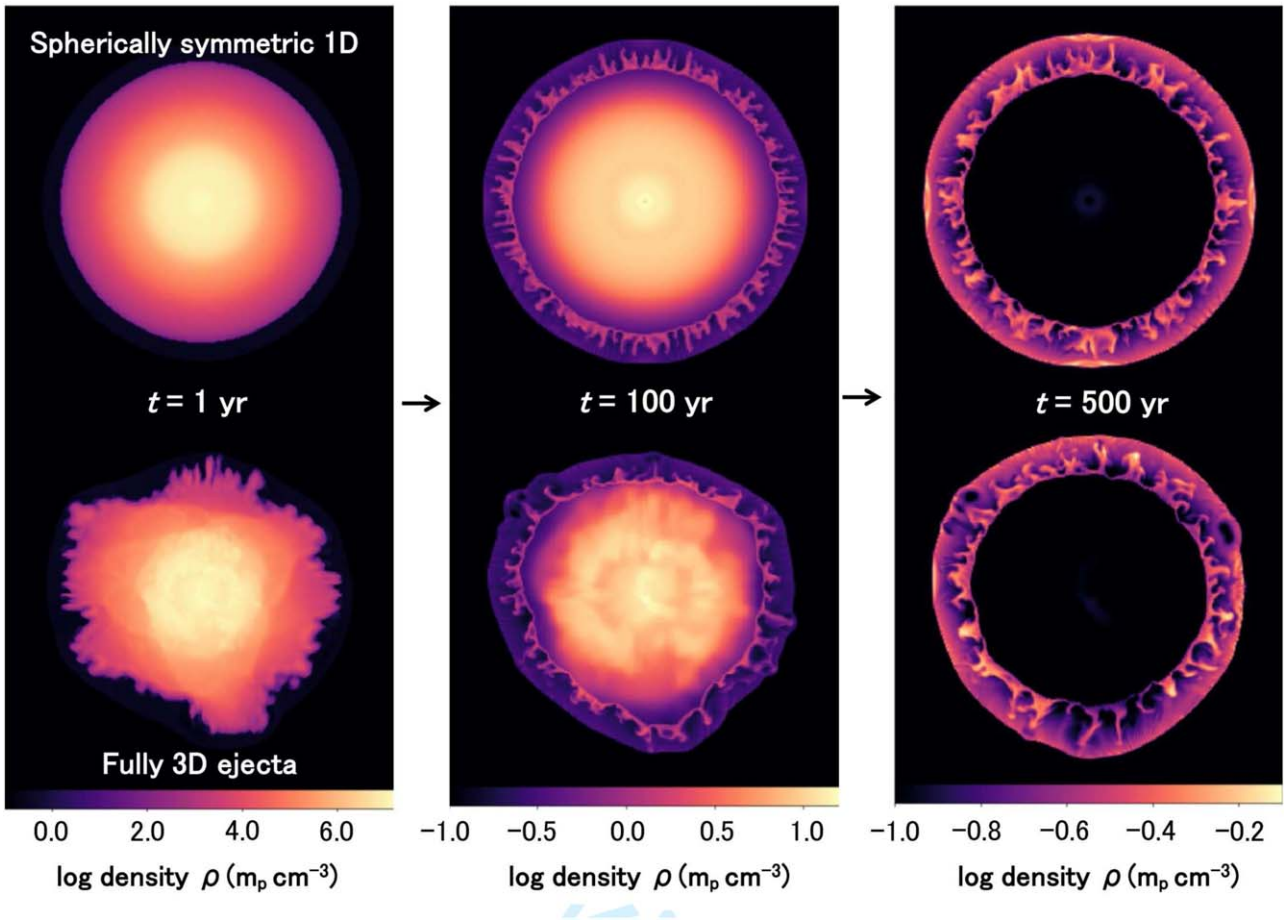


Figure 16. An example of how asymmetries in SN Ia ejecta contribute to the shaping of SNRs. The figure illustrates slices of mass density of all material at $t = 1$ yr (*left*), $t = 100$ yr (*middle*) and $t = 500$ yr (*right*) from 3D hydrodynamical SNR simulations (i.e., the ejecta-CSM/ISM interaction) of Ferrand et al. (2019) by adopting either a 1D angle averaged spherically symmetric ejecta model (*top panels*) or a fully 3D ejecta model (*bottom panels*; the N100 delayed detonation model of Seitenzahl et al. 2013b) as the initial condition. Note that different length scales are used in diagrams at different ages, which are respectively given in the order of 0.085 pc, 5 pc and 13 pc from *left to right*. The figure is reprinted from Ferrand et al. (2019, see their Figure 3) with the permission of the AAS.

5.5. Polarization Features

Scattering from electrons distributed in the ejecta of the explosion can linearly polarize light. Measuring polarization features of SNe Ia through spectropolarimetry is an important tool for revealing the geometry of SN Ia ejecta and the distribution of various elements in them. This can provide constraints on the explosion geometry and thus may be helpful for disentangling progenitor models and explosion mechanisms (see Wang & Wheeler 2008, for a review). Observations commonly find low levels of continuum polarization in SNe Ia ($\lesssim$1% Wang & Wheeler 2008; Cikota et al. 2019), typically 0.2–0.3 per cent in normal SNe Ia, and 0.3–0.8 per cent in subluminous SNe Ia. However, a few events do show higher polarization, e.g., SN 1999by (Howell 2001), SN 2004dt (Wang et al. 2006) and SN 2005ke (Patat et al. 2012). In contrast to the low-level continuum polarization, the polarization across the line profiles of spectral features associated with IMEs, such as Ca, Si, sulfur (S) and Mg, has been found to be quite significant in some SNe Ia (up to ∼2 per cent; Wang et al. 2003, 2006; Kasen et al. 2003; Patat et al. 2009, 2012; Maund et al. 2010). This suggests significant asymmetries in the element distribution in SN ejecta (Wang & Wheeler 2008). Also, it has been suggested that there may exist correlations between the polarization of Si II and either the pseudo equivalent width (pEW) or the velocity of Si II features (Meng et al. 2017; Cikota et al. 2019). Some earlier attempts to model the spectropolarimetry of SNe Ia assumed either an ellipsoidal ejecta shape—which is predicted in the explosion of a rapidly rotating WD (Hoflich 1991; Howell 2001; Wang et al. 1997, 2001)—or clumped and toroidal shells in the outer ejecta layers (Kasen et al. 2003) and the results have been compared to spectropolarimetry observations of SNe Ia (Höflich et al. 2006; Patat et al. 2012; Kasen et al. 2003).

Asymmetric ejecta from SN Ia explosions themselves (i.e., asymmetries in the geometry and element distribution) have been predicted by many multi-dimensional SN Ia explosion models (Hillebrandt et al. 2013; see Section 3.2). Recently, synthetic spectropolarimetry has been calculated by performing Monte Carlo radiative transfer calculations for different possible explosion models, including violent mergers of two WDs (Bulla et al. 2016a), sub-Chandrasekhar-mass double-detonation and Chandrasekhar-mass delayed-detonation models (Bulla et al. 2016b), and WD head-on collisions (Livneh & Katz 2022). Bulla et al. (2016b) found that the sub-Chandrasekhar-mass double-detonation model and the Chandrasekhar-mass delayed detonation model produce a low continuum polarization around maximum light of about 0.1–0.3 per cent and it decreases after maximum light, which is in good agreement with spectropolarimetric observations of normal SNe Ia. In contrast, Bulla et al. (2016a) showed that the violent merger model produces high Si II line polarization of ∼0.5%–3.2%, which is too strong to fit the observations of most SNe Ia. Livneh & Katz (2022) predict a low continuum polarization of ∼0.5% for the head-on WD collision model but they find a very high Si II line polarization of ∼3%, which is inconsistent with the observations.

All these simulations ignored the potential effect of the ejecta–companion interaction on the predicted polarization features. Kasen et al. (2004) addressed the effect of an ejecta-hole asymmetry due to the ejecta–companion interaction on the variation of the spectrum, luminosity and polarization with viewing angle by using multi-dimensional radiative transfer calculations. They found that high continuum polarization can be seen when looking down the hole carved by the companion almost directly. However, a simplified structure and composition of the SN ejecta was used in their modeling. Bulla et al. (2020) predicted spectropolarimetric features originating from a Chandrasekhar-mass pure deflagration explosion simulation and the subsequent ejecta–companion interaction. They report a reasonable agreement between predicted polarization features and those observed in SN 2005hk (see Figure 17) and suggest that the polarization seen at blue wavelengths around maximum-light was mainly caused by ejecta asymmetries due to the ejecta–companion interaction (Bulla et al. 2020). However, only a 1D averaged spherically symmetric ejecta model (which ignores the asymmetries of the SN explosion itself) was used in their simulations of ejecta–companion interaction.

For stronger conclusions on the effect of the presence of a companion star on polarization features of SNe Ia, realistic SN ejecta structures directly computed from simulations of ejecta–companion interaction are needed as inputs to calculate synthetic spectropolarimetry of SNe Ia in the context of different explosion mechanisms.

5.6. Late-Time Photometry

Seitenzahl et al. (2009) pointed out that the slow decay of ^{57}Co, ^{55}Fe and ^{44}Ti can contribute significantly to the light curve evolution of SNe Ia, slowing down their decline later than ∼900 days after the SN explosion (see also Seitenzahl & Townsley 2017). Different nucleosynthetic yields (e.g., ^{57}Co, ^{55}Fe and ^{44}Ti) are expected from different explosion models. Therefore, comparing the predictions from different explosion models (e.g., Röpke et al. 2012) with observed late-time light curves of SNe Ia is a potential way to constrain the explosion conditions (Graur et al. 2016; Tucker et al. 2022b; Tiwari et al. 2022; Kosakowski et al. 2023). The following important decay chains are generally considered in the study of SN Ia late-time photometry (Seitenzahl et al. 2009):

$$^{56}\mathrm{Ni} \xrightarrow{t_{1/2} = 6.08\ \mathrm{d}} {}^{56}\mathrm{Co} \xrightarrow{t_{1/2} = 77.2\ \mathrm{d}} {}^{56}\mathrm{Fe},$$
$$^{57}\mathrm{Ni} \xrightarrow{t_{1/2} = 35.60\ \mathrm{h}} {}^{57}\mathrm{Co} \xrightarrow{t_{1/2} = 271.79\ \mathrm{d}} {}^{57}\mathrm{Fe},$$
$$^{55}\mathrm{Co} \xrightarrow{t_{1/2} = 17.53\ \mathrm{h}} {}^{55}\mathrm{Fe} \xrightarrow{t_{1/2} = 999.67\ \mathrm{d}} {}^{55}\mathrm{Mn},$$
$$^{44}\mathrm{Ti} \xrightarrow{t_{1/2} = 58.90\ \mathrm{yr}} {}^{44}\mathrm{Sc} \xrightarrow{t_{1/2} = 3.97\ \mathrm{h}} {}^{44}\mathrm{Ca}.$$

To date, very late-time photometry has been observed only for a limited sample of events, including SN 2011fe (Shappee et al. 2017; Dimitriadis et al. 2017; Kerzendorf et al. 2017; Tucker et al. 2022b), SN 2012cg (Childress et al. 2015; Graur et al. 2016), SN 2013aa (Jacobson-Galán et al. 2018), SN 2014J (Yang et al. 2018; Graur 2019; Li et al. 2019b), ASASN-14lp (Graur et al. 2018a) and SN 2015F (Graur et al. 2018b). The ratios of ^{57}Ni/^{56}Ni and/or ^{55}Fe/^{57}Co of these SNe Ia were estimated and then compared with the predictions of different explosion models. For instance, based on photometry of SN 2011fe out to about 2,400 d after maximum light, Tucker et al. (2022b) suggested that the late-time light curve of SN 2011fe was powered by the energy released from the decay of both ^{57}Co and ^{55}Fe, giving rise to mass ratios of $\log(^{57}\mathrm{Co}/^{56}\mathrm{Co}) \approx -1.69$ (which is reasonably consistent with the estimates for other SNe Ia; Graur et al. 2016, 2018b; Shappee et al. 2017; Dimitriadis et al. 2017; Jacobson-Galán et al. 2018; Yang et al. 2018; Li et al. 2019b) and $\log(^{55}\mathrm{Fe}/^{57}\mathrm{Co}) \approx -0.66$. They pointed out that this was the first detection of ^{55}Fe in SNe Ia. Tucker et al. (2022b) further concluded that these late-time photometry observations of SN 2011fe are consistent with the predictions either from a delayed detonation of a near-Chandrasekhar-mass WD (1.2–1.3 $M_\odot$) with a low central density or from a sub-Chandrasekhar-mass WD (1.0–1.1 $M_\odot$) experiencing a thin-shell double-detonation. Tiwari et al. (2022) carried out a comprehensive comparison between late-time light curves of five SNe Ia (SN 2011fe, SN 2012cg, SN 2013aa, SN 2014J and SN 2015F) and nucleosynthetic yields of publicly-available SN Ia models, suggesting that SN 2015F favors the sub-Chandrasekhar progenitor model, and other SNe Ia are consistent with both

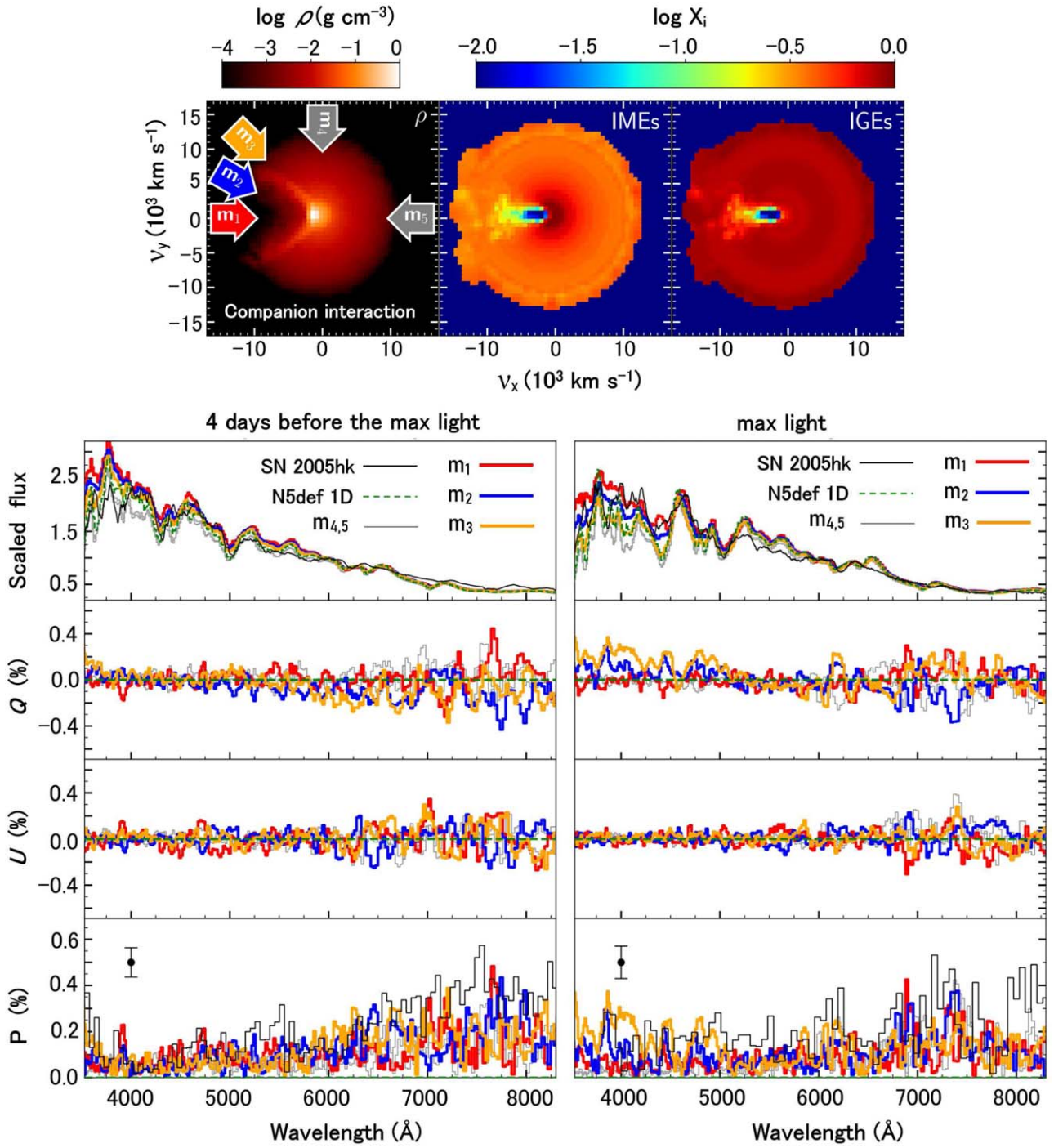


Figure 17. Theoretical flux and polarization spectra of a weak pure deflagration explosion model (i.e., N5def model of Fink et al. 2014) by considering the effect of the presence of a non-degenerate companion star. *Top panels*: Distribution of density (*left*), IMEs (*middle*) and IGEs (*right*) of post-impact SN ejecta in the $x - y$ plane from a 3D hydrodynamical simulation of ejecta-companion interaction of Liu et al. (2013a). *Bottom panels*: Predicted flux, Q, U and P spectra at pre- and around maximum light are displayed from *top to bottom*. Different colored lines give the results viewed from the five different orientations (m1-m5) shown in the *top left panel*. Here, Q and U are the Stokes parameters. The results are compared with those of SN 2005hk (*black solid lines*). The figure is reproduced from Bulla et al. (2020, see their Figure 3) with permission © ESO.

near-Chandrasekhar and sub-Chandrasekhar progenitor models.

Either a non-degenerate or WD companion star (in the SD or D[6] model; see Section 5.3) or a bound WD remnant (in weak pure deflagration explosion model; see Section 5.3.3) is expected to survive the explosion. These surviving stars could become more luminous than their pre-explosion brightnesses after the explosion due to significant heating by the explosion and the radioactive decay of captured SN Ia ejecta onto the star. As SNe Ia fade at late time phases, the shocked companion star and/or WD remnant could become more luminous than the SN itself (Podsiadlowski 2003; Pan et al. 2012a, 2013; Shappee et al. 2013a; Shen et al. 2017; Liu & Zeng 2021; Liu et al. 2021, 2023; Zeng et al. 2022a). This suggests that the surviving companion star or WD remnant could begin to dominate light curves of SNe Ia at late-time phases, causing the light curves to decline more slowly than those of SN explosions themselves.

5.7. X-ray and EUV Emission from Accreting WDs

In the SD scenario, the accreting WDs are expected to respectively undergo an extreme UV (EUV) radiation phase and an SSS phase (0.3–0.7 keV; van den Heuvel et al. 1992; Iben & Tutukov 1994; Kahabka & Ergma 1997; Yoon & Langer 2003; Nomoto et al. 2007; Chen et al. 2015) before the SN explosions during the stable nuclear burning and the optically thick wind regimes. Chen et al. (2015) conducted a population synthesis study of accreting WDs in the context of SD scenario to make predictions on X-ray and EUV emissions from populations of accreting WDs.

Comparisons of the observed SSSs in galaxies of different morphological types with X-ray expectations from the SD model have been used to put constraints on SN Ia progenitor models (e.g., Di Stefano 2010a, 2010b; Gilfanov & Bogdán 2010; Woods et al. 2017, 2018; Kuuttila et al. 2019). For instance, Gilfanov & Bogdán (2010) reported that the observed X-ray flux from six nearby elliptical galaxies and galaxy bulges is lower than the predictions from the SD scenario by a factor of 30–50. They therefore concluded that no more than five per cent of SNe Ia in early-type galaxies can be produced by the SD scenario. However, Hachisu et al. (2010) pointed out that there are still uncertainties on the theoretical X-ray luminosity of the SSSs, such as the atmospheric models of accreting WDs and absorption of soft X-rays. Depending on the different mass-accretion rates, the accreting WDs would undergo optically thick wind evolution, SSS phases and nova outbursts. Hachisu et al. (2010) further argued that the SSS phase should be short in duration, because most of the accreting WDs in the SD scenario spend a large portion of time in the optically thick wind phase and the recurrent nova phase. However, Chen et al. (2015) predicted that also the optically thick wind evolution is expected to produce significant EUV emission.

6. Summary and Future Perspectives

Despite substantial efforts, the progenitor systems and explosion mechanisms of SNe Ia have been established neither observationally nor theoretically, although there is consensus that SNe Ia arise from thermonuclear explosions of WDs in binary systems. Different progenitor models and explosion mechanisms have been proposed for SNe Ia in the literature. We have reviewed theoretical predictions for observables of SNe Ia at different stages of the explosion and their comparison with observations in the context of currently proposed progenitor models. Despite substantial progress in the understanding of the origin and the explosion physics of SNe Ia over the past years, there are still many open questions that need to be answered by future studies taking both theoretical and observational approaches.

1. *How can different progenitor and explosion scenarios be related to the diverse zoo of SN Ia subclasses?* SNe Ia have been used as excellent cosmological distance indicators because of the so-called Phillips relation, an empirical tight correlation between the peak luminosity of SNe Ia and the width of the light curve (Pskovskii 1977; Phillips 1993; Phillips et al. 1999). However, the physics causing the Phillips relation is still unknown. There is growing evidence for different subclasses of SNe Ia that are in various characteristics clearly distinct from normal SNe Ia and deviate from the Phillips relation (Taubenberger 2017). Connections between potential explosion models and some subclasses of SNe Ia have been established. For instance, SNe Iax have been associated with off-center ignited deflagrations in Chandrasekhar-mass WDs (Phillips et al. 2007; Jordan et al. 2012a; Kromer et al. 2013a, 2015), and a violent merger of two WDs seems to be a possible explanation of observed features of a subluminous, slowly declining SN 2002es-like event, SN 2010lp (Kromer et al. 2013b; Pakmor et al. 2013). However, the origin of the diversity of SNe Ia is still far from being resolved.
2. *How do the WDs reach an explosive state? What are the progenitor systems of SNe Ia?* Despite the substantial efforts undertaken from both the theoretical and observational side, the questions of how the WD reaches an explosive state and what progenitor systems are more likely to produce SNe Ia remain open. No single published model is able to consistently explain the observational features and full diversity of SNe Ia. A new progenitor paradigm might be needed if all SNe Ia arise from the same origin. Otherwise, a contribution of several distinct progenitor channels may be an alternative.
3. *What is the efficiency of mass accumulation onto an accreting WD?* In the SD scenario, the accreting WD does not retain a significant fraction of the transferred material. Only a fairly narrow range of accretion rates

allows for steady mass accumulation, which makes it difficult to explain the observed SN Ia rates in the context of that scenario. However, the exact mass-retention efficiency is still not well-constrained because of uncertainties in the nova phase at low mass transfer rates and the treatment at high mass transfer rates. BPS calculations have indicated that different retention efficiencies could have a strong influence on the predicted rates and delayed times of SNe Ia (Bours et al. 2013; Ruiter et al. 2014; Toonen et al. 2014). The so-called optically thick wind model (Hachisu et al. 1999) is generally adopted at high mass transfer rates to avoid the formation of a CE. However, the optically thick wind does not work at low metallicities, which seems to be in conflict with the detection of high-redshift ($z > 2$) SNe Ia. Also, the mixing between the accreted envelope and the WD during the nova phase is still poorly constrained, leading to uncertainties in the mass retention during the nova outbursts (Yaron et al. 2005; Denissenkov et al. 2013). Furthermore, the donor is expected to be irradiated by nova eruptions. How the nova irradiation affects the donor star and thus the mass transfer rate is not well understood (Ginzburg & Quataert 2021).

4. *What is the critical He shell mass in the sub-Chandrasekhar double-detonation model?* Early studies have suggested that double detonations of sub-Chandrasekhar-mass WDs produce heavy elements in the outer ejecta layers that drive the flux too far into red colors to be consistent with the observations of normal SNe Ia (Kromer et al. 2010). But it seems possible that a He detonation could already trigger after accreting a rather thin He shell (Bildsten et al. 2007; Shen & Bildsten 2009; Shen et al. 2018a; Woosley & Kasen 2011) and then lead to a core detonation (Fink et al. 2007, 2010; Gronow et al. 2020, 2021a; Boos et al. 2021). It has been suggested that explosions caused with thin accreted He layers may be a viable scenario for normal SNe Ia (Townsley et al. 2019; Boos et al. 2021; Shen et al. 2021b). However, the critical He-shell mass that can successfully trigger double-detonations of sub-Chandrasekhar-mass WDs remains uncertain, as well as its dependency on the mass of the accreting WD.
5. *Can stripped H/He in the SD scenario be hidden?* Current hydrodynamic simulations predict that a significant amount of H/He can be stripped off from the companion surface by the SN blast wave. This seems to imply the presence of H/He lines in late-time spectra. However, no H/He lines have been detected in normal SNe Ia but only in two fast-declining, subluminous events (see Section 5.2.1). This poses a serious challenge to the SD scenario. However, such conclusions are based on models with an analytical ejecta structure or the so-called 1D W7 model to represent an SN Ia explosion. The properties of this simplified SN Ia ejecta model differ from those directly derived from 3D explosion modeling. This leads to uncertainties not only on the amount of stripped H/He masses, but also on the prediction of late-time H/He lines and properties of surviving companion stars. To determine whether the stripped-off H/He companion material would be observable in SN Ia late-time spectra, a new quality of impact simulations based on realistic 3D ejecta structures is required. The output ejecta structure predicted from such impact simulations should be used directly as input for subsequent 3D radiative transfer modeling to test for H/He lines in late-time spectra.
6. *Where are surviving companions in the SD scenario?* Searching for the surviving companion stars in SNRs is thought to be a promising way to potentially identify SD progenitor systems of SNe Ia. Although a few surviving WD candidates of the sub-Chandrasekhar-mass double-detonation model have been reported in the literature, no promising surviving companion star predicted by the SD scenario has been identified yet beyond doubt in SNRs (Ruiz-Lapuente 2019). Some results seem to support an SD origin for at least a few SNe Ia, for instance, the detection of variable blueshifted absorption lines associated with CSM in some SNe Ia. Also, Seitenzahl et al. (2013a) suggested that at least a certain fraction of Chandrasekhar-mass WD explosions are needed to explain the solar manganese-to-iron ratio, which seems to favor the SD scenario. The question is whether the surviving companion stars of SD SNe Ia do exist. The spin-up/spin-down model predicts that the companion star could either be an MS star, an RG, a subdwarf-B (sdB) star, or a WD (depending on the unknown spin-down timescale), which may explain the non-detection of surviving companion stars. Because of this, Meng & Li (2019) suggested that searches for such stars should be done preferentially in the U/UV bands. Observations are still needed to search for such surviving companions to test the SD scenario. As mentioned above, the predictions on the observational signatures should be improved by adopting realistic 3D ejecta structures in hydrodynamical impact simulations.
7. *Do early excess emissions observed in SNe Ia share the same origin?* For a growing list of SNe Ia early excess emission has been reported. These objects are sometimes referred to as "early-excess SNe Ia". Different mechanisms have been proposed to produce the observed bumps in the early light curves of SNe Ia (see Section 5.2.2). It remains unclear, however, whether these early-time features share the same origin. The discovery of more early excess SNe Ia in future observations will enable us to conduct statistical studies of their observational

properties, and therefore provide deeper insight into the origin of this feature.

8. *What imprint leaves the companion star on SN Ia observables from different stages of the explosion?* Over the past years, the SN Ia explosion mechanism and the evolution of potential progenitors have been studied in quite some detail. However, the presence of a binary companion star in the explosion process and its implications for observations have received less attention. Taking this effect into account holds promise for identifying viable progenitor systems. Conversely, its ignorance leads to a lack of realism in the observables predicted from explosion simulations. Future studies are encouraged to address the role of a companion star in shaping the observables of SNe Ia from different phases of the explosion, such as the effect on late-time spectra, polarization signals and SNRs. Such investigations are needed to better constrain SN Ia progenitor systems and explosion mechanisms.
9. *How can the "spin-up/spin-down" model be identified observationally?* It seems that the spin-up/spin-down model is able to provide good explanations for different observational facts on SNe Ia such as the non-detection of a pre-explosion companion star, the lack of radio/X-ray emission, and the absence of surviving companion stars and swept-up H/He in late-time spectra. On the one hand, the constraints on the exact spin-down timescale are still quite weak. On the other hand, a smoking gun is needed to observationally identify the spin-up/spin-down model. This requires numerical modeling in the context of the spin-up/spin-down model to make predictions for detectable signatures of this model and to identify the properties of the donor star.
10. *How can we improve the SN Ia peak-brightness calibration?* With the Phillips relation, SNe Ia have been successfully used as cosmic distance indicators to measure the accelerated expansion of the Universe. To further advance the precision of SN Ia cosmology and to constrain the properties of dark energy, the peak-brightness standardization of SNe Ia needs to be improved. The underlying causes of the variability of peak luminosities should be understood in order to unveil the physics behind the Phillips relation and to reduce potential systematic errors of the distance measurements. One of the keys is to understand the dependence of SN Ia properties on the redshift, galaxy type and host environment by statistical studies with large samples of well-observed SNe Ia.

Further understanding of the nature of SN Ia progenitors and their explosion mechanism relies not only on the improvements to theoretical modeling (binary evolution and population synthesis calculations, impact simulations, explosion modeling, radiative transfer calculations, etc) but also on better observational constraints. This requires both individual studies of well-observed SNe Ia and systematical investigations of different subclasses of SN Ia, which can be realized with ongoing surveys and projects like ZTF (Smith et al. 2014; Bellm et al. 2019), Gaia (Gaia Collaboration et al. 2016, 2018), JWST (Gardner et al. 2006), ATLAS (Tonry et al. 2018), PTF/iPTF (Law et al. 2009; Rau et al. 2009), ASAS-SN (Shappee et al. 2014), Pan-STARRS (Kaiser et al. 2002), YSE (Jones et al. 2021), DES (Dark Energy Survey Collaboration et al. 2016), SkyMapper (Keller et al. 2007), CRTS (Drake et al. 2009), OGLE-IV (Wyrzykowski et al. 2014), La Silla-QUEST (Baltay et al. 2013) and Subaru Hyper Suprime-Cam Transient Survey (Tanaka et al. 2016), and forthcoming projects with the Vera C. Rubin Observatory LSST (Ivezic et al. 2008; Ivezić et al. 2019). In particular, LSST is expected to discover ten million SNe during a ten-year survey, which will yield hundreds of thousands of SNe Ia with a broad range in redshifts. The combination of statistical investigations of such large samples of SNe Ia with individual studies of well-observed objects will allow addressing many questions about SNe Ia (like the rates, the progenitor systems, the explosion mechanism, the host properties, the origin of diversity and the details of variation in peak luminosity) in more detail, and will also lead to major advances in the precision of SN Ia cosmology (LSST Science Collaboration et al. 2009).

Acknowledgments

We thank the anonymous referee for useful comments that helped to improve this article. We are grateful to Robert Izzard, Xuefei Chen, Ji-An Jiang, Takashi Moriya, Xiangcun Meng and Hai-Liang Chen for very fruitful discussions. We thank Ji-An Jiang for sharing the data of their double-detonation models for partly reproducing Figure 12 of this article. Also, Figure 12 made use of the Heidelberg Supernova Model Archive (HESMA, see https://hesma.h-its.org; Kromer et al. 2017). This work is supported by the National Natural Science Foundation of China (NSFC, Grant Nos. 12288102, 12090040/1, 11873016), the National Key R&D Program of China (Nos. 2021YFA1600401 and 2021YFA1600400), the Chinese Academy of Sciences (CAS), the International Centre of Supernovae, Yunnan Key Laboratory (No. 202302AN360001), the Yunnan Fundamental Research Projects (grant Nos. 202 201BC070003, 202001AW070007) and the "Yunnan Revitalization Talent Support Program" Science & Technology Champion Project (No. 202305AB350003). The work of FR is supported by the Klaus Tschira Foundation and by the Deutsche Forschungsgemeinschaft (DFG, German Research Foundation)—Project-ID 138 713 538—SFB 881 ("The Milky Way System", Subproject A10).

ORCID iDs

Zheng-Wei Liu https://orcid.org/0000-0002-7909-4171
Friedrich K. Röpke https://orcid.org/0000-0002-4460-0097
Zhanwen Han https://orcid.org/0000-0001-9204-7778

References

Ablimit, I., Maeda, K., & Li, X.-D. 2016, ApJ, 826, 53
Ablimit, I., Xu, X.-j., & Li, X. D. 2014, ApJ, 780, 80
Ablimit, I., Podsiadlowski, P., Di Stefano, R., Rappaport, S. A., & Wicker, J. 2022, ApJL, 941, L33
Amaro-Seoane, P., Audley, H., Babak, S., et al. 2017, arXiv:1702.00786
Antoniadis, J., Chanlaridis, S., Gräfener, G., & Langer, N. 2020, A&A, 635, A72
Applegate, J. H., & Terman, J. L. 1989, ApJ, 340, 380
Arnett, W. D. 1969, Astrophysics and Space Science, 5, 180
Arnett, W. D. 1982, ApJ, 253, 785
Ashall, C., Lu, J., Hsiao, E. Y., et al. 2021, ApJ, 922, 205
Ashall, C., Lu, J., Shappee, B. J., et al. 2022, ApJL, 932, L2
Badenes, C., Hughes, J. P., Bravo, E., & Langer, N. 2007, ApJ, 662, 472
Badenes, C., Mullally, F., Thompson, S. E., & Lupton, R. H. 2009, ApJ, 707, 971
Baltay, C., Rabinowitz, D., Hadjiyska, E., et al. 2013, PASP, 125, 683
Bauer, E. B., Chandra, V., Shen, K. J., & Hermes, J. J. 2021, ApJL, 923, L34
Bauer, E. B., White, C. J., & Bildsten, L. 2019, ApJ, 887, 68
Bedin, L. R., Ruiz-Lapuente, P., González Hernández, J. I., et al. 2014, MNRAS, 439, 354
Bellm, E. C., Kulkarni, S. R., Graham, M. J., et al. 2019, PASP, 131, 018002
Benetti, S., Cappellaro, E., Mazzali, P. A., et al. 2005, ApJ, 623, 1011
Benetti, S., Cappellaro, E., Turatto, M., et al. 2006, ApJL, 653, L129
Benz, W., Bowers, R. L., Cameron, A. G. W., & Press, W. H. 1990, ApJ, 348, 647
Benz, W., Thielemann, F.-K., & Hills, J. G. 1989, ApJ, 342, 986
Bildsten, L., Shen, K. J., Weinberg, N. N., & Nelemans, G. 2007, ApJL, 662, L95
Blondin, J. M., & Ellison, D. C. 2001, ApJ, 560, 244
Blondin, S., Kasen, D., Röpke, F. K., Kirshner, R. P., & Mandel, K. S. 2011, MNRAS, 417, 1280
Blondin, S., Matheson, T., Kirshner, R. P., et al. 2012, AJ, 143, 126
Blondin, S., Prieto, J. L., Patat, F., et al. 2009, ApJ, 693, 207
Bloom, J. S., Kasen, D., Shen, K. J., et al. 2012, ApJL, 744, L17
Boehner, P., Plewa, T., & Langer, N. 2017, MNRAS, 465, 2060
Bondi, H., & Hoyle, F. 1944, MNRAS, 104, 273
Boos, S. J., Townsley, D. M., Shen, K. J., Caldwell, S., & Miles, B. J. 2021, ApJ, 919, 126
Borkowski, K. J., Gwynne, P., Reynolds, S. P., et al. 2017, ApJL, 837, L7
Borkowski, K. J., Reynolds, S. P., Hwang, U., et al. 2013, ApJL, 771, L9
Botticella, M. T., Riello, M., Cappellaro, E., et al. 2008, A&A, 479, 49
Botyánszki, J., Kasen, D., & Plewa, T. 2018, ApJL, 852, L6
Bours, M. C. P., Toonen, S., & Nelemans, G. 2013, A&A, 552, A24
Branch, D., Doggett, J. B., Nomoto, K., & Thielemann, F. K. 1985, ApJ, 294, 619
Branch, D., Fisher, A., & Nugent, P. 1993, AJ, 106, 2383
Bravo, E., & García-Senz, D. 2006, ApJL, 642, L157
Bravo, E., & García-Senz, D. 2008, A&A, 478, 843
Bravo, E., & García-Senz, D. 2009, ApJ, 695, 1244
Bravo, E., García-Senz, D., Cabezón, R. M., & Domínguez, I. 2009, ApJ, 695, 1257
Breedt, E., Steeghs, D., Marsh, T. R., et al. 2017, MNRAS, 468, 2910
Brown, J. S., Stanek, K. Z., Holoien, T. W. S., et al. 2019, MNRAS, 484, 3785
Brown, P. J., Dawson, K. S., de Pasquale, M., et al. 2012b, ApJ, 753, 22
Brown, P. J., Dawson, K. S., Harris, D. W., et al. 2012a, ApJ, 749, 18
Brown, W. R., Gianninas, A., Kilic, M., Kenyon, S. J., & Allende Prieto, C. 2016, ApJ, 818, 155
Brown, W. R., Kilic, M., Allende Prieto, C., & Kenyon, S. J. 2010, ApJ, 723, 1072
Brown, W. R., Kilic, M., Kosakowski, A., et al. 2020, ApJ, 889, 49
Bulla, M., Liu, Z. W., Röpke, F. K., et al. 2020, A&A, 635, A179
Bulla, M., Sim, S. A., Kromer, M., et al. 2016b, MNRAS, 462, 1039
Bulla, M., Sim, S. A., Pakmor, R., et al. 2016a, MNRAS, 455, 1060
Burdge, K. B., Coughlin, M. W., Fuller, J., et al. 2020, ApJL, 905, L7
Burke, J., Howell, D. A., Sand, D. J., et al. 2022b, arXiv:2207.07681
Burke, J., Howell, D. A., Sand, D. J., & Hosseinzadeh, G. 2022a, arXiv:2208.11201
Burkey, M. T., Reynolds, S. P., Borkowski, K. J., & Blondin, J. M. 2013, ApJ, 764, 63
Cao, Y., Kulkarni, S. R., Howell, D. A., et al. 2015, Natur, 521, 328
Cappellaro, E., Turatto, M., Tsvetkov, D. Y., et al. 1997, A&A, 322, 431
Cartier, R., Sullivan, M., Firth, R. E., et al. 2017, MNRAS, 464, 4476
Cendes, Y., Drout, M. R., Chomiuk, L., & Sarbadhicary, S. K. 2020, ApJ, 894, 39
Chandra, V., Hwang, H.-C., Zakamska, N. L., et al. 2022, MNRAS, 512, 6122
Chen, H.-L., Woods, T. E., Yungelson, L. R., Gilfanov, M., & Han, Z. 2015, MNRAS, 453, 3024
Chen, M. C., Herwig, F., Denissenkov, P. A., & Paxton, B. 2014, MNRAS, 440, 1274
Chen, X., Han, Z., & Tout, C. A. 2011, ApJL, 735, L31
Cheng, A. 1974, Astrophysics and Space Science, 31, 49
Chevalier, R. A. 1977, ARA&A, 15, 175
Chevalier, R. A. 1982, ApJ, 258, 790
Chevalier, R. A. 1998, ApJ, 499, 810
Chevalier, R. A., & Fransson, C. 2006, ApJ, 651, 381
Chevalier, R. A., Blondin, J. M., Emmering, R. T., et al. 1992, ApJ, 392, 118
Childress, M. J., Hillier, D. J., Seitenzahl, I., et al. 2015, MNRAS, 454, 3816
Chiotellis, A., Schure, K. M., Vink, J., et al. 2012, A&A, 537, A139
Chomiuk, L., Soderberg, A., Simon, J., & Foley, R. 2012a, The Astronomer's Telegram, 4453
Chomiuk, L., Soderberg, A. M., Chevalier, R. A., et al. 2016, ApJ, 821, 119
Chomiuk, L., Soderberg, A. M., Moe, M., et al. 2012b, ApJ, 750, 164
Chugai, N. N. 1986, SvA, 30, 563
Ciaraldi-Schoolmann, F., Seitenzahl, I. R., & Röpke, F. K. 2013, A&A, 559, A117
Cikota, A., Patat, F., Wang, L., et al. 2019, MNRAS, 490, 578
Claeys, J. S. W., Pols, O. R., Izzard, R. G., Vink, J., & Verbunt, F. W. M. 2014, A&A, 563, A83
Colgate, S. A. 1970, Natur, 225, 247
Colgate, S. A., & McKee, C. 1969, ApJ, 157, 623
Collins, C. E., Gronow, S., Sim, S. A., & Röpke, F. K. 2022, MNRAS, 517, 5289
Contreras, C., Phillips, M. M., Burns, C. R., et al. 2018, ApJ, 859, 24
Dan, M., Rosswog, S., Guillochon, J., & Ramirez-Ruiz, E. 2011, ApJ, 737, 89
Dark Energy Survey Collaboration, Abbott, T., Abdalla, F. B., et al. 2016, MNRAS, 460, 1270
De, K., Kasliwal, M. M., Tzanidakis, A., et al. 2020, ApJ, 905, 58
De Marco, O., Passy, J.-C., Moe, M., et al. 2011, MNRAS, 411, 2277
Deng, J., Kawabata, K. S., Ohyama, Y., et al. 2004, ApJL, 605, L37
Denissenkov, P. A., Herwig, F., Bildsten, L., & Paxton, B. 2013, ApJ, 762, 8
Denissenkov, P. A., Truran, J. W., Herwig, F., et al. 2015, MNRAS, 447, 2696
Dessart, L., Leonard, D. C., & Prieto, J. L. 2020, A&A, 638, A80
Deufel, B., Barwig, H., Šimić, D., Wolf, S., & Drory, N. 1999, A&A, 343, 455
Di Stefano, R. 2010a, ApJ, 712, 728
Di Stefano, R. 2010b, ApJ, 719, 474
Di Stefano, R., Voss, R., & Claeys, J. S. W. 2011, ApJL, 738, L1
Diehl, R., Siegert, T., Hillebrandt, W., et al. 2014, Science, 345, 1162
Diehl, R., Siegert, T., Hillebrandt, W., et al. 2015, A&A, 574, A72
Dilday, B., Howell, D. A., Cenko, S. B., et al. 2012, Science, 337, 942
Dimitriadis, G., Foley, R. J., Rest, A., et al. 2019, ApJL, 870, L1
Dimitriadis, G., Maguire, K., Karambelkar, V. R., et al. 2023, MNRAS, 521, 1162
Dimitriadis, G., Sullivan, M., Kerzendorf, W., et al. 2017, MNRAS, 468, 3798
Drake, A. J., Djorgovski, S. G., Mahabal, A., et al. 2009, ApJ, 696, 870
Drout, M. R., Soderberg, A. M., Mazzali, P. A., et al. 2013, ApJ, 774, 58
Dubay, L. O., Tucker, M. A., Do, A., Shappee, B. J., & Anand, G. S. 2022, ApJ, 926, 98
Dutta, A., Sahu, D. K., Anupama, G. C., et al. 2022, ApJ, 925, 217
Edwards, Z. I., Pagnotta, A., & Schaefer, B. E. 2012, ApJL, 747, L19
Elias-Rosa, N., Chen, P., Benetti, S., et al. 2021, A&A, 652, A115
Ferrand, G., Tanikawa, A., Warren, D. C., et al. 2022, ApJ, 930, 92

Ferrand, G., Warren, D. C., Ono, M., et al. 2019, ApJ, 877, 136
Filippenko, A. V. 1997, ARA&A, 35, 309
Filippenko, A. V., Richmond, M. W., Branch, D., et al. 1992b, AJ, 104, 1543
Filippenko, A. V., Richmond, M. W., Matheson, T., et al. 1992a, ApJL, 384, L15
Fink, M., Hillebrandt, W., & Röpke, F. K. 2007, A&A, 476, 1133
Fink, M., Kromer, M., Seitenzahl, I. R., et al. 2014, MNRAS, 438, 1762
Fink, M., Röpke, F. K., Hillebrandt, W., et al. 2010, A&A, 514, A53
Firth, R. E., Sullivan, M., Gal-Yam, A., et al. 2015, MNRAS, 446, 3895
Foley, R. J., Challis, P. J., Chornock, R., et al. 2013, ApJ, 767, 57
Foley, R. J., McCully, C., Jha, S. W., et al. 2014, ApJ, 792, 29
Foley, R. J., Rest, A., Stritzinger, M., et al. 2010, AJ, 140, 1321
Foley, R. J., Simon, J. D., Burns, C. R., et al. 2012, ApJ, 752, 101
Foley, R. J., Van Dyk, S. D., Jha, S. W., et al. 2015, ApJL, 798, L37
Fransson, C., Lundqvist, P., & Chevalier, R. A. 1996, ApJ, 461, 993
Fryer, C. L., Ruiter, A. J., Belczynski, K., et al. 2010, ApJ, 725, 296
Fryxell, B. A., & Arnett, W. D. 1981, ApJ, 243, 994
Fuhrmann, K. 2005, MNRAS, 359, L35
Fujimoto, M. Y. 1982a, ApJ, 257, 767
Fujimoto, M. Y. 1982b, ApJ, 257, 752
Gaia Collaboration, Brown, A. G. A., Vallenari, A., et al. 2018, A&A, 616, A1
Gaia Collaboration, Prusti, T., de Bruijne, J. H. J., et al. 2016, A&A, 595, A1
Gal-Yam, A. 2017, in Handbook of Supernovae, ed. A. W. Alsabti & P. Murdin (Berlin: Springer), 195
Gamezo, V. N., Khokhlov, A. M., & Oran, E. S. 2005, ApJ, 623, 337
Gamezo, V. N., Khokhlov, A. M., Oran, E. S., Chtchelkanova, A. Y., & Rosenberg, R. O. 2003, Science, 299, 77
Ganeshalingam, M., Li, W., Filippenko, A. V., et al. 2010, ApJS, 190, 418
Ganeshalingam, M., Li, W., Filippenko, A. V., et al. 2012, ApJ, 751, 142
García-Berro, E., Ritossa, C., & Iben, I., Jr. 1997, ApJ, 485, 765
García-Senz, D., Badenes, C., & Serichol, N. 2012, ApJ, 745, 75
García-Senz, D., & Bravo, E. 2005, A&A, 430, 585
Gardner, J. P., Mather, J. C., Clampin, M., et al. 2006, SSRv, 123, 485
Geier, S., Fürst, F., Ziegerer, E., et al. 2015, Science, 347, 1126
Geier, S., Heber, U., Kupfer, T., & Napiwotzki, R. 2010, A&A, 515, A37
Geier, S., Marsh, T. R., Wang, B., et al. 2013, A&A, 554, A54
Geier, S., Nesslinger, S., Heber, U., et al. 2007, A&A, 464, 299
Gilfanov, M., & Bogdán, Á. 2010, Natur, 463, 924
Ginzburg, S., & Quataert, E. 2021, MNRAS, 507, 475
González Hernández, J. I., Ruiz-Lapuente, P., Filippenko, A. V., et al. 2009, ApJ, 691, 1
González Hernández, J. I., Ruiz-Lapuente, P., Tabernero, H. M., et al. 2012, Natur, 489, 533
Goobar, A., Kromer, M., Siverd, R., et al. 2015, ApJ, 799, 106
Goobar, A., & Leibundgut, B. 2011, Annual Review of Nuclear and Particle Science, 61, 251
Graham, M. L., Harris, C. E., Nugent, P. E., et al. 2019, ApJ, 871, 62
Graham, M. L., Kumar, S., Hosseinzadeh, G., et al. 2017, MNRAS, 472, 3437
Graham, M. L., Nugent, P. E., Sullivan, M., et al. 2015, MNRAS, 454, 1948
Graur, O. 2019, ApJ, 870, 14
Graur, O., & Maoz, D. 2013, MNRAS, 430, 1746
Graur, O., Maoz, D., & Shara, M. M. 2014a, MNRAS, 442, L28
Graur, O., Rodney, S. A., Maoz, D., et al. 2014b, ApJ, 783, 28
Graur, O., Zurek, D., Shara, M. M., et al. 2016, ApJ, 819, 31
Graur, O., Zurek, D. R., Cara, M., et al. 2018a, ApJ, 866, 10
Graur, O., Zurek, D. R., Rest, A., et al. 2018b, ApJ, 859, 79
Graur, O., Bianco, F. B., Modjaz, M., et al. 2017, ApJ, 837, 121
Gray, W. J., Raskin, C., & Owen, J. M. 2016, ApJ, 833, 62
Griffeth Stone, A., Johnson, H. T., Blondin, J. M., et al. 2021, ApJ, 923, 233
Gronow, S., Collins, C., Ohlmann, S. T., et al. 2020, A&A, 635, A169
Gronow, S., Collins, C. E., Sim, S. A., & Röpke, F. K. 2021a, A&A, 649, A155
Gronow, S., Côté, B., Lach, F., et al. 2021b, A&A, 656, A94
Guerrero, J., García-Berro, E., & Isern, J. 2004, A&A, 413, 257
Guillochon, J., Dan, M., Ramirez-Ruiz, E., & Rosswog, S. 2010, ApJL, 709, L64
Hachinger, S., Röpke, F. K., Mazzali, P. A., et al. 2017, MNRAS, 471, 491
Hachisu, I., & Kato, M. 2001, ApJ, 558, 323
Hachisu, I., Kato, M., Kato, T., & Matsumoto, K. 2000, ApJL, 528, L97
Hachisu, I., Kato, M., & Nomoto, K. 1996, ApJL, 470, L97
Hachisu, I., Kato, M., & Nomoto, K. 1999, ApJ, 522, 487
Hachisu, I., Kato, M., & Nomoto, K. 2010, ApJL, 724, L212
Hachisu, I., Kato, M., & Nomoto, K. 2012a, ApJL, 756, L4
Hachisu, I., Kato, M., Saio, H., & Nomoto, K. 2012b, ApJ, 744, 69
Hallakoun, N., Maoz, D., Kilic, M., et al. 2016, MNRAS, 458, 845
Hamers, A. S., Pols, O. R., Claeys, J. S. W., & Nelemans, G. 2013, MNRAS, 430, 2262
Hamuy, M., Phillips, M. M., Suntzeff, N. B., et al. 2003, Natur, 424, 651
Han, Z. 1998, MNRAS, 296, 1019
Han, Z. 2008, ApJL, 677, L109
Han, Z., & Podsiadlowski, P. 2004, MNRAS, 350, 1301
Han, Z., & Podsiadlowski, P. 2006, MNRAS, 368, 1095
Han, Z.-W., Ge, H.-W., Chen, X.-F., & Chen, H.-L. 2020, Res. Astron. Astrophys., 20, 161
Harris, C. E., Chomiuk, L., & Nugent, P. E. 2021, ApJ, 912, 23
Hayden, B. T., Garnavich, P. M., Kasen, D., et al. 2010, ApJ, 722, 1691
Hermes, J. J., Putterman, O., Hollands, M. A., et al. 2021, ApJL, 914, L3
Hicken, M., Garnavich, P. M., Prieto, J. L., et al. 2007, ApJL, 669, L17
Hillebrandt, W., Kromer, M., Röpke, F. K., & Ruiter, A. J. 2013, Frontiers of Physics, 8, 116
Hillebrandt, W., & Niemeyer, J. C. 2000, ARA&A, 38, 191
Hoeflich, P., & Khokhlov, A. 1996, ApJ, 457, 500
Hoeflich, P., Khokhlov, A., Wheeler, J. C., et al. 1996, ApJL, 472, L81
Hoeflich, P., Khokhlov, A. M., & Wheeler, J. C. 1995, ApJ, 444, 831
Hoflich, P. 1991, A&A, 246, 481
Höflich, P., Gerardy, C. L., Marion, H., & Quimby, R. 2006, NewAR, 50, 470
Holmbo, S., Stritzinger, M. D., Shappee, B. J., et al. 2019, A&A, 627, A174
Horesh, A., Kulkarni, S. R., Fox, D. B., et al. 2012, ApJ, 746, 21
Hosseinzadeh, G., Sand, D. J., Lundqvist, P., et al. 2022, ApJL, 933, L45
Hosseinzadeh, G., Sand, D. J., Sarbadhicary, S. K., et al. 2023, arXiv:2305.03071
Hosseinzadeh, G., Sand, D. J., Valenti, S., et al. 2017, ApJL, 845, L11
Howell, D. A. 2001, ApJL, 554, L193
Howell, D. A. 2011, Nat. Commun., 2, 350
Howell, D. A., Sullivan, M., Nugent, P. E., et al. 2006, Natur, 443, 308
Howell, S. B., Sobeck, C., Haas, M., et al. 2014, PASP, 126, 398
Hoyle, F., & Fowler, W. A. 1960, ApJ, 132, 565
Hsiao, E. Y., Hoeflich, P., Ashall, C., et al. 2020, ApJ, 900, 140
Huang, S.-J., Hu, Y.-M., Korol, V., et al. 2020, PhRvD, 102, 063021
Iben, I. J., & Renzini, A. 1983, ARA&A, 21, 271
Iben, I., Jr., Nomoto, K., Tornambe, A., & Tutukov, A. V. 1987, ApJ, 317, 717
Iben, I., Jr., & Tutukov, A. V. 1984, ApJ, 284, 719
Iben, I., Jr., & Tutukov, A. V. 1994, ApJ, 431, 264
Igoshev, A. P., Perets, H., & Hallakou, N. 2023, MNRAS, 518, 6223
Ihara, Y., Ozaki, J., Doi, M., et al. 2007, PASJ, 59, 811
Ilkov, M., & Soker, N. 2012, MNRAS, 419, 1695
Im, M., Choi, C., Yoon, S.-C., et al. 2015, ApJS, 221, 22
Immler, S., Brown, P. J., Milne, P., et al. 2006, ApJL, 648, L119
Inserra, C., Smartt, S. J., Scalzo, R., et al. 2014, MNRAS, 437, L51
Isern, J., Jean, P., Bravo, E., et al. 2016, A&A, 588, A67
Ivanova, L. N., Imshennik, V. S., & Chechetkin, V. M. 1974, Astrophysics and Space Science, 31, 497
Ivanova, N., Justham, S., Chen, X., et al. 2013, Astronomy and Astrophysics Review, 21, 59
Ivezic, Z., Axelrod, T., Brandt, W. N., et al. 2008, Serbian Astronomical Journal, 176, 1
Jacobson-Galán, W. V., Dimitriadis, G., Foley, R. J., & Kilpatrick, C. D. 2018, ApJ, 857, 88
Jacobson-Galán, W. V., Foley, R. J., Schwab, J., et al. 2019, MNRAS, 487, 2538
Jeffery, D. J., Leibundgut, B., Kirshner, R. P., et al. 1992, ApJ, 397, 304
Jha, S., Branch, D., Chornock, R., et al. 2006, AJ, 132, 189
Jha, S. W. 2017, Type Iax Supernovae, Handbook of Supernovae (Berlin: Springer)
Jha, S. W., Maguire, K., & Sullivan, M. 2019, NatAs, 3, 706
Ji, S., Fisher, R. T., García-Berro, E., et al. 2013, ApJ, 773, 136
Jiang, J.-A., Doi, M., Maeda, K., et al. 2017, Natur, 550, 80
Jiang, J.-a., Doi, M., Maeda, K., & Shigeyama, T. 2018, ApJ, 865, 149
Jiang, J.-a., Maeda, K., Kawabata, M., et al. 2021, ApJL, 923, L8
Johansson, J., Woods, T. E., Gilfanov, M., et al. 2014, MNRAS, 442, 1079

Jones, D. O., Foley, R. J., Narayan, G., et al. 2021, ApJ, 908, 143
Jordan, G. C. I., Fisher, R. T., Townsley, D. M., et al. 2008, ApJ, 681, 1448
Jordan, G. C. I., Graziani, C., Fisher, R. T., et al. 2012b, ApJ, 759, 53
Jordan, G. C., IV, Perets, H. B., Fisher, R. T., & van Rossum, D. R. 2012a, ApJL, 761, L23
Justham, S. 2011, ApJL, 730, L34
Justham, S., Wolf, C., Podsiadlowski, P., & Han, Z. 2009, A&A, 493, 1081
Kahabka, P., & Ergma, E. 1997, A&A, 318, 108
Ivezić, Ž, Kahn, S. M., Tyson, J. A., et al. 2019, ApJ, 873, 111
Kaiser, N., Aussel, H., Burke, B. E., et al. 2002, Proc. SPIE, 4836, 154
Kasen, D. 2010, ApJ, 708, 1025
Kasen, D., Nugent, P., Thomas, R. C., & Wang, L. 2004, ApJ, 610, 876
Kasen, D., Nugent, P., Wang, L., et al. 2003, ApJ, 593, 788
Kasen, D., Röpke, F. K., & Woosley, S. E. 2009, Natur, 460, 869
Kasen, D., Thomas, R. C., & Nugent, P. 2006, ApJ, 651, 366
Kashi, A., & Soker, N. 2011, MNRAS, 417, 1466
Kashyap, R., Fisher, R., García-Berro, E., et al. 2015, ApJL, 800, L7
Kasliwal, M. M., Kulkarni, S. R., Gal-Yam, A., et al. 2010, ApJL, 723, L98
Kasliwal, M. M., Kulkarni, S. R., Gal-Yam, A., et al. 2012, ApJ, 755, 161
Kasuga, T., Sato, T., Mori, K., Yamaguchi, H., & Bamba, A. 2018, PASJ, 70, 88
Kasuga, T., Vink, J., Katsuda, S., et al. 2021, ApJ, 915, 42
Kato, M., & Hachisu, I. 2003, ApJL, 598, L107
Katz, B., & Dong, S. 2012, arXiv:1211.4584
Kawabata, M., Maeda, K., Yamanaka, M., et al. 2021, PASJ, 73, 1295
Kawai, Y., Saio, H., & Nomoto, K. 1987, ApJ, 315, 229
Kawka, A., Briggs, G. P., Vennes, S., et al. 2017, MNRAS, 466, 1127
Keller, S. C., Schmidt, B. P., Bessell, M. S., et al. 2007, PASA, 24, 1
Kelly, P. L., Fox, O. D., Filippenko, A. V., et al. 2014, ApJ, 790, 3
Kerzendorf, W. E., Childress, M., Scharwächter, J., Do, T., & Schmidt, B. P. 2014, ApJ, 782, 27
Kerzendorf, W. E., Long, K. S., Winkler, P. F., & Do, T. 2018a, MNRAS, 479, 5696
Kerzendorf, W. E., McCully, C., Taubenberger, S., et al. 2017, MNRAS, 472, 2534
Kerzendorf, W. E., Schmidt, B. P., Asplund, M., et al. 2009, ApJ, 701, 1665
Kerzendorf, W. E., Schmidt, B. P., Laird, J. B., Podsiadlowski, P., & Bessell, M. S. 2012, ApJ, 759, 7
Kerzendorf, W. E., Strampelli, G., Shen, K. J., et al. 2018b, MNRAS, 479, 192
Kerzendorf, W. E., Yong, D., Schmidt, B. P., et al. 2013, ApJ, 774, 99
Khokhlov, A. M. 1989, MNRAS, 239, 785
Khokhlov, A. M. 1991, A&A, 245, 114
Kilpatrick, C. D., Coulter, D. A., Dimitriadis, G., et al. 2018, MNRAS, 481, 4123
Kool, E. C., Johansson, J., Sollerman, J., et al. 2023, Natur, 617, 477
Korol, V., Hallakoun, N., Toonen, S., & Karnesis, N. 2022, MNRAS, 511, 5936
Kosakowski, D., Ugalino, M. I., Fisher, R., et al. 2023, MNRAS, 519, L74
Wyrzykowski, Ł., Kostrzewa-Rutkowska, Z., Kozłowski, S., et al. 2014, AcA, 64, 197
Kromer, M., Fink, M., Stanishev, V., et al. 2013a, MNRAS, 429, 2287
Kromer, M., Fremling, C., Pakmor, R., et al. 2016, MNRAS, 459, 4428
Kromer, M., Ohlmann, S., & Röpke, F. K. 2017, Mem. Soc. Astron. Italiana, 88, 312
Kromer, M., Ohlmann, S. T., Pakmor, R., et al. 2015, MNRAS, 450, 3045
Kromer, M., Pakmor, R., Taubenberger, S., et al. 2013b, ApJL, 778, L18
Kromer, M., Sim, S. A., Fink, M., et al. 2010, ApJ, 719, 1067
Kudritzki, R. P., & Simon, K. P. 1978, A&A, 70, 653
Kundu, E., Lundqvist, P., Pérez-Torres, M. A., Herrero-Illana, R., & Alberdi, A. 2017, ApJ, 842, 17
Kupfer, T., Bauer, E. B., van Roestel, J., et al. 2022, ApJL, 925, L12
Kushnir, D., Katz, B., Dong, S., Livne, E., & Fernández, R. 2013, ApJL, 778, L37
Kutsuna, M., & Shigeyama, T. 2015, PASJ, 67, 54
Kuuttila, J., Gilfanov, M., Seitenzahl, I. R., Woods, T. E., & Vogt, F. P. A. 2019, MNRAS, 484, 1317
Lach, F., Callan, F. P., Bubeck, D., et al. 2022a, A&A, 658, A179
Lach, F., Callan, F. P., Sim, S. A., & Röpke, F. K. 2022c, A&A, 659, A27
LSST Science Collaboration, Abell, P. A., Allison, J., et al. 2009, arXiv:0912.0201
Law, N. M., Kulkarni, S. R., Dekany, R. G., et al. 2009, PASP, 121, 1395
Leaman, J., Li, W., Chornock, R., & Filippenko, A. V. 2011, MNRAS, 412, 1419
Leibundgut, B. 2001, ARA&A, 39, 67
Leibundgut, B. 2008, Gen. Relativ. Gravitation, 40, 221
Leibundgut, B., Kirshner, R. P., Phillips, M. M., et al. 1993, AJ, 105, 301
Leonard, D. C. 2007, ApJ, 670, 1275
Li, C.-J., Chu, Y.-H., Gruendl, R. A., et al. 2017, ApJ, 836, 85
Li, C.-J., Kerzendorf, W. E., Chu, Y.-H., et al. 2019a, ApJ, 886, 99
Li, L., Zhang, J., Dai, B., et al. 2022, ApJ, 924, 35
Li, W., Bloom, J. S., Podsiadlowski, P., et al. 2011b, Natur, 480, 348
Li, W., Chornock, R., Leaman, J., et al. 2011a, MNRAS, 412, 1473
Li, W., Filippenko, A. V., Chornock, R., et al. 2003, PASP, 115, 453
Li, W., Filippenko, A. V., Treffers, R. R., et al. 2001, ApJ, 546, 734
Li, W., Leaman, J., Chornock, R., et al. 2011c, MNRAS, 412, 1441
Li, W., Wang, X., Hu, M., et al. 2019b, ApJ, 882, 30
Li, W., Wang, X., Vinkó, J., et al. 2019c, ApJ, 870, 12
Litke, K. C., Chu, Y.-H., Holmes, A., et al. 2017, ApJ, 837, 111
Liu, D., Wang, B., Ge, H., Chen, X., & Han, Z. 2019, A&A, 622, A35
Liu, D., Wang, B., & Han, Z. 2018, MNRAS, 473, 5352
Liu, D. D., Wang, B., Podsiadlowski, P., & Han, Z. 2016, MNRAS, 461, 3653
Liu, Z., & Stancliffe, R. J. 2020, A&A, 641, A20
Liu, Z.-W., Kromer, M., Fink, M., et al. 2013a, ApJ, 778, 121
Liu, Z.-W., Moriya, T. J., & Stancliffe, R. J. 2015a, MNRAS, 454, 1192
Liu, Z.-W., Moriya, T. J., Stancliffe, R. J., & Wang, B. 2015b, A&A, 574, A12
Liu, Z. W., Pakmor, R., Röpke, F. K., et al. 2012, A&A, 548, A2
Liu, Z.-W., Pakmor, R., Röpke, F. K., et al. 2013b, A&A, 554, A109
Liu, Z.-W., Pakmor, R., Seitenzahl, I. R., et al. 2013c, ApJ, 774, 37
Liu, Z.-W., Roepke, F. K., & Zeng, Y. 2023, ApJ, 928, 146
Liu, Z.-W., Röpke, F. K., Zeng, Y., & Heger, A. 2021, A&A, 654, A103
Liu, Z.-W., & Stancliffe, R. J. 2016, MNRAS, 459, 1781
Liu, Z.-W., & Stancliffe, R. J. 2017, MNRAS, 470, L72
Liu, Z.-W., & Stancliffe, R. J. 2018, MNRAS, 475, 5257
Liu, Z.-W., Stancliffe, R. J., Abate, C., & Wang, B. 2015c, ApJ, 808, 138
Liu, Z.-W., & Zeng, Y. 2021, MNRAS, 500, 301
Livio, M., & Mazzali, P. 2018, PhR, 736, 1
Livio, M., Prialnik, D., & Regev, O. 1989, ApJ, 341, 299
Livio, M., & Riess, A. G. 2003, ApJL, 594, L93
Livne, E. 1990, ApJL, 354, L53
Livne, E., & Arnett, D. 1995, ApJ, 452, 62
Livne, E., & Glasner, A. S. 1990, ApJ, 361, 244
Livne, E., Tuchman, Y., & Wheeler, J. C. 1992, ApJ, 399, 665
Livneh, R., & Katz, B. 2022, MNRAS, 511, 2994
Long, M., Jordan, G. C. I., van Rossum, D. R., et al. 2014, ApJ, 789, 103
Lorén-Aguilar, P., Isern, J., & García-Berro, E. 2009, A&A, 500, 1193
Lundqvist, P., Kundu, E., Pérez-Torres, M. A., et al. 2020, ApJ, 890, 159
Lundqvist, P., Mattila, S., Sollerman, J., et al. 2013, MNRAS, 435, 329
Lundqvist, P., Nyholm, A., Taddia, F., et al. 2015, A&A, 577, A39
Lunnan, R., Kasliwal, M. M., Cao, Y., et al. 2017, ApJ, 836, 60
Luo, J., Chen, L.-S., Duan, H.-Z., et al. 2016, Classical Quantum Gravity, 33, 035010
Lyman, J. D., James, P. A., Perets, H. B., et al. 2013, MNRAS, 434, 527
Ma, H., Woosley, S. E., Malone, C. M., Almgren, A., & Bell, J. 2013, ApJ, 771, 58
Maeda, K., Jiang, J.-a., Shigeyama, T., & Doi, M. 2018, ApJ, 861, 78
Maeda, K., Kutsuna, M., & Shigeyama, T. 2014, ApJ, 794, 37
Maeda, K., Röpke, F. K., Fink, M., et al. 2010, ApJ, 712, 624
Maeda, K., & Terada, Y. 2016, International Journal of Modern Physics D, 25, 1630024
Magee, M. R., Cuddy, C., Maguire, K., et al. 2022, MNRAS, 513, 3035
Magee, M. R., Kotak, R., Sim, S. A., et al. 2016, A&A, 589, A89
Magee, M. R., & Maguire, K. 2020, A&A, 642, A189
Magee, M. R., Maguire, K., Kotak, R., et al. 2020, A&A, 634, A37
Magee, M. R., Maguire, K., Kotak, R., & Sim, S. A. 2021, MNRAS, 502, 3533
Magee, M. R., Sim, S. A., Kotak, R., & Kerzendorf, W. E. 2018, A&A, 614, A115
Maguire, K., Sullivan, M., Patat, F., et al. 2013, MNRAS, 436, 222
Maguire, K., Taubenberger, S., Sullivan, M., & Mazzali, P. A. 2016, MNRAS, 457, 3254
Mannucci, F., Maoz, D., Sharon, K., et al. 2008, MNRAS, 383, 1121
Maoz, D., & Graur, O. 2017, ApJ, 848, 25

Maoz, D., & Mannucci, F. 2008, MNRAS, 388, 421
Maoz, D., & Mannucci, F. 2012, PASA, 29, 447
Maoz, D., Mannucci, F., & Brandt, T. D. 2012, MNRAS, 426, 3282
Maoz, D., Mannucci, F., Li, W., et al. 2011, MNRAS, 412, 1508
Maoz, D., Mannucci, F., & Nelemans, G. 2014, ARA&A, 52, 107
Maoz, D., Sharon, K., & Gal-Yam, A. 2010, ApJ, 722, 1879
Margutti, R., Parrent, J., Kamble, A., et al. 2014, ApJ, 790, 52
Margutti, R., Soderberg, A. M., Chomiuk, L., et al. 2012, ApJ, 751, 134
Marietta, E., Burrows, A., & Fryxell, B. 2000, ApJS, 128, 615
Marion, G. H., Brown, P. J., Vinkó, J., et al. 2016, ApJ, 820, 92
Marquardt, K. S., Sim, S. A., Ruiter, A. J., et al. 2015, A&A, 580, A118
Mattila, S., Lundqvist, P., Sollerman, J., et al. 2005, A&A, 443, 649
Maund, J. R., Wheeler, J. C., Wang, L., et al. 2010, ApJ, 722, 1162
Maxted, P. F. L., Marsh, T. R., & North, R. C. 2000, MNRAS, 317, L41
Mazzali, P. A., Röpke, F. K., Benetti, S., & Hillebrandt, W. 2007, Science, 315, 825
McCully, C., Jha, S. W., Foley, R. J., et al. 2014, Natur, 512, 54
McCully, C., Jha, S. W., Scalzo, R. A., et al. 2022, ApJ, 925, 138
McCutcheon, C., Zeng, Y., Liu, Z. W., et al. 2022, MNRAS, 514, 4078
Meng, X., Chen, X., & Han, Z. 2007, PASJ, 59, 835
Meng, X., Chen, X., & Han, Z. 2009, MNRAS, 395, 2103
Meng, X., & Li, J. 2019, MNRAS, 482, 5651
Meng, X., & Podsiadlowski, P. 2013, ApJL, 778, L35
Meng, X., & Podsiadlowski, P. 2014, ApJL, 789, L45
Meng, X., & Podsiadlowski, P. 2017, MNRAS, 469, 4763
Meng, X., & Yang, W. 2010, ApJ, 710, 1310
Meng, X.-C., & Luo, Y.-P. 2021, MNRAS, 507, 4603
Meng, X., Zhang, J., & Han, Z. 2017, ApJ, 841, 62
Meng, X., & Podsiadlowski, P. 2018, ApJ, 861, 127
Mennekens, N., Vanbeveren, D., De Greve, J. P., & De Donder, E. 2010, A&A, 515, A89
Miller, A. A., Cao, Y., Piro, A. L., et al. 2018, ApJ, 852, 100
Miller, A. A., Magee, M. R., Polin, A., et al. 2020, ApJ, 898, 56
Minkowski, R. 1941, PASP, 53, 224
Mohamed, S., & Podsiadlowski, P. 2007, in ASP Conf. Ser. 372, 15th European Workshop on White Dwarfs, ed. R. Napiwotzki & M. R. Burleigh (San Francisoc, CA: ASP), 397
Moll, R., Raskin, C., Kasen, D., & Woosley, S. E. 2014, ApJ, 785, 105
Moll, R., & Woosley, S. E. 2013, ApJ, 774, 137
Moore, K., & Bildsten, L. 2012, ApJ, 761, 182
Moore, K., Townsley, D. M., & Bildsten, L. 2013, ApJ, 776, 97
Moriya, T. J., Liu, D., Wang, B., & Liu, Z.-W. 2019, MNRAS, 488, 3949
Moriya, T. J., Mazzali, P. A., Ashall, C., & Pian, E. 2023, MNRAS, 522, 6035
Napiwotzki, R., Christlieb, N., Drechsel, H., et al. 2001, Astron. Nachr., 322, 411
Napiwotzki, R., Karl, C. A., Lisker, T., et al. 2020, A&A, 638, A131
Nelemans, G., & Tauris, T. M. 1998, A&A, 335, L85
Nelemans, G., Yungelson, L. R., Portegies Zwart, S. F., & Verbunt, F. 2001, A&A, 365, 491
Neunteufel, P. 2020, A&A, 641, A52
Neunteufel, P., Preece, H., Kruckow, M., et al. 2022, A&A, 663, A91
Neunteufel, P., Yoon, S. C., & Langer, N. 2016, A&A, 589, A43
Neunteufel, P., Yoon, S. C., & Langer, N. 2019, A&A, 627, A14
Ni, Y. Q., Moon, D.-S., Drout, M. R., et al. 2022, NatAs, 6, 568
Ni, Y. Q., Moon, D.-S., Drout, M. R., et al. 2023, ApJ, 946, 7
Noebauer, U. M., Kromer, M., Taubenberger, S., et al. 2017, MNRAS, 472, 2787
Nomoto, K. 1982a, ApJ, 257, 780
Nomoto, K. 1982b, ApJ, 253, 798
Nomoto, K., & Iben, I., Jr. 1985, ApJ, 297, 531
Nomoto, K., & Kondo, Y. 1991, ApJL, 367, L19
Nomoto, K., Saio, H., Kato, M., & Hachisu, I. 2007, ApJ, 663, 1269
Nomoto, K., Thielemann, F.-K., & Yokoi, K. 1984, ApJ, 286, 644
Nonaka, A., Aspden, A. J., Zingale, M., et al. 2012, ApJ, 745, 73
Nugent, P. E., Sullivan, M., Cenko, S. B., et al. 2011, Natur, 480, 344
Olling, R. P., Mushotzky, R., Shaya, E. J., et al. 2015, Natur, 521, 332
Orlando, S., Bocchino, F., Miceli, M., Petruk, O., & Pumo, M. L. 2012, ApJ, 749, 156
Paczynski, B. 1976, in IAU Symp. 73, Structure and Evolution of Close Binary Systems, ed. P. Eggleton, S. Mitton, & J. Whelan (Dordrecht: Reidel Publishing Co.), 75
Pagnotta, A., & Schaefer, B. E. 2015, ApJ, 799, 101
Pagnotta, A., Walker, E. S., & Schaefer, B. E. 2014, ApJ, 788, 173
Pakmor, R., Callan, F. P., Collins, C. E., et al. 2022, MNRAS, 517, 5260
Pakmor, R., Hachinger, S., Röpke, F. K., & Hillebrandt, W. 2011, A&A, 528, A117
Pakmor, R., Kromer, M., Röpke, F. K., et al. 2010, Natur, 463, 61
Pakmor, R., Kromer, M., Taubenberger, S., et al. 2012, ApJL, 747, L10
Pakmor, R., Kromer, M., Taubenberger, S., & Springel, V. 2013, ApJL, 770, L8
Pakmor, R., Röpke, F. K., Weiss, A., & Hillebrandt, W. 2008, A&A, 489, 943
Pakmor, R., Zenati, Y., Perets, H. B., & Toonen, S. 2021, MNRAS, 503, 4734
Pan, K.-C., Ricker, P. M., & Taam, R. E. 2010, ApJ, 715, 78
Pan, K.-C., Ricker, P. M., & Taam, R. E. 2012a, ApJ, 760, 21
Pan, K.-C., Ricker, P. M., & Taam, R. E. 2012b, ApJ, 750, 151
Pan, K.-C., Ricker, P. M., & Taam, R. E. 2013, ApJ, 773, 49
Pan, L., Wheeler, J. C., & Scalo, J. 2008, ApJ, 681, 470
Panagia, N., Van Dyk, S. D., Weiler, K. W., et al. 2006, ApJ, 646, 369
Papish, O., & Perets, H. B. 2016, ApJ, 822, 19
Parrent, J., Friesen, B., & Parthasarathy, M. 2014, Astrophysics and Space Science, 351, 1
Patat, F., Baade, D., Höflich, P., et al. 2009, A&A, 508, 229
Patat, F., Chandra, P., Chevalier, R., et al. 2007, Science, 317, 924
Patat, F., Höflich, P., Baade, D., et al. 2012, A&A, 545, A7
Pelisoli, I., Neunteufel, P., Geier, S., et al. 2021, NatAs, 5, 1052
Perets, H. B., Badenes, C., Arcavi, I., Simon, J. D., & Gal-yam, A. 2011, ApJ, 730, 89
Perets, H. B., Gal-Yam, A., Mazzali, P. A., et al. 2010, Natur, 465, 322
Pérez-Torres, M. A., Lundqvist, P., Beswick, R. J., et al. 2014, ApJ, 792, 38
Perlmutter, S., Aldering, G., Goldhaber, G., et al. 1999, ApJ, 517, 565
Phillips, M. M. 1993, ApJL, 413, L105
Phillips, M. M., Ashall, C., Burns, C. R., et al. 2022, ApJ, 938, 47
Phillips, M. M., Li, W., Frieman, J. A., et al. 2007, PASP, 119, 360
Phillips, M. M., Lira, P., Suntzeff, N. B., et al. 1999, AJ, 118, 1766
Phillips, M. M., Wells, L. A., Suntzeff, N. B., et al. 1992, AJ, 103, 1632
Piersanti, L., Tornambé, A., & Yungelson, L. R. 2014, MNRAS, 445, 3239
Piro, A. L. 2015, ApJ, 801, 137
Piro, A. L., & Morozova, V. S. 2016, ApJ, 826, 96
Piro, A. L., & Nakar, E. 2013, ApJ, 769, 67
Planck Collaboration, Aghanim, N., Akrami, Y., et al. 2020, A&A, 641, A6
Plewa, T. 2007, ApJ, 657, 942
Plewa, T., Calder, A. C., & Lamb, D. Q. 2004, ApJL, 612, L37
Podsiadlowski, P. 2003, arXiv e-prints, astro
Polin, A., Nugent, P., & Kasen, D. 2019, ApJ, 873, 84
Poludnenko, A. Y., Chambers, J., Ahmed, K., Gamezo, V. N., & Taylor, B. D. 2019, Science, 366, aau7365
Poznanski, D., Chornock, R., Nugent, P. E., et al. 2010, Science, 327, 58
Prieto, J. L., Chen, P., Dong, S., et al. 2020, ApJ, 889, 100
Pskovskii, I. P. 1977, SvA, 21, 675
Rabinak, I., Livne, E., & Waxman, E. 2012, ApJ, 757, 35
Raddi, R., Hollands, M. A., Gänsicke, B. T., et al. 2018, MNRAS, 479, L96
Raddi, R., Hollands, M. A., Koester, D., et al. 2019, MNRAS, 489, 1489
Rappaport, S., Chiang, E., Kallman, T., & Malina, R. 1994, ApJ, 431, 237
Rasio, F. A., & Shapiro, S. L. 1995, ApJ, 438, 887
Raskin, C., & Kasen, D. 2013, ApJ, 772, 1
Raskin, C., Kasen, D., Moll, R., Schwab, J., & Woosley, S. 2014, ApJ, 788, 75
Raskin, C., Scannapieco, E., Fryer, C., Rockefeller, G., & Timmes, F. X. 2012, ApJ, 746, 62
Raskin, C., Scannapieco, E., Rockefeller, G., et al. 2010, ApJ, 724, 111
Raskin, C., Timmes, F. X., Scannapieco, E., Diehl, S., & Fryer, C. 2009, MNRAS, 399, L156
Rau, A., Kulkarni, S. R., Law, N. M., et al. 2009, PASP, 121, 1334
Rau, S.-J., & Pan, K.-C. 2022, ApJ, 933, 38
Reindl, N., Schaffenroth, V., Miller Bertolami, M. M., et al. 2020, A&A, 638, A93
Reinecke, M., Hillebrandt, W., & Niemeyer, J. C. 2002, A&A, 391, 1167
Riess, A. G., Filippenko, A. V., Challis, P., et al. 1998, AJ, 116, 1009
Rivas, F., Harris, J. A., Hix, W. R., & Messer, O. E. B. 2022, ApJ, 937, 2
Rodríguez-Gil, P., Santander-García, M., Knigge, C., et al. 2010, MNRAS, 407, L21
Röpke, F. K. 2007, ApJ, 668, 1103

Röpke, F. K. 2017, in Handbook of Supernovae, ed. A. W. Alsabti & P. Murdin (Berlin: Springer), 1185
Röpke, F. K., & De Marco, O. 2023, LRCA, 9, 2
Röpke, F. K., Gieseler, M., Reinecke, M., Travaglio, C., & Hillebrandt, W. 2006a, A&A, 453, 203
Röpke, F. K., & Hillebrandt, W. 2005, A&A, 431, 635
Röpke, F. K., Hillebrandt, W., Niemeyer, J. C., & Woosley, S. E. 2006b, A&A, 448, 1
Röpke, F. K., Hillebrandt, W., Schmidt, W., et al. 2007a, ApJ, 668, 1132
Röpke, F. K., Kromer, M., Seitenzahl, I. R., et al. 2012, ApJL, 750, L19
Röpke, F. K., & Niemeyer, J. C. 2007, A&A, 464, 683
Röpke, F. K., & Sim, S. A. 2018, SSRv, 214, 72
Röpke, F. K., Woosley, S. E., & Hillebrandt, W. 2007b, ApJ, 660, 1344
Rosswog, S., Kasen, D., Guillochon, J., & Ramirez-Ruiz, E. 2009a, ApJL, 705, L128
Rosswog, S., Ramirez-Ruiz, E., & Hix, W. R. 2009b, ApJ, 695, 404
Roy, N. C., Tiwari, V., Bobrick, A., et al. 2022, ApJL, 932, L24
Ruan, W.-H., Guo, Z.-K., Cai, R.-G., & Zhang, Y.-Z. 2018, arXiv:1807.09495
Ruffini, N. J., & Casey, A. R. 2019, MNRAS, 489, 420
Ruiter, A. J. 2020, IAU Symposium, 357, 1
Ruiter, A. J., Belczynski, K., & Fryer, C. 2009, ApJ, 699, 2026
Ruiter, A. J., Belczynski, K., Sim, S. A., et al. 2011, MNRAS, 417, 408
Ruiter, A. J., Belczynski, K., Sim, S. A., Seitenzahl, I. R., & Kwiatkowski, D. 2014, MNRAS, 440, L101
Ruiter, A. J., Sim, S. A., Pakmor, R., et al. 2013, MNRAS, 429, 1425
Ruiz-Lapuente, P. 2014, NewAR, 62, 15
Ruiz-Lapuente, P. 2019, NewAR, 85, 101523
Ruiz-Lapuente, P., Comeron, F., Méndez, J., et al. 2004, Natur, 431, 1069
Ruiz-Lapuente, P., Damiani, F., Bedin, L., et al. 2018, ApJ, 862, 124
Ruiz-Lapuente, P., González Hernández, J. I., Cartier, R., et al. 2023, ApJ, 947, 90
Russell, B. R., & Immler, S. 2012, ApJL, 748, L29
Sai, H., Wang, X., Elias-Rosa, N., et al. 2022, MNRAS, 514, 3541
Saio, H., & Nomoto, K. 1998, ApJ, 500, 388
Sand, D. J., Amaro, R. C., Moe, M., et al. 2019, ApJL, 877, L4
Sand, D. J., Graham, M. L., Botyánszki, J., et al. 2018, ApJ, 863, 24
Sand, D. J., Sarbadhicary, S. K., Pellegrino, C., et al. 2021, ApJ, 922, 21
Santander-García, M., Rodríguez-Gil, P., Corradi, R. L. M., et al. 2015, Natur, 519, 63
Sarbadhicary, S. K., Chomiuk, L., Badenes, C., et al. 2019, ApJ, 872, 191
Sato, Y., Nakasato, N., Tanikawa, A., et al. 2015, ApJ, 807, 105
Sato, Y., Nakasato, N., Tanikawa, A., et al. 2016, ApJ, 821, 67
Scalzo, R. A., Aldering, G., Antilogus, P., et al. 2010, ApJ, 713, 1073
Schaefer, B. E., & Pagnotta, A. 2012, Natur, 481, 164
Schmidt, B. P., Suntzeff, N. B., Phillips, M. M., et al. 1998, ApJ, 507, 46
Schmidt, W., Ciaraldi-Schoolmann, F., Niemeyer, J. C., Röpke, F. K., & Hillebrandt, W. 2010, ApJ, 710, 1683
Schreiber, M. R., Belloni, D., Zorotovic, M., et al. 2022, MNRAS, 513, 3090
Schwab, J. 2021, ApJ, 906, 53
Schwab, J., Quataert, E., & Kasen, D. 2016, MNRAS, 463, 3461
Seaquist, E. R., & Taylor, A. R. 1990, ApJ, 349, 313
Segretain, L., Chabrier, G., & Mochkovitch, R. 1997, ApJ, 481, 355
Seitenzahl, I. R., Cescutti, G., Röpke, F. K., Ruiter, A. J., & Pakmor, R. 2013a, A&A, 559, L5
Seitenzahl, I. R., Ciaraldi-Schoolmann, F., Röpke, F. K., et al. 2013b, MNRAS, 429, 1156
Seitenzahl, I. R., Kromer, M., Ohlmann, S. T., et al. 2016, A&A, 592, A57
Seitenzahl, I. R., Taubenberger, S., & Sim, S. A. 2009, MNRAS, 400, 531
Seitenzahl, I. R., & Townsley, D. M. 2017, in Handbook of Supernovae, ed. A. W. Alsabti & P. Murdin (Berlin: Springer), 1955
Shappee, B., Prieto, J., Stanek, K. Z., et al. 2014, American Astronomical Society Meeting Abstracts, Vol. 223, 236.03
Shappee, B. J., Holoien, T. W. S., Drout, M. R., et al. 2019, ApJ, 870, 13
Shappee, B. J., Kochanek, C. S., & Stanek, K. Z. 2013a, ApJ, 765, 150
Shappee, B. J., Piro, A. L., Stanek, K. Z., et al. 2018, ApJ, 855, 6
Shappee, B. J., Stanek, K. Z., Kochanek, C. S., & Garnavich, P. M. 2017, ApJ, 841, 48
Shappee, B. J., Stanek, K. Z., Pogge, R. W., & Garnavich, P. M. 2013b, ApJL, 762, L5
Sharma, Y., Sollerman, J., Fremling, C., et al. 2023, ApJ, 948, 52
Shen, K. J., & Bildsten, L. 2007, ApJ, 660, 1444
Shen, K. J., & Bildsten, L. 2009, ApJ, 699, 1365
Shen, K. J., Bildsten, L., Kasen, D., & Quataert, E. 2012, ApJ, 748, 35
Shen, K. J., Blondin, S., Kasen, D., et al. 2021a, ApJL, 909, L18
Shen, K. J., Boos, S. J., Townsley, D. M., & Kasen, D. 2021b, ApJ, 922, 68
Shen, K. J., Boubert, D., Gänsicke, B. T., et al. 2018b, ApJ, 865, 15
Shen, K. J., Guillochon, J., & Foley, R. J. 2013, ApJL, 770, L35
Shen, K. J., Kasen, D., Miles, B. J., & Townsley, D. M. 2018a, ApJ, 854, 52
Shen, K. J., Kasen, D., Weinberg, N. N., Bildsten, L., & Scannapieco, E. 2010, ApJ, 715, 767
Shen, K. J., & Moore, K. 2014, ApJ, 797, 46
Shen, K. J., Toonen, S., & Graur, O. 2017, ApJL, 851, L50
Shields, J. V., Kerzendorf, W., Hosek, M. W., et al. 2022, ApJL, 933, L31
Siebert, M. R., Dimitriadis, G., Polin, A., & Foley, R. J. 2020, ApJL, 900, L27
Silverman, J. M., Foley, R. J., Filippenko, A. V., et al. 2012, MNRAS, 425, 1789
Silverman, J. M., Ganeshalingam, M., Li, W., et al. 2011, MNRAS, 410, 585
Silverman, J. M., Nugent, P. E., Gal-Yam, A., et al. 2013, ApJS, 207, 3
Sim, S. A., Fink, M., Kromer, M., et al. 2012, MNRAS, 420, 3003
Sim, S. A., Röpke, F. K., Hillebrandt, W., et al. 2010, ApJL, 714, L52
Sim, S. A., Seitenzahl, I. R., Kromer, M., et al. 2013, MNRAS, 436, 333
Simon, J. D., Gal-Yam, A., Gnat, O., et al. 2009, ApJ, 702, 1157
Smith, R. M., Dekany, R. G., Bebek, C., et al. 2014, Proc. SPIE, 9147, 914779
Soker, N. 2018, Science China Physics, Mechanics, and Astronomy, 61, 49502
Soker, N. 2019, NewAR, 87, 101535
Soker, N., García-Berro, E., & Althaus, L. G. 2014, MNRAS, 437, L66
Soker, N., Kashi, A., García-Berro, E., Torres, S., & Camacho, J. 2013, MNRAS, 431, 1541
Srivastav, S., Smartt, S. J., Huber, M. E., et al. 2023, ApJL, 943, L20
Starrfield, S., Truran, J. W., Sparks, W. M., & Kutter, G. S. 1972, ApJ, 176, 169
Stauffer, C. M., Margutti, R., Linford, J. D., et al. 2021, MNRAS, 505, 1153
Sternberg, A., Gal-Yam, A., Simon, J. D., et al. 2011, Science, 333, 856
Stritzinger, M. D., Valenti, S., Hoeflich, P., et al. 2015, A&A, 573, A2
Sullivan, M., Kasliwal, M. M., Nugent, P. E., et al. 2011, ApJ, 732, 118
Swaruba Rajamuthukumar, A., Hamers, A., Neunteufel, P., Pakmor, R., & de Mink, S. E. 2023, ApJ, 950, 9
Taam, R. E. 1980, ApJ, 242, 749
Taam, R. E., & Fryxell, B. A. 1984, ApJ, 279, 166
Tanaka, M., Tominaga, N., Morokuma, T., et al. 2016, ApJ, 819, 5
Tanikawa, A., Nomoto, K., Nakasato, N., & Maeda, K. 2019, ApJ, 885, 103
Taubenberger, S. 2017, in Handbook of Supernovae, ed. A. W. Alsabti & P. Murdin (Berlin: Springer), 317
Taubenberger, S., Benetti, S., Childress, M., et al. 2011, MNRAS, 412, 2735
Timmes, F. X., Woosley, S. E., & Taam, R. E. 1994, ApJ, 420, 348
Tiwari, V., Graur, O., Fisher, R., et al. 2022, MNRAS, 515, 3703
Tonry, J. L., Denneau, L., Heinze, A. N., et al. 2018, PASP, 130, 064505
Toonen, S., Claeys, J. S. W., Mennekens, N., & Ruiter, A. J. 2014, A&A, 562, A14
Toonen, S., Nelemans, G., & Portegies Zwart, S. 2012, A&A, 546, A70
Toonen, S., Perets, H. B., & Hamers, A. S. 2018, A&A, 610, A22
Tout, C. A. 2005, in ASP Conf. Ser. 330, The Astrophysics of Cataclysmic Variables and Related Objects, ed. J. M. Hameury & J. P. Lasota (San Francisco, CA: ASP), 279
Tovmassian, G., Yungelson, L., Rauch, T., et al. 2010, ApJ, 714, 178
Townsley, D. M., Calder, A. C., Asida, S. M., et al. 2007, ApJ, 668, 1118
Townsley, D. M., Miles, B. J., Shen, K. J., & Kasen, D. 2019, ApJL, 878, L38
Truran, J. W., Arnett, W. D., & Cameron, A. G. W. 1967, Can. J. Phys., 45, 2315
Tucker, M. A., Ashall, C., Shappee, B. J., et al. 2022a, ApJL, 926, L25
Tucker, M. A., Shappee, B. J., Kochanek, C. S., et al. 2022b, MNRAS, 517, 4119
Tucker, M. A., Shappee, B. J., Vallely, P. J., et al. 2020, MNRAS, 493, 1044
Tucker, M. A., Shappee, B. J., & Wisniewski, J. P. 2019, ApJL, 872, L22
Tutukov, A., & Yungelson, L. 1996, MNRAS, 280, 1035
Vallely, P. J., Fausnaugh, M., Jha, S. W., et al. 2019, MNRAS, 487, 2372
van den Bergh, S., & Tammann, G. A. 1991, ARA&A, 29, 363
van den Heuvel, E. P. J., Bhattacharya, D., Nomoto, K., & Rappaport, S. A. 1992, A&A, 262, 97
Vassiliadis, E., & Wood, P. R. 1993, ApJ, 413, 641

Vennes, S., Kawka, A., O'Toole, S. J., Németh, P., & Burton, D. 2012, ApJL, 759, L25
Vennes, S., Nemeth, P., Kawka, J. R., et al. 2017, Science, 357, 680
Vigh, C. D., Velázquez, P. F., Gómez, D. O., et al. 2011, ApJ, 727, 32
Waldman, R., Sauer, D., Livne, E., et al. 2011, ApJ, 738, 21
Wang, B. 2018, Res. Astron. Astrophys., 18, 049
Wang, B., Chen, X., Meng, X., & Han, Z. 2009, ApJ, 701, 1540
Wang, B., & Han, Z. 2012, NewAR, 56, 122
Wang, B., Justham, S., & Han, Z. 2013, A&A, 559, A94
Wang, B., Justham, S., Liu, Z. W., et al. 2014a, MNRAS, 445, 2340
Wang, B., Li, X.-D., & Han, Z.-W. 2010, MNRAS, 401, 2729
Wang, B., Meng, X., Liu, D.-D., Liu, Z.-W., & Han, Z. 2014b, ApJL, 794, L28
Wang, L., Baade, D., Höflich, P., et al. 2003, ApJ, 591, 1110
Wang, L., Baade, D., Höflich, P., et al. 2006, ApJ, 653, 490
Wang, L., Howell, D. A., Höflich, P., & Wheeler, J. C. 2001, ApJ, 550, 1030
Wang, L., & Wheeler, J. C. 2008, ARA&A, 46, 433
Wang, L., Wheeler, J. C., & Höflich, P. 1997, ApJL, 476, L27
Wang, Q., Rest, A., Dimitriadis, G., et al. 2023, arXiv:2305.03779
Warner, B. 2003, Cataclysmic Variable Stars (Cambridge : Cambridge Univ. Press)
Warren, J. S., Hughes, J. P., Badenes, C., et al. 2005, ApJ, 634, 376
Webbink, R. F. 1984, ApJ, 277, 355
Webbink, R. F., Livio, M., Truran, J. W., & Orio, M. 1987, ApJ, 314, 653
Wheeler, J. C. 2012, ApJ, 758, 123
Wheeler, J. C., Lecar, M., & McKee, C. F. 1975, ApJ, 200, 145
Whelan, J., & Iben, I. J. 1973, ApJ, 186, 1007
White, C. J., Kasliwal, M. M., Nugent, P. E., et al. 2015, ApJ, 799, 52
Willcox, D. E., Townsley, D. M., Calder, A. C., Denissenkov, P. A., & Herwig, F. 2016, ApJ, 832, 13
Williams, B. J., Borkowski, K. J., Ghavamian, P., et al. 2013, ApJ, 770, 129
Williams, B. J., Coyle, N. M., Yamaguchi, H., et al. 2017, ApJ, 842, 28
Winkler, P. F., Williams, B. J., Reynolds, S. P., et al. 2014, ApJ, 781, 65
Wiseman, P., Sullivan, M., Smith, M., et al. 2021, MNRAS, 506, 3330
Wolf, W. M., Bildsten, L., Brooks, J., & Paxton, B. 2013, ApJ, 777, 136
Woltjer, L. 1972, ARA&A, 10, 129
Wong, T. L. S., Schwab, J., & Götberg, Y. 2021, ApJ, 922, 241
Woods, T. E., Ghavamian, P., Badenes, C., & Gilfanov, M. 2017, NatAs, 1, 800
Woods, T. E., Ghavamian, P., Badenes, C., & Gilfanov, M. 2018, ApJ, 863, 120
Woods, T. E., & Gilfanov, M. 2013, MNRAS, 432, 1640
Woosley, S. E., & Kasen, D. 2011, ApJ, 734, 38
Woosley, S. E., Kerstein, A. R., & Aspden, A. J. 2011, ApJ, 734, 37
Woosley, S. E., Kerstein, A. R., Sankaran, V., Aspden, A. J., & Röpke, F. K. 2009, ApJ, 704, 255
Woosley, S. E., Taam, R. E., & Weaver, T. A. 1986, ApJ, 301, 601
Woosley, S. E., & Weaver, T. A. 1994, ApJ, 423, 371
Yamaguchi, H., Badenes, C., Foster, A. R., et al. 2015, ApJL, 801, L31
Yang, Y., Wang, L., Baade, D., et al. 2018, ApJ, 852, 89
Yaron, O., Prialnik, D., Shara, M. M., & Kovetz, A. 2005, ApJ, 623, 398
Yoon, S.-C., & Langer, N. 2003, A&A, 412, L53
Yoon, S. C., Podsiadlowski, P., & Rosswog, S. 2007, MNRAS, 380, 933
York, D. G., Adelman, J., Anderson, J. E. J., et al. 2000, AJ, 120, 1579
Yungelson, L., & Livio, M. 1998, ApJ, 497, 168
Yungelson, L. R. 2010, Astron. Lett., 36, 780
Yungelson, L. R., & Kuranov, A. G. 2017, MNRAS, 464, 1607
Zeng, Y., Liu, Z.-W., & Han, Z. 2020, ApJ, 898, 12
Zeng, Y., Liu, Z.-W., Heger, A., et al. 2022a, ApJ, 933, 65
Zeng, Y., Liu, Z.-W., Meng, X., & Han, Z. 2022b, RAA, 22, 075004
Zhang, M., Fuller, J., Schwab, J., & Foley, R. J. 2019, ApJ, 872, 29
Zheng, W., Silverman, J. M., Filippenko, A. V., et al. 2013, ApJL, 778, L15
Zorotovic, M., Schreiber, M. R., Gänsicke, B. T., & Nebot Gómez-Morán, A. 2010, A&A, 520, A86